Uncertainty in Probabilistic Open Pit Slope Stability Analyses: Implications for Reliability-Based Designs

by

Myzael Jacob Valdivia Paucar

A thesis submitted in partial fulfillment of the requirements for the degree of

Master of Science

in

Geotechnical Engineering

Department of Civil and Environmental Engineering
University of Alberta

Abstract

The presence of uncertainty is acknowledged in various fields of Engineering. Also, there are many sources of uncertainties. In geotechnical engineering, probabilistic slope stability analysis (PSSA) is a tool used to quantify parameter uncertainty. It achieves this by considering any strength parameter of a material as a random variable with a specific probability distribution. The outcomes of such analyses are evaluated through design acceptance criteria (DAC) that incorporate uncertainty in terms of design reliability – also known as Reliability-Based Design Acceptance Criteria (RBDAC) – having different ranges of DAC depending on the level of reliability, but also based on the potential consequence of the failure. Nevertheless, other forms of uncertainty are not usually accounted for in PSSA. Open pit slopes, akin to other mining earth structures, are subject to various types of uncertainties. This leads to the question of what emerges when these other sources of uncertainties are considered in PSSA and evaluated within the RBDAC.

This work is performed to study specific sources of uncertainty within open pits slopes, especially those referred to as parameter uncertainty, geometrical uncertainty, and computational uncertainty. These sources of uncertainty are explored using PSSA and subsequently evaluated within the RBDAC matrix proposed by Macciotta et al. (2020). The research is divided into two parts. The first part of the work primarily focuses on parameter uncertainty in the rock mass strength. It is an in-depth exploration of rock strength variability in terms of the Hoek-Brown failure criterion and Mohr-Coulomb failure criterion, considering univariate and bivariate distributions using two rock mass strength parameters. The aim of this work is to demonstrate consistent results whether Hoek-Brown or Mohr-Coulomb are being used and to comprehend the underlying reasons for

any disparities. The second part of the work stress tests the applicability of the RBDAC proposed by Macciotta et al. (2020) for open pit slopes, while also exploring the implications of introducing additional uncertainties (geometrical and computational) in addition to parameter uncertainty. This is performed through the integration of diverse scenarios, allowing for the creation of designs at different reliability levels and evaluations at different areas of the RBDAC matrix. Both works were conducted on a modified open pit slope, inspired by the geotechnical, geological, and hydrological characteristics of an implemented pit slope located in British Columbia, Canada.

The outcomes of this research yield significant insights for forthcoming probabilistic open pit slope stability analyses. The results of the first work underline that there will be differences in the outcomes of the PSSA between considering the variability of the rock mass strength using Mohr-Coulomb and Hoek-Brown unless an inherent correlation between the Mohr-Coulomb strength parameters is considered and estimated from the equations provided by Rafiei and Martin (2019) and through Monte Carlo simulations. This inherent correlation tends to be negative, consistent with considerations taken in soils, but it shifts to positive values as the GSI decreases or the confining stress increases. The results of the second work showed that our case study can be optimized in terms of computational time by reducing the number of realizations from 10 000 to 1000 with minimal influences of statistical uncertainty. Nonetheless, it was found significant differences (attributed to computational simplifications) when PSSA is performed with fixed slip surfaces compared to the results using iteration-specific slip surface generation. It was observed that the former significantly overestimated the design stability. The work also demonstrated that the introduction of additional scenarios (meaning an increase in

epistemic uncertainty), leads to higher coefficients of variation and thus an elevated probability of failure. These results can be the defining factor between designs deemed acceptable or not, as per the RBDAC criteria.

Based on these outcomes, it is suggested that practitioners consider, depending on the necessity of the design, the integration of other sources of uncertainty in the assessment of open pit slopes, beyond the consideration of parameter uncertainty alone. This will ensure a more precise and consistent interpretation of the design, enabling well-informed decisions on open pit design. This also is facilitated in a practicable manner by utilizing the RBDAC matrix proposed by Macciotta et al. (2020), where uncertainty is evaluated in a transparent manner.

Preface

Chapters 3 and 4 of this thesis have been submitted for publication, with details outlined below:

Chapter 3 was submitted to the CIM Journal in June 2023 under the title “Rock mass strength variability for probabilistic open pit slope stability analyses”. I am the author, while my supervisor is the co-author. My contributions encompassed conceptualization, data analysis, data interpretation, discussion, and composition. Dr. Macciotta provided supervision, guidance, critical review, commentary, and editing of the work.

Chapter 4 was submitted to the Geotechnical and Geological Engineering Journal in October 2023, titled “Testing the application of reliability-based design acceptance criteria for open pit slopes”. Similarly, I am the author, and my supervisor is the co-author. I undertook all data analysis, data interpretation, discussion, and composition. Dr. Macciotta initiated the conceptual framework for this work. As with Chapter 3, he contributed through supervision, guidance, critical review, commentary, and editing of the work.

Acknowledgment

I would like to express my sincere gratitude to my supervisor, Dr. Renato Macciotta, for his consistent support, valuable guidance, and the knowledge he shared during the development of this research. His profound insights were invaluable in the completion of this work. I am also grateful for the meaningful discussions and the constructive feedback he generously provided to enhance this study. I am deeply indebted to him for granting me this research opportunity at the University of Alberta.

I would also like to extend my thanks to Ashley Creighton from Rio Tinto and Phil de Graaf from De Beers Group for their valuable insight gained from the review of this research. Their comments are greatly appreciated.

My gratitude for the SoutherhPeru/ProUNI 2021 scholarship and the Graduate Recruitment 2022 Scholarship that I received at the National University of Engineering in Lima, Peru, and at the University of Alberta respectively. Their financial support was instrumental in making this research journey possible.

My appreciation extends to the University of Alberta and the professors who shared their knowledge in the various courses of the program. Their teachings have played a pivotal role in my professional growth. I am also grateful for the new friends I made during my time at the university and the wonderful moments we shared. I'd like to offer a special thanks to my office mate, Gustavo, for the numerous discussions on the technical aspects of this research, which were immensely helpful in understanding the concepts behind this work.

I extend my deepest gratitude to my family for their unwavering love and belief in me. Finally, I am profoundly grateful to my wife for being with me in Edmonton throughout this new challenge. Her support over the last two years has been instrumental in reaching this point in my life.

Table of Contents

List of Tables

List of Figures

List of Abbreviations

DAC	Design Acceptance Criteria
DSSA	Deterministic Slope Stability Analysis
CDF	Cumulative Density Function
COV	Coefficient of Variation
COV_C	Coefficient of Variation of cohesion
COV_{FoS}	Coefficient of Variation of FoS
COV_{GSI}	Coefficient of Variation of GSI
COV_{mi}	Coefficient of Variation of Constant Parameter m_i
COV_{UCS}	Coefficient of Variation of UCS
COV_{φ}	Coefficient of Variation of friction angle
FDA	Finite Difference Analyses
FEA	Finite Element Analyses
FoS	Factor of Safety
GDP	Gross Domestic Product
GSI	Geological Strength Index
HCC2002	Equivalent Mohr-Coulomb Parameters Estimated using Hoek et al. (2002)
LEA	Limit Equilibrium Analyses
MAC	Mining Association of Canada
PDF	Probability Density Function
PoF	Probability of Failure
PSSA	Probabilistic Slope Stability Analysis
RBD	Reliability-Based Design
RBDAC	Reliability-Based Design Acceptance Criteria (RBDAC)
RM2019	Equivalent Mohr-Coulomb Parameters Estimated using Rafiei and Martin (2019)
TARPS	Triger Action and Response Plans
UCS	Uniaxial Compression Strength
θ	Spatial Correlation Length

σ_{ci}	Unconfined Compressive Strength
σ_{cm}	Rock Mass Strength
σ_{3max}	Upper Limit of Confining Stress
σ_1	Major Principal Stress
σ_3	Minor Principal Stress
δ_{12}	Pearson Correlation Coefficient (or Correlation Coefficient)
$\delta_{\sigma m}$	Correlation Coefficient between σ_{ci} and m_i
$\delta_{c\phi}$	Correlation Coefficient between cohesion and friction angle

Glossary of Key Terms

Bivariate distribution	It is related to probability distribution involving two random variables. It provides the PDF of two different values occurring together by considering a correlation parameter.
Coefficient of Variation (COV)	Ratio between the standard deviation and the mean of a set of data.
Cumulative density function (CDF)	It is a mathematical function that provides the probability that a random variable takes on a value less than or equal to a given point.
Factor of Safety (FoS)	Ratio between the geotechnical capacity of the slope and the driving forces acting on the slope.
Probability of Failure (PoF)	Probability that the FoS will be 1 or less than 1.
Probability density function (PDF)	It is a mathematical function that provides the probability that a random variable takes on a specific value or falls within a certain range.
Reliability	Uncertainty in the relation between the loads a system must carry and its ability to carry those loads. It is commonly related to the PoF.
Univariate distribution	It is related to probability distribution involving one random variable. It is commonly represented by a PDF.

1. Introduction

According to the Mining Association of Canada (MAC), the industry of mining, quarrying and oil and gas extraction has contributed in a 7.9% to the Gross Domestic Product (GDP) in 2021 (MAC, 2023). It ranks as the third industry with the highest GDP share, following manufacturing and real estate and rental and leasing. Every province in Canada is home to mining operations, as shown in Figure 1. These mining activities encompass the extraction of metals, non-metals and coal, with a significant presence of coal mining in British Columbia and Alberta.

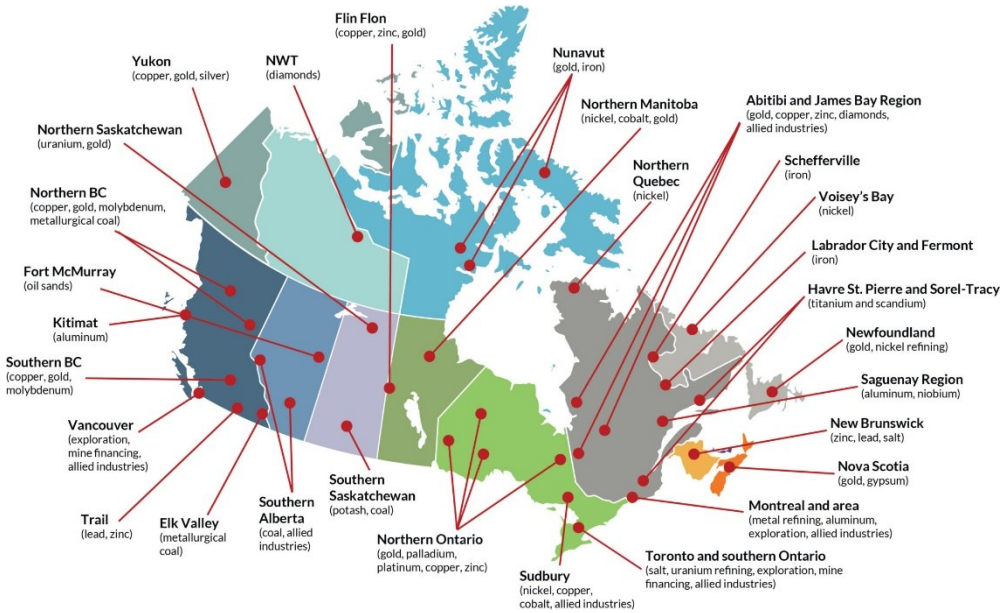

Figure 1: Mines in Canada (MAC, 2023)

Furthermore, the extraction of these materials involves the utilization of either open pit or underground mines. As indicated by the MAC (2023) and the mining operation data from 2021, approximately 122 out of 200 mine sites, accounting for around 60% of mining activities in Canada, rely on open pit mining. Moreover, open pit mining is responsible for

over 80% of mining operations in Nova Scotia, New Brunswick, Alberta, and British Columbia.

From the information provided above, it can be inferred that open pit mining is a prevalent method employed in Canada, indicating its reliability and efficiency in material extraction. Consequently, the geotechnical design of these mining structures is considered robust, yet it continues to evolve. Furthermore, the ongoing evolution of geotechnical design in open pit mining can be attributed, in part, to the gradual acceptance of reliability-based design (RBD) within the geotechnical community, as highlighted by Phoon and Kulhawy (1999a). Also, RBD incorporates probabilistic slope stability analysis (PSSA) as a crucial component, which is progressively being adopted in open pit slope design. Thus, the growing acceptance of RBD and PSSA has contributed to the continuous refinement and robustness of geotechnical design practices in open pit mining operations.

Macciotta et al. (2020) stated that there is an ongoing need to incorporate design acceptance criteria (DAC) which takes into account both the uncertainty (in terms of design reliability) and the risk tolerance of the business. In their research, they proposed DAC considering these two factors building upon previous DAC proposed by Wesseloo and Read (2009) in the Guidelines for Open Pit Slope Desing. The proposed DAC emphasizes the need for understanding uncertainty involved in the open pit mining design and how it can influence in the application of reliability-based DAC (RBDAC).

Some of these uncertainties are related to (1) understanding of rock mass strength variability, which is the first input in the evaluation of PSSA and (2) other but common uncertainties which are not usually accounted for PSSA. Apart from these uncertainties

there is a need to demonstrate the applicability of the proposed RBDAC by evaluating the flexibility of the suggested RBDAC matrix in terms of design reliability and the risk tolerance of the business. This flexibility can be evaluated considering a case study and analyzing the following (1) results of PSSA in terms of Factor of Safety (FoS), Probability of Failure (PoF) and the resulting coefficient of variation of the FoS from PSSA (COV_{FoS}) for different reliability levels of design and its location in the RBDAC matrix, (2) comparison of the statistical distribution of FoS obtained in the PSSA with the statistical distributions adopted to build the RBDAC matrix in Macciotta et al. (2020).

1.1 Problem statement

DAC for open pit slope design aims at targeting tolerable levels of economic risk for the operation (it is assumed safety risks are controlled by monitoring and emergency responses). DAC that only considers FoS/PoF and potential consequences, will not be targeting a similar level of risk if the knowledge available for the analysis is not consistent. Adopting RBDAC that considers the level of knowledge (reliability) in the designs is a means to resolve this in a practicable manner, however, a robust understanding of the effect of different sources of geotechnical uncertainty (particularly Epistemic uncertainty) is required to evaluate the applicability of RBDAC to open pit slope design.

1.2 Objectives of this thesis

- Quantify and address uncertainties related to rock mass strength variability in the evaluation of PSSA, considering common failure criteria such as Hoek-Brown and the equivalent Mohr-Coulomb parameters. Identify uncertainties associated with these simplifications on parameter variability in PSSA.

- Identify and address uncertainties that are acknowledged by practitioners but not typically quantified in PSSA and analyze their impact when adopting the RBDAC framework.
- Demonstrate the applicability of the proposed RBDAC developed by Macciotta et al. (2020) by evaluating its flexibility in terms of design reliability and business risk tolerance, using an ideal case study based on a real scenario.
- Evaluate the statistical distributions of FoS obtained in PSSA and compare them with the distributions adopted for the development of the proposed RBDAC developed by Macciotta et al. (2020).

1.3 Methodology

To accomplish these objectives, the following methodology was employed:

- Review of current practice for the design of open pit slopes, publications of probabilistic open pit slope stability analysis, rock mass strength variability, and current practices of using DAC for open pit slopes.
- Parametric study of rock mass strength variability in terms of Hoek-Brown and Mohr-Coulomb for understanding the impact of strength variability for different failure criteria. Estimation of the differences and consequences of considering one failure criterion over the other.
- Parametric study through different levels of reliability in an open pit slope as part of making informed decisions regarding the adoption of RBDAC, as well as assessing the validity of the assumptions behind RBDAC.

1.4 Thesis outline

The content of the subsequent chapters, following the previous introduction, is summarized as follows:

- Chapter 2 presents a brief literature review of the different topics to be discussed. It first introduces the concept of uncertainty in the geotechnical field, moving later to uncertainty in open pit designs. Other information about rock mass strength variability, PSSA, and DAC for open pits are briefly discussed. The information is complemented with literature review presented in first and second journal paper which are presented in Chapters 3 and 4, respectively.
- Chapter 3 focuses on a parametric study of rock mass strength variability considering the failure criteria of Hoek-Brown and equivalent Mohr-Coulomb. The parametric study is performed in a modified open pit inspired by the characteristics of an implement pit slope located in British Columbia. The analyses are carried out in Slide2 (Rocscience Inc 2023) which accounts for the method of limit equilibrium in probabilistic analysis using Monte Carlo simulations. For the study, univariate and bivariate distributions are analyzed. The goal in this manuscript is to observe the difference of results in PSSA when Hoek-Brown and equivalent Mohr-Coulomb are used in the parametric study, and present recommendations for obtaining consistent results in terms of FoS, PoF and COV_{FoS} when one failure criteria is considered over the other.
- Chapter 4 examines the suitability of the proposed RBDAC by Macciotta et al. (2020) through a parametric study in the modified open pit slope mentioned previously. The study analyzes different reliability levels of the open pit slope

created by combining multiple scenarios which have different levels of uncertainties (depending on the reliability level). Different types of uncertainties are studied inspired by the geotechnical, geological, and hydrological characteristics of the implemented pit-slope. Also, other uncertainties are studied primarily pertaining to computational simplifications and spatial variability. The results from the different scenarios created will be shown in the proposed RBDAC matrix to study its flexibility in terms of the design reliability, and therefore to the level of uncertainty, considered for the open pit slope.

- Chapter 5 comprises the conclusion and recommendations for future work, aiming to supplement and enhance the findings presented in this study.

2. Literature Review

2.1 Design Acceptance Criteria (DAC) for Open Pit

This section is complemented with the summaries in Chapter 4. PSSA is used to quantify uncertainty in slope stability analysis. Also, it is the combination of probability and the consequence of the failure that determines the risk of the structure (Baecher and Christian, 2006). Therefore, the basis behind DAC for probabilistic analysis is to assess and control this risk. DAC for probabilistic analysis has been proposed since the mid-1970s (Phoon and Kulhawy, 1999a), being close in time to the early works in PSSA.

For the design of open pits, various DAC have been proposed for evaluating the adequacy of design through PSSA. One of the early DAC, presented in Table 1, was introduced by Priest and Brown (1983). Subsequent works by different authors, such as Swan and Sepulveda (2000), Wesseloo and Read (2009) in the Guidelines for Open Pit Slope Design, Adams (2015), Gaida et al. (2021), and Macciotta et al. (2020), have further contributed to this field. The latter is a quantitative RBDAC and evaluates design reliability by analyzing the resulting coefficient of variation (COV) of the FoS obtained from PSSA (COV_{FoS}). The method was built upon the previous DAC proposed by Wesseloo and Read (2009) and following previous case studies conducted on earth and tailing dams by Meyerhof (1970), Lambe (1985), and Silva et al. (2008).

A matrix presenting the recommended values of FoS and PoF for different categories of the economic consequence of failure as well as design reliability is illustrated in Figure 35 (see Chapter 4). Also, a similar matrix where the pairs of FoS and PoF are combined with COV_{FoS} is presented in Figure 2. These ranges align with previous reports by Meyerhof

(1970) and Lambe (1985) for earth and tailing dams, indicating different levels of engineering. The best design practices correspond to COV_{FoS} values lower than 0.07 and the poor design practices correspond to COV_{FoS} values higher than 0.3. Therefore, the variation in COV_{FoS} can be attributed to the current reliability level, and consequently, the level of epistemic uncertainty.

Table 1: DAC proposed by Priest and Brown (1983)

Category of slope	Types of Geo-hazards		Acceptable values		
	Consequences of failure	Examples	Minimum PoF for FoS<1	Maxima PoF for FoS<1	PoF for FoS<1.5
1	Not serious	Individual benches, small* temporary slopes not adjacent to haulage roads.	1.3	0.1	0.2
2	Moderately serious	Any slopes of a permanent or semi-permanent nature.	1.6	0.01	0.1
3	Very serious	Medium-size and high slopes carrying major haulage roads or underlying permanent mine installations.	2.0	0.003	0.05

*Small, height < 50 m; medium, height 50-150 m; high, height > 150 m.

The RBDAC is proposed for inter-ramp and overall slopes, and it is not applicable for bench slopes. The distinctions between these slopes, which describe the geometric arrangement in open pit slopes and are illustrated in Figure 3, are presented below:

- Bench slope: refers to the slope between toe and crest of each bench. Open pits are often designed with multiple benches to facilitate efficient mining operations and provide stable working surfaces.

- Inter-ramp slope: refers to the slope that occurs between two adjacent ramps or haul roads and it is measured for the line connecting the bench toes in that area.
- Overall Slope: refers to the slope that is that measured from the toe of the slope to the pit crest. The slope is measured across the entire vertical extent of the open pit, reflecting the overall angle from the bottom to the crest.

Design reliability	COV_{FoS} (For reference)		Economic Consequence Category				
			Very low	Low	Moderate	High	Very high
Very low	COVFoS>0.30	FoS	1.40 →	1.70	≥ 1.70 (≥ *2.00*)	Not acceptable	Not acceptable
Low	$0.25<COV_{FoS}\leq0.30$	PoF FoS	20% → 1.35		5% 1.70 (*2.00*)	≤ 5% ≥ 1.70 (*2.00*)	Not acceptable
Moderate	$0.20<COV_{FoS}\leq0.25$	PoF FoS	25% → 1.25		10% → 1.40 (*1.50*)	→	≤ 5% ≥ 1.55 (*1.70*)
High	$0.10<COV_{FoS}\leq0.20$	PoF FoS	30% → 1.15		15% → 1.25	→	5% ≥ 1.40 (*1.50*)
Very high	$COV_{FoS}\leq0.10$	PoF FoS	≤ 30% → ≥ 1.10		20% → 1.15	→	10% ≥ 1.20

Figure 2: Proposed RBDAC for open pits slopes with COV (Macciotta et al, 2020, with permission)

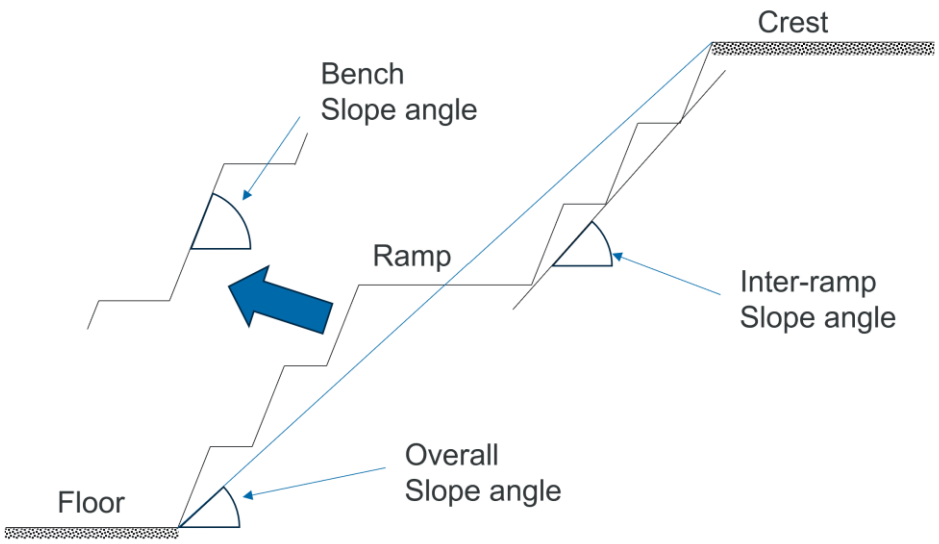

Figure 3: Open pit slope terminology

2.2 Uncertainty in geotechnical engineering

Uncertainty is universal, it has been widely recognized in different fields of Engineering. In geotechnical engineering, early approaches to control uncertainty were established by the application of the observational method from Peck (1969) - as stated by Christian et al. (1994). Also, there has been many definitions and taxonomies to describe uncertainty. Guo and Du (2007) and Huan et al. (2018) stated that the most common taxonomy categorized uncertainty in two different aspects: aleatory uncertainty and epistemic uncertainty. This combination in uncertainty is described by Guo and Du (2007) as the difference between present state of knowledge and the complete knowledge, as shown in Figure 4. Epistemic uncertainty arises from a lack of knowledge, higher epistemic uncertainty leads to the complete ignorance of the aleatory (inherent) uncertainty within the system, as both types of uncertainty coexist simultaneously. Nonetheless, epistemic uncertainty is reducible, meaning that as more data is collected the level of uncertainty is reduced until aleatory uncertainty is left. On the other hand, aleatory uncertainty is referred to the inherent variability of the system. It is irreducible, meaning that as more data is obtained in the system the variability is constant.

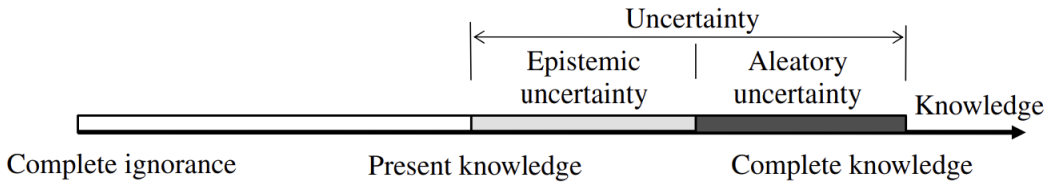

Figure 4: Uncertainty types (Guo and Du, 2007, with permission)

The extend of epistemic uncertainty within the field of mining geotechnical engineering can be represented by the progression of a project from its conceptual stage to the operational stage. Macciotta et al. (2020) have presented this progression in terms of

design confidence (also referred to design reliability) and COV, illustrated in Figure 5. During the initial stages of design, high uncertainty is associated with low design reliability and a high COV. However, as the project advances, uncertainty levels decrease, resulting in higher design reliability and a lower COV. This reduction is achieved by augmenting the available data through field geotechnical investigations and instrumentation data.

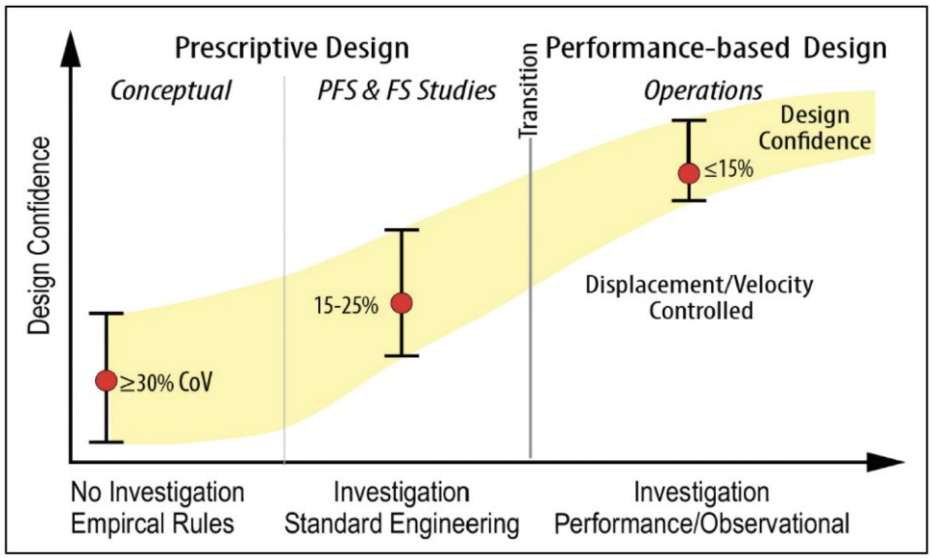

Figure 5: Design confidence and uncertainty for life-of-mine stages (Macciotta et al., 2020, with permission)

2.3 Uncertainties in open pit slope design

Considering uncertainty in the geotechnical design is an intricate undertaking, Phoon and Kulhawy (1999a) emphasized the importance of comprehending three key sources of uncertainties – soil variability, measurement error, and transformation uncertainty – for designing with soil parameters. In a subsequent study, Phoon and Kulhawy (1999b) quantified soil variability in terms of COV and for different soil parameters. Prakoso (2002) conducted a similar work to estimate COV for various rock mass properties. Subsequent investigations by Doruk (1991), Rafiei et al. (2019) and Pozo (2022), among others, have

also focused on estimating variability in rock mass parameters. Chapter 3 provides a review of these studies.

While considerable progress has been achieved in estimating uncertainty associated with rock mass parameters, it is important to acknowledge that open pit design is subject to various other types of uncertainties. Furthermore, as noted by Huan et al. (2018), it is important to recognize that there may exist other types of uncertainties that extend beyond the taxonomy of defining uncertainty in terms of aleatory and epistemic uncertainty. Moreover, the studies mentioned in the preceding paragraphs focused on uncertainty pertaining to variability in material properties.

Different taxonomy to define other type of uncertainty have been presented by Wesseloo and Read (2009), Adams, (2015), Macciotta et al. (2020), and Gaida et al. (2021). Adams (2015) identified six common sources of uncertainty that play a role in this context, namely (1) parameter uncertainty, (2) geometrical uncertainty, (3) temporal uncertainty, (4) slope behavior uncertainty, (5) computational uncertainty, and (6) human uncertainty. A description of each of these sources of uncertainty are provided in Figure 6.

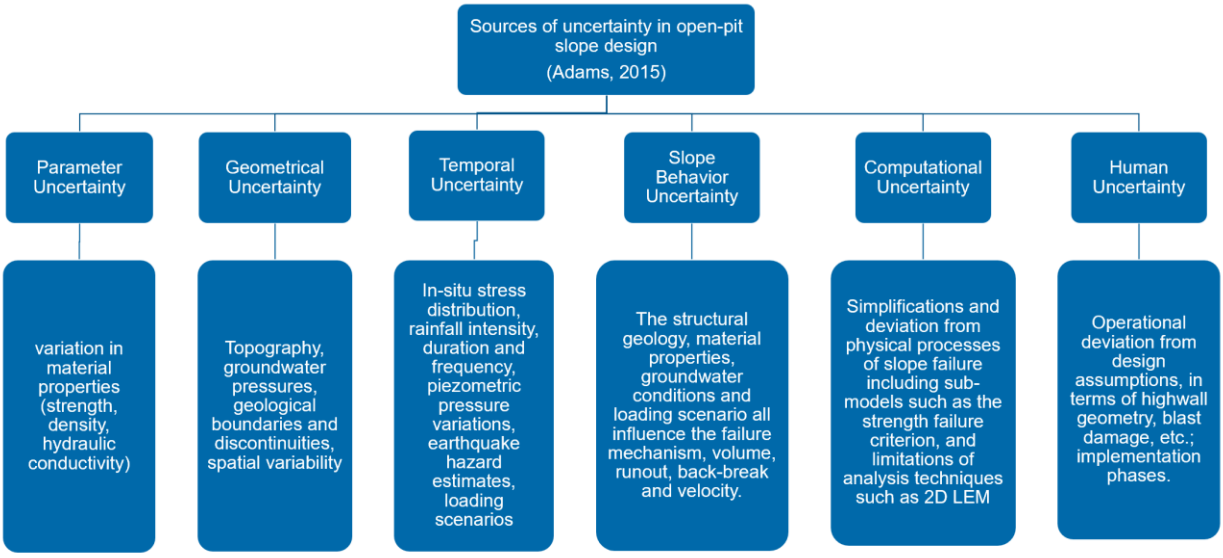

Figure 6: Sources of uncertainty in open pit slope design (after Adams, 2015)

These uncertainties highlight that while parameter uncertainty accounts for soil or rock variability, there are additional factors to consider. Geometrical uncertainty, for instance, encompasses spatial variability and changes in geological structures or loading uncertainty for hydrological characterization when utilizing a piezometric elevation in stability analyses. Computational uncertainty arises from simplifications made in the software used for performing PSSA, as well as the failure criterion employed.

This prompts the question of what emerges when other sources of uncertainty (apart from parameter uncertainty) are taken into account in PSSA and evaluated within the RBDAC. According to Adams (2015) PSSA may not capture all the uncertainty involved in slope design. Consequently, the computed PoF obtained through PSSA is expected to be lower than the global PoF. However, in cases of high or very high design reliability, particularly for operating conditions, the global PoF is considered to be close to the computed PoF.

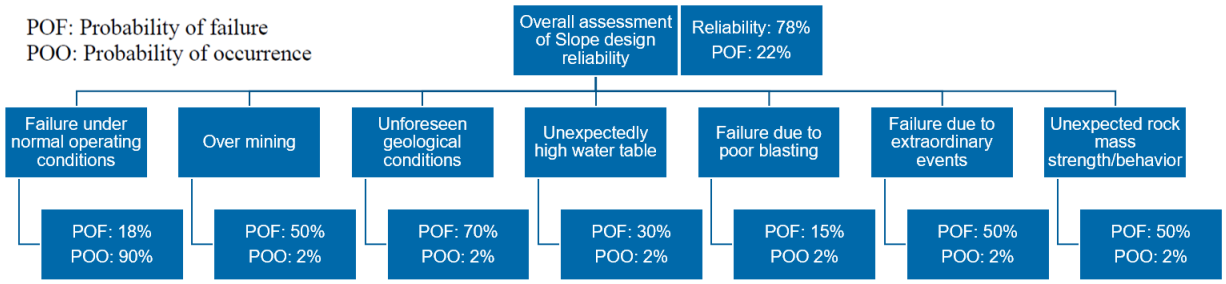

Figure 7: Fault tree analysis for slope failure (after Steffen et al., 2006)

This can be explained by the analysis conducted by Steffen et al. (2006) in an even tree analysis, as shown in Figure 7. The figure illustrates that 90% of the PoF is under normal operating conditions when appropriate slope behavior and numerical model are utilized. However, it is also expected to be a different condition for lower reliability levels in the design. In that case, epistemic uncertainty is high, and it can be related to increased uncertainty in strength, geometry, behavior, and uncertainty in the type of computational performance as well as human error. Consequently, the computed PoF under these conditions is expected to drop below 90% of the global PoF, emphasizing the need to account for other failure scenarios.

2.4 Rock Strength Variability (RSV)

RSV is discussed in Chapters 3 and 4, as part of the literature review presented in the respective manuscripts. A summary with examples is only presented below to complement the information related to parameter variability, parameter correlation and spatial variability.

2.4.1 Parameter variability

Parameter variability refers to the variation of any parameter used to describe the strength, permeability or deformation behavior of intact rock, the rock mass, and

discontinuities. It can be described using univariate distributions. An example using Unconfined Compressive Strength (σ_{ci}) as a single strength parameter in the Hoek-Brown failure criterion and following a lognormal distribution is presented in Figure 8. The mean σ_{ci} is equal to 70 MPa with a COV equal to 0.40 as indicated in the figure.

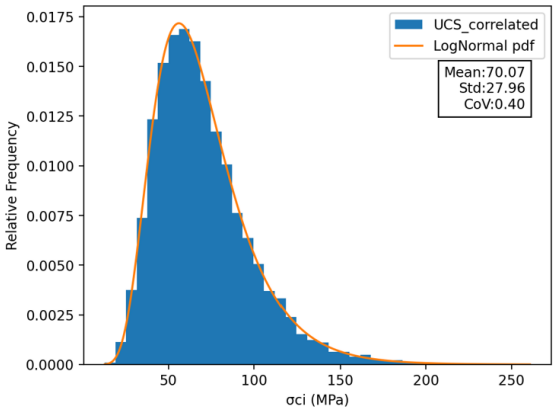

Figure 8: Example of σ_{ci} as random variable

2.4.2 Parameter Correlation (Correlation Coefficient)

Additional strength parameters can also be modelled as univariate distributions in either the Hoek-Brown failure criterion or in the equivalent Mohr-Coulomb (in terms of cohesion and friction angle). Yet, solely relying on these univariate distributions might disregard the interdependencies between parameters. To address these dependencies, bivariate or multivariate distributions are necessary (Phoon and Ching, 2015). A bivariate distribution is defined as two pairs of data that are correlated using the Pearson correlation coefficient (δ_{12}), also referred to as the cross-correlation coefficient (Javankhoshdel and Bathurst, 2016, Javankhoshdel et al. 2016). An example of a bivariate distribution is presented in Figure 9 between σ_{ci} and the rock material constant m_i with a correlation coefficient set at -0.9. On the left, it is shown a lognormal distribution of m_i and on the right the correlation between σ_{ci} and m_i. The distribution for σ_{ci} is that previously presented in Figure 8.

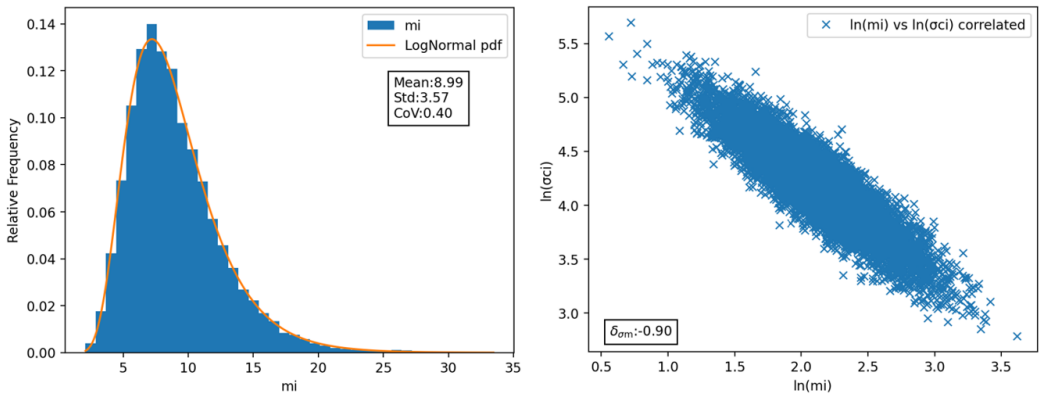

Figure 9: Example of a bivariate distribution between σ_{ci} and m_i

Chapter 3 provides more details about results in terms of univariate and bivariate distribution using Hoek-Brown and equivalent Mohr-Coulomb and the influence that correlation coefficient has in PSSA.

2.4.3 Spatial Variability

Spatial variability of strength can be modelled through random field generation techniques. A parameter called the spatial correlation length (θ) is used to determine how similar the strength parameters are between samples in different locations. The distribution of any strength parameter in space is determined using a spatial correlation function. The most commonly used function is the Markovian function, which is expressed as:

$$\rho = \exp\left(-2\,{}^{d}/_{\theta}\right) \qquad [1]$$

Where ρ represents the correlation of a strength parameter between two locations at a distance d. The function rapidly decreases when the radio d/θ exceeds 2. In such cases, the strength parameters are considered independent throughout the space.

An example of a 150 m open pit height for one realization (of many) and considering two spatial correlation lengths of 5 m and 10 m is illustrated in Figure 10. The profile was generated using Slide2 (Rocscience Inc 2023) and incorporates a single strength parameter following a lognormal distribution with COV of 0.4. In the figure, the dark elements represent strength parameters associated with a weaker strength, while the lighter elements represent strength parameters associated with a stronger strength. These examples clearly demonstrate that, when compared to the height of the open pit, the spatial variability of strength can have a significant impact on the results of PSSA.

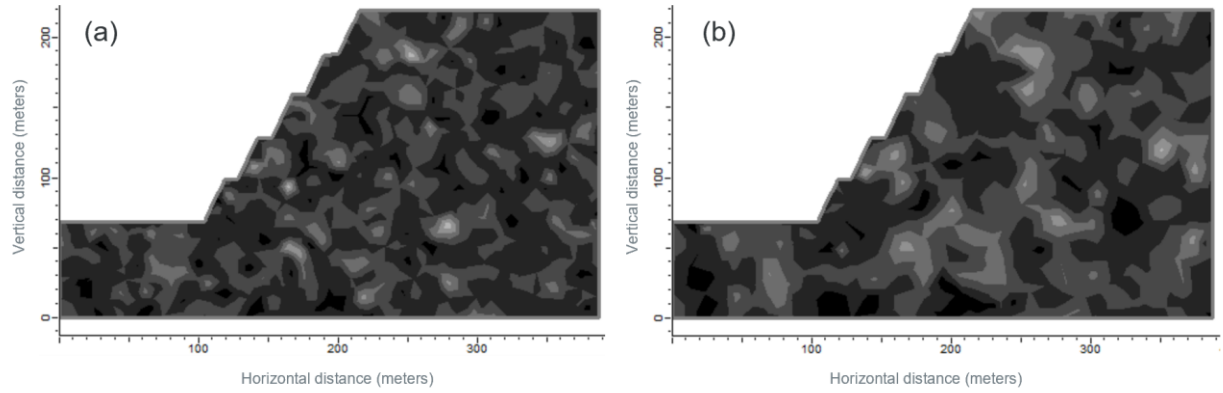

Figure 10: Example of strength spatial variability in a 150 m height open pit for θ equal to (a) 5 m and (b) 10 m.

2.5 Probabilistic Slope Stability Analysis (PSSA)

Early works in PSSA, as noted by Christian et al. (1994) and Rafiei et al. (2019), date back to the 1970s and include contributions from Alonso (1976), Tang et al. (1976), Harr (1977), Vanmarcke (1977), among others. PSSA allows the evaluation of the mean FoS, PoF, and understanding the reliability of calculations of stability analysis through the resulting COV_{FoS}. Therefore, probability in slope stability analysis is performed to quantify uncertainty, which is not possible in deterministic slope stability analysis (DSSA). DSSA

usually accounts for uncertainty by providing a conservative threshold FoS above 1. Nevertheless, this threshold FoS is without any relation to the level of uncertainty involved in the design.

To carry out a PSSA, strength parameters are treated as random variables with specific probability distributions. Analyses are generated based on these considerations, using methods such as Limit Equilibrium Analyses (LEA), Finite Element Analyses (FEA), or Finite Difference Analyses (FDA), and the statistical distribution of the output is calculated using Monte Carlo simulations (computationally adequate for LEA) or other statistical techniques such as Point Estimate Method or First Order Second Moment method which are more computationally compatible for FEA and FDA (Baecher and Cristian, 2003).

Point Estimate Method and First Order Second Method typically involve assuming the statistical distribution of the FoS results, often a normal distribution as indicated by Baecher and Cristian (2003), to estimate PoF based on the mean and standard deviation obtained in the analysis. However, Monte Carlo simulation does not require any assumption about the statistical distribution. Instead, it utilizes the actual realizations from the slope stability analysis to obtain the distribution and therefore the mean, standard deviation, and consequently, the PoF. By increasing the number of simulations in this method, the results become more accurate, leading to smoother curves in either the probability density function (PDF) or the cumulative density function (CDF). A comparison of a PDF related to the output values of FoS from PSSA, using Monte Carlo simulation, between 1000 and 10 000 realizations is presented in Figure 11. Although there are similar results in FoS, PoF and COV_{FoS}, it is observed clear differences in the distribution of the data. Furthermore, it is worth nothing that the lognormal distribution exhibits a better

fit in the data in comparison to the normal distribution, which is commonly assumed in the other two methods previously indicated.

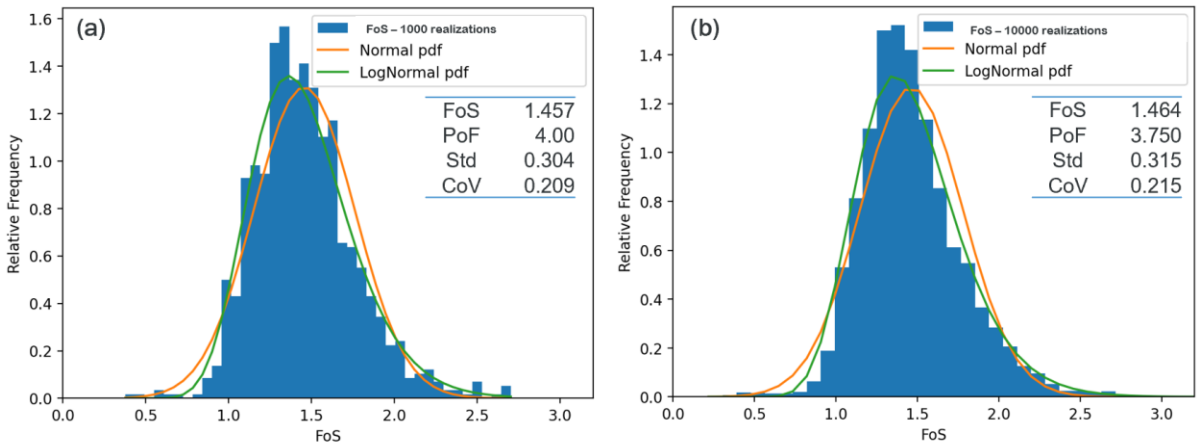

Figure 11: Example of results from PSSA for (7a) 1000 realizations and (7b) 10 000 realizations

Publications related to probability analyses in slope stability are reported in Macciotta et al. (2020) and Rafiei et al. (2019). Also, some publications with examples applications of PSSA for open pit and rock slope design are reported in Chapter 3. These works have highlighted the different considerations taken when defining the variability of the rock mass in terms of parameter variability and parameter correlation, as indicated in the previous section 2.4.

3. Rock Mass Strength Variability for Probabilistic Open Pit Slope Stability Analyses

This chapter was submitted for publication under the title *Rock Mass Strength Variability for Probabilistic Open Pit Slope Stability Analyses* in the CIM Journal on June 21st, 2023.

3.1 Introduction

Reliability-based design (RBD) has been adopted for different geotechnical structures. Part of RBD is the use of probabilistic slope stability analysis (PSSA), which is increasingly being used for open pit slope design. PSSA allows the evaluation of the mean Factor of Safety (FoS) and Probability of Failure (PoF) against design criteria, and understanding the reliability of calculations through the resulting Coefficient of Variation of FoS (COV_{FoS}). Lately, reliability-based design acceptance criteria (RBDAC) have been proposed for open pit slopes (Macciotta et al. 2020). This approach allows pit optimization on the basis of increased design reliability, qualified by the effort in engineering design and supported by the relationships between FoS and PoF from PSSA. One aspect of consideration in RBDAC is that the design of open pits through PSSA requires understanding the rock mass strength variability, where resulting FoS, PoF and COV_{FoS} depend on the strategies used to model rock strength. Understanding the impact of strength variability approaches becomes important for informed adoption of RBDAC, and the validity of assumptions behind RBDAC.

To carry out a PSSA, strength parameters are treated as random variables with specific probability distributions. Analyses are generated based on these, using methods such as Limit Equilibrium Analyses (LEA), Finite Element Analyses (FEA), or Finite Difference

Analyses (FDA), and the statistical distribution of the output is calculated using Monte Carlo simulations (computationally adequate for LEA) or other statistical techniques such as Point Estimate Methods or First Order Second Moment methods which are more computationally compatible for FEA and FDA (Baecher and Cristian, 2003). Finally, the results are compared to design acceptance criteria such as those proposed in the Guidelines for Open Pit Slope Design (Wesseloo and Read, 2009) or the RBDAC by Macciotta et al. (2020), in terms of FoS and PoF. Geotechnical strength parameter variability is a key consideration for undertaking these analyses. The mean value and standard deviation (or Coefficient of Variation - COV) are usually required to describe a random variable. One or more parameters can be considered random variables in PSSA, which requires an understanding if those parameters are correlated, for example following bivariate distributions of two random strength variables.

Publications with example applications of PSSA for open pit and rock slope design keep increasing, with different design criteria being adopted. Previous work by Chiwaye and Stacey (2010), Sina et al. (2018), Rafiei et al. (2019), Abdulai and Sharifzadeh (2021), and others; highlight some important considerations: (1) Mohr-Coulomb strength parameters are commonly used, and is attributed to the familiarity of the users with cohesion and friction and the increased functionality of software tools for PSSA as opposed to Hoek-Brown strength models, (2) The use of Hoek-Brown models consider univariate distributions neglecting parameter correlation (bivariate distribution) between the Hoek-Brown strength parameters (3) Monte Carlo simulations and univariate distributions are used to transform rock strength variability from the Hoek-Brown failure criterion to the Mohr-Coulomb failure criterion. Two relationships have been proposed to

estimate the equivalent Mohr-Coulomb strength parameters from Hoek-Brown, each having different implications for PSSA; and (4) input parameter correlation between equivalent cohesion and friction angle used for rocks typically follows that used in soils.

This paper aims to explore rock mass strength variability, considering the effects of bivariate random variables and the selection of approaches to calculate equivalent Mohr-Coulomb strength parameters for use in PSSA. The work starts with a review of COV values reported in the literature for rock strength parameters, followed by a case study in an open pit to estimate the rock strength variability in terms of respectively the Hoek-Brown failure criterion and equivalent Mohr-Coulomb failure parameters, the latter using the relationships provided by Hoek et al. (2002) and Rafiei and Martin (2019) and following the criteria presented by Rafiei et al. (2019). The study considers univariate distributions for the variability in Unconfined Compressive Strength (σ_{ci}) and the rock material constant m_i, as well as a more realistic scenario of bivariate distributions. The paper also analyzes the trends observed in the variability of the equivalent Mohr-Coulomb parameters from these distributions, including an inherent correlation between cohesion and friction angle due to the expressions used to estimate the equivalent Mohr-Coulomb parameters. The influence of GSI and the confining stress on this correlation is also examined for completeness, such that the key inputs in slope stability analyses are evaluated.

3.2 Rock Strength variability (RSV) and equivalent Mohr-Coulomb parameters

3.2.1 COV for material parameters

Different COV values have been reported in the literature for soils and rocks. Phoon and Kulhawy (1999) reported COV values for soils classified as sands and clays in relation to the effective friction angle and undrained shear strength (s_u). Figure 12a shows the variation of COV for the effective friction angle. It is seen that the COV for clays is higher than for sands. It is also observed that while the friction angle increases, the COV decreases as these appear to be inversely correlated. Figure 12b shows the variation of COV for the s_u reported on clays. Similarly, it is observed that the COV decreases as the mean value of s_u increases. These results are typical of soils. This implies that strength is inversely correlated to COV, at least for some materials reported in literature.

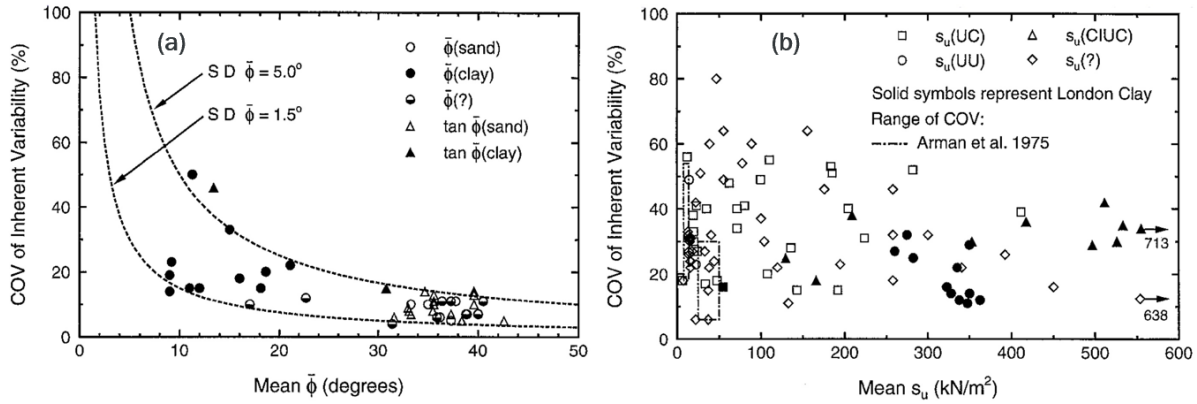

Figure 12: (a) COV of the effective friction angle (φ) for sands and clay. (b) COV for undrained shear strength (s_u) in clays (Phoon and Kulhawy 1999, with permission).

Prakoso (2002) presented guidelines for estimating the COV of different rock properties. In relation to the Uniaxial Compression Strength (UCS), he reported COV of UCS (referred to as COV_{UCS}) values between 0.008 and 0.61 related to unweathered rocks. Clastic and chemical sedimentary rocks dominated the database. Figure 13 shows the

mean UCS value for every data group analyzed. It is observed that only one group for clastic sedimentary rock and metamorphic non-foliated rock has a COV_{UCS} value close to 0.6, while the majority of the data is below 0.4.

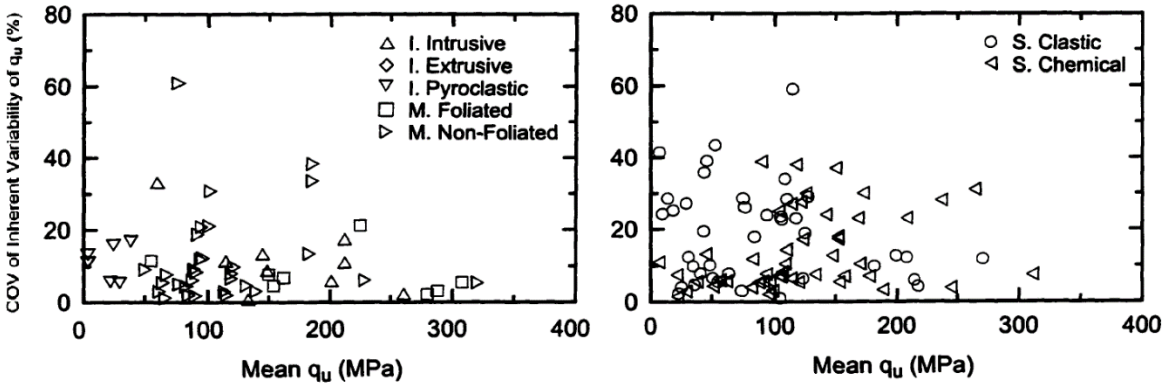

Figure 13: COV_{UCS} versus Mean UCS (Prakoso, 2002, with permission). Note Prakoso (2002) refer to UCS as q_u.

Phoon et al. (2016) also reported the mean COV_{UCS} for the same group of data presented by Prakoso (2002). The trend is presented in Figure 14a. Higher values of COV_{UCS} were reported by Rafiei et al. (2019) for the case of highly heterogeneous porphyry deposits. They compared these values with other rock types, and as shown in Figure 14b the values of COV_{UCS} were in the range of 0.1 for massive rocks (Lac du Bonnet granite) to almost 1 for the altered (or weathered) rocks. The data also shows the COV_{UCS} for sedimentary rocks being as high as 0.4.

Doruk (1991) presented COV values of the Hoek-Brown parameter m_i (referred to as COV_{mi}) for different rock types (Table 2). It is observed that COV_{mi} in their database had different ranges depending on the rock type. The values are significantly greater than the mean COV_{UCS} reported elsewhere in the literature (Phoon et al., 2016). Also, Zhang et al. (2018) reported COV_{mi} for igneous rocks between 0.16 and 0.42. It is observed from

this data that the COV_{mi} is at least twice the COV of σ_{ci} (referred to as $COV_{\sigma ci}$) with a strong negative correlation coefficient of -0.9. In this study, we assume that UCS values are very close to σ_{ci} and can be considered equal so that the variability reported for UCS can be used to inform the expected variability in σ_{ci}.

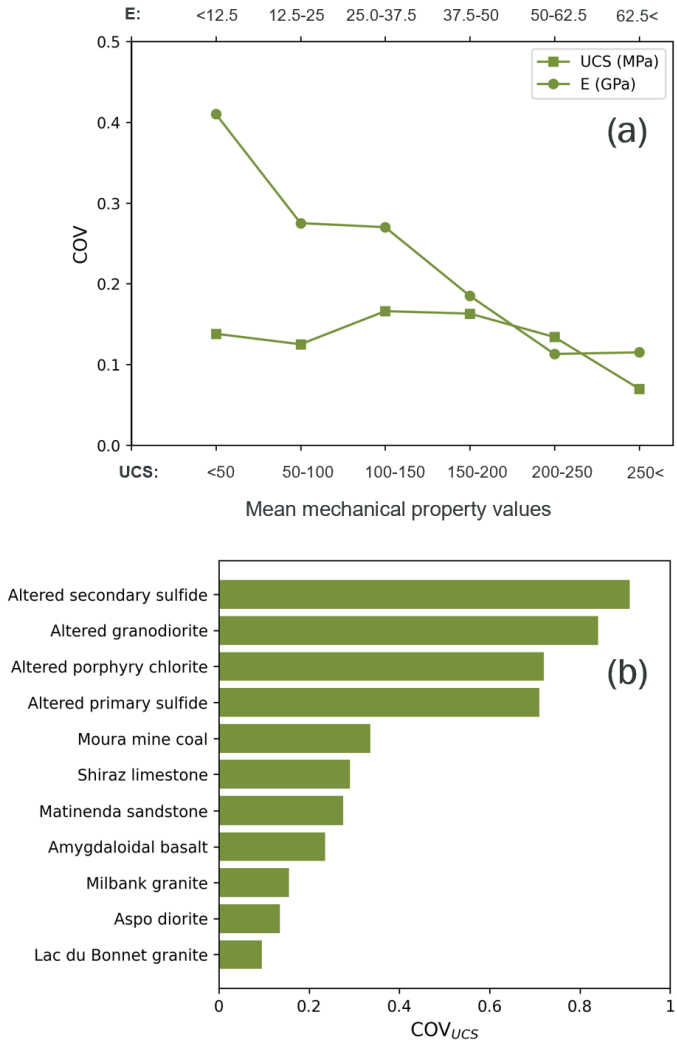

Figure 14: COV_{UCS} for rocks after (a) Phoon et al. (2016) and (b) Rafiei et al. (2019)

COV of GSI (referred to as COV_{GSI}) in the range of 0.15 to 0.22 was reported by Abdulai and Sharifzadeh (2021) for an open pit case study. Also, Prakoso (2002) mentioned that the variability of the GSI leads to an increase in the variability (COV) of the rock mass

strength between 0.2 to 0.3. Nonetheless, Pozo's (2022) research reveals that the use of quantitative methods results in a range of COV_{GSI} between 0.06 and 0.15. This range suggests that the variability of the rock mass strength, caused by variability in GSI, is lower than previously anticipated by other studies. The trend presented by Pozo (2022) using four different rock types showed that COV_{GSI} decreases as GSI increases. Others report this parameter should be considered independent as the equations presented by Hoek-Brown to estimate the rock mass strength capture the co-dependency between intact and rock mass constants (Langford and Diederichcs, 2015).

Table 2: Variability reported in the Hoek-Brown m_i parameter (Data from Doruk, 1991 and table reported by Phoon et al., 2016)

Type of rock	Number of data groups	Mean m_i	Range m_i	COV m_i
Granite	18	25.3	8 – 43	0.377
Dolerite	4	13.2	11 – 15	0.147
Granodiorite	4	26.0	16 – 35	0.314
Sandstone	57	16.0	3 – 42	0.538
Mudstone	7	19.2	9 – 47	0.758
Shale	3	14.6	3 – 29	0.919
Chalk	2	7.2	-	-
Limestone	25	9.6	4 – 26	0.473
Dolostone	8	11.4	5 – 18	0.377
Carnallitite	5	20.8	3 – 46	0.947
Amphibolite	3	27.8	24 – 33	0.167
Quartzite	6	20.4	15 – 28	0.249
Marble	14	8.1	5 – 16	0.395

Based on this information, it is possible to estimate the expected $COV_{\sigma ci}$ and COV_{mi}, as well as the correlation coefficient between these two parameters in order to estimate the rock mass strength variability using the nonlinear Hoek-Brown failure criterion (Hoek et al. 2002). The work can also be extended to estimate COV in its equivalent cohesion and friction angle from the linear Mohr-Coulomb failure criterion hereafter referred to as COV_c and COV_φ, respectively. In this study, GSI is considered a constant value due to its small variability and for purposes of only studying the results obtained from σ_{ci} and m_i. Nevertheless, it is possible to further expand the scope of this work by considering GSI as an independent random variable.

3.2.2 Hoek-Brown failure criterion for rocks and equivalent Mohr-Coulomb strength

The Hoek-Brown failure criterion (Hoek et al. 2002, Hoek and Brown 2018) is a commonly used empirical failure criterion for rocks that accounts for the nonlinear behavior observed in these materials due to the change in the microscopic failure mechanism from tensile stresses to shear stresses. It is derived from Griffith's crack theory (Griffith 1924), and is expressed as:

$$\sigma_1 = \sigma_3 + \sigma_{ci}(m_b \frac{\sigma_3}{\sigma_{ci}} + \mathrm{s})^a \quad [2]$$

Where m_b, s, and a are constants for the rock mass given by the following relationship:

$$m_\mathrm{b} = m_i \exp(\frac{GSI-100}{28-14D}) \quad [3]$$

$$s = \exp(\frac{GSI-100}{9-3D}) \quad [4]$$

$$a = \frac{1}{2} + \frac{1}{6}(e^{-GSI/15} - e^{-20/3}) \quad [5]$$

and m_i being a constant for the intact rock and D a disturbance factor that depends on the level of damage by blasting and stress relaxation. The GSI is used to represent the behavior of an isotropic rock mass in the field, from the behavior of a small-scale intact rock tested in the lab to an isotropic heavily jointed rock mass at the scale of a pit slope. The parameter m_b would be analogous to the rock mass frictional component of strength, and s is related to the rock mass cohesive component (Eberhardt, 2012).

Hoek et al. (2002) related the criterion to the linear Mohr-Coulomb as follows:

$$\phi = \sin^{-1}\left[\frac{6am_b(s+m_b\sigma_{3n})^{a-1}}{2(1+a)(2+a)+6am_b(s+m_b\sigma_{3n})^{a-1}}\right] \quad [6]$$

$$c = \frac{\sigma_{ci}[(1+2a)s+(1-a)m_b\sigma_{3n}](s+m_b\sigma_{3n})^{a-1}}{(1+a)(2+a)\sqrt{1+(6am_b(s+m_b\sigma_{3n})^{a-1})/((1+a)(2+a))}} \quad [7]$$

Where:

$$\sigma_{3n} = \sigma_{3max}/\sigma_{ci} \quad [8]$$

$$\sigma_{3max} = \sigma_{cm}0.72\left(\frac{\sigma_{cm}}{\gamma H}\right)^{-0.91} \quad [9]$$

$$\sigma_{cm} = \sigma_{ci}.\frac{(m_b+4s-a(m_b-8s))(m_b/4+s)^{a-1}}{2(1+a)(2+a)} \quad [10]$$

Conversion to equivalent parameters requires selecting a range of confining stresses representative of the geometry of analysis. This is done through selection of the upper limit of confining stress (σ_{3max}) over which the relationship between the Hoek-Brown and the equivalent Mohr-Coulomb criteria is considered. In relation to equation 9 (for slope stability problem), it can be said that σ_{3max} depends on the unit weight of the rock mass (γ), the height of the slope (H) and the rock mass strength (σ_{cm}).

Equation 9 was estimated based on circular slip surfaces and using Bishop's method for LEA. However, an updated equation was proposed by Rafiei and Martin (2019) that considers the Morgenstern-Price method (Morgenstern and Price, 1965) and non-circular slip surfaces. The proposed relationship is presented in equation 11, being independent of σ_{cm}, but controlled by the slope angle (β).

$$\sigma_{3\max} = \gamma H\left(\frac{0.175}{\tan(\beta)}\right) \quad [11]$$

It should be noted that Rafiei and Martin (2019) demonstrated that using equation 11 to estimate the equivalent cohesion and friction angle has given adequate results of FoS when it is compared with the original slip surface using Hoek-Brown in deterministic slope stability analyses.

3.3 Open pit slope case study

For the purpose of investigating the rock strength variability and the impact on its representation on PSSA for RBD of pit slopes, the researchers have opted to perform PSSA using 2D LEA to a case study inspired by the geometry and geologic context of an implemented pit slope, which provides an existing set of rock strength parameters, and complemented by assumptions on material variability informed by literature. The adoption of LEA does not capture the complexities of progressive failure in rock slopes for kinematically admissible failure modes; however, it reflects the state of practice for slope design in mining practice, where numerical techniques are deployed only to a subset of slopes and pushbacks. In this way, we can evaluate the effect of uncertainty in commonly adopted slope design approaches.

The base case study corresponds to an open pit in operation in southeastern British Columbia, Canada, as reported by Barnett et al. (2017) and Clayton et al. (2020). The study area is located within the Elk Valley Coalfield. The geology comprises the Mist Mountain Formation which overlies the Moose Mountain Formation, part of the Kootenay Group of the Lower Jurassic to Lower Cretaceous (Grieve and Price, 1987). A cross section of the case study is shown in Figure 15.

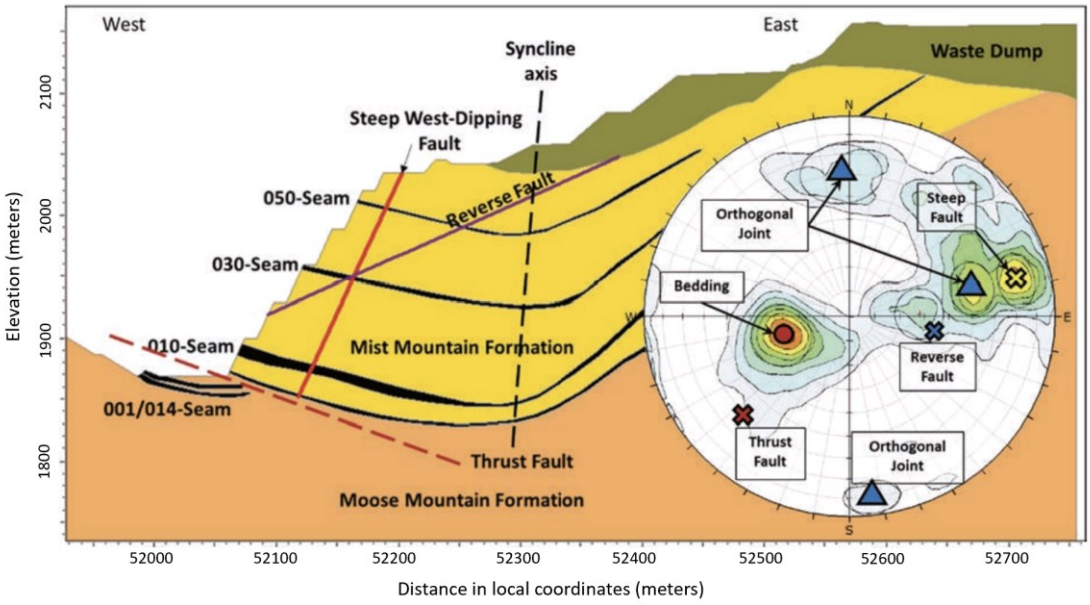

Figure 15: Cross section of the base case study. Units in meters (Clayton et al. 2020, with permission).

The first rock type corresponds to a group of interbedded sedimentary units from the Mist Mountain Formation ranging from fine-grained (mudstone, siltstone, and shale) to coarse-grained (sandstone and conglomerate) rocks. Rafiei et al. (2019) reported the $COV_{\sigma ci}$ for sedimentary rocks ranging between 0.28 to 0.38. Clayton et al. (2020) reported the $COV_{\sigma ci}$ for this unit equal to 0.40.

The second rock type is coal, also hosted in the Mist Mountain Formation. However, the material is separated from the previous group because (1) there might be over 30 seams in the Formation having a cumulative thickness of more than 70 m (British Columbia Ministry of Energy, 2018), and (2) some seams might be related to sheared-weak coals having a weak behavior compared to that in the interbedded sedimentary unit and competent coals. Medhurst and Brown (1998) reported σ_{ci} values for Australian coals ranged between 8.8 MPa and 40 MPa. Near the study area, Gentzis et al. (2007) reported σ_{ci} values between 8.6 MPa and 21.9 MPa and an average of 16.4 MPa. Medhurst and Brown (1998) reported a $COV_{\sigma ci}$ of 0.38 from the Australian coal tested. Ivor Evans and Pomeroy (1966) and Bieniawski (1968) reported $COV_{\sigma ci}$ in coals ranging from 0.17 to 0.30. This is somewhat consistent with an upper $COV_{\sigma ci}$ limit of 0.4 observed for the group of interbedded sedimentary units.

The Hoek-Brown strength parameters and the $COV_{\sigma ci}$ values adopted in this work are presented in Table 3. The σ_{ci} for coals is below the average value reported by Gentzis et al. (2007) to account for the lower values of σ_{ci} reported by Clayton et al. (2020) for competent coals in the study area. Regarding weak coals, Barnett et al. (2017) pointed out the limited information in the literature about strength in weak coals. They conducted triaxial strength testing in weak-sheared coal in a soil testing laboratory due to the difficulty of performing these tests in a rock testing laboratory. To estimate Hoek-Brown strength parameters for weak coals we reduced some of the Hoek-Brown strength parameters reported for competent coal so that the failure envelope matched the results of the triaxial drained tests in weak coal. Although in practice coals are usually modelled using Mohr-Coulomb failure criterion (due to their thickness typically very thin compared to the scale

of the slope and therefore modelled as a weak contact), this consideration was adopted in this work to compare the variability when transforming Hoek-Brown parameters to Mohr-Coulomb in weaker materials. Furthermore, LEA with Mohr-Coulomb parameters in these materials is still consistent with practice. Table 3 also shows the Hoek-Brown strength parameters reported by Rafiei et al. (2019) for what they named “unit 1”, as a means of reference.

The Hoek-Brown failure envelopes for these four rock mass materials are shown in Figure 16. The figure also shows results from triaxial strength testing conducted in competent and weak coals reported in the literature. Figure 16 shows that unit 1 (Rafiei et al., 2019) is the weakest material compared to the different rock types investigated in this work.

Table 3: Rock mass properties for the Hoek-Brown failure criterion and $COV_{\sigma ci}$ for the case study materials

Rock mass	γ (kN/m3)	σ_{ci} (Mpa)	GSI	m_i	m_b	s	a	$COV_{\sigma ci}$
Interbedded sedimentary rock	26	70	59	9	2.081	1.05E-2	0.503	0.4
Competent coal	17	10	85	15	8.779	1.89E-1	0.501	0.4
Weak coal	17	6	75	15	1.677	3.87E-3	0.506	0.4
Unit 1	26.5	25	-	-	0.177	5.36E-5	0.511	0.4

γ: unit weight GSI: Geological Strength Index σ_{ci}: Unconfined Compressive Strength
m_b, s, and a: Constant parameters for the rock mass m_i: Constant parameter for intact rock

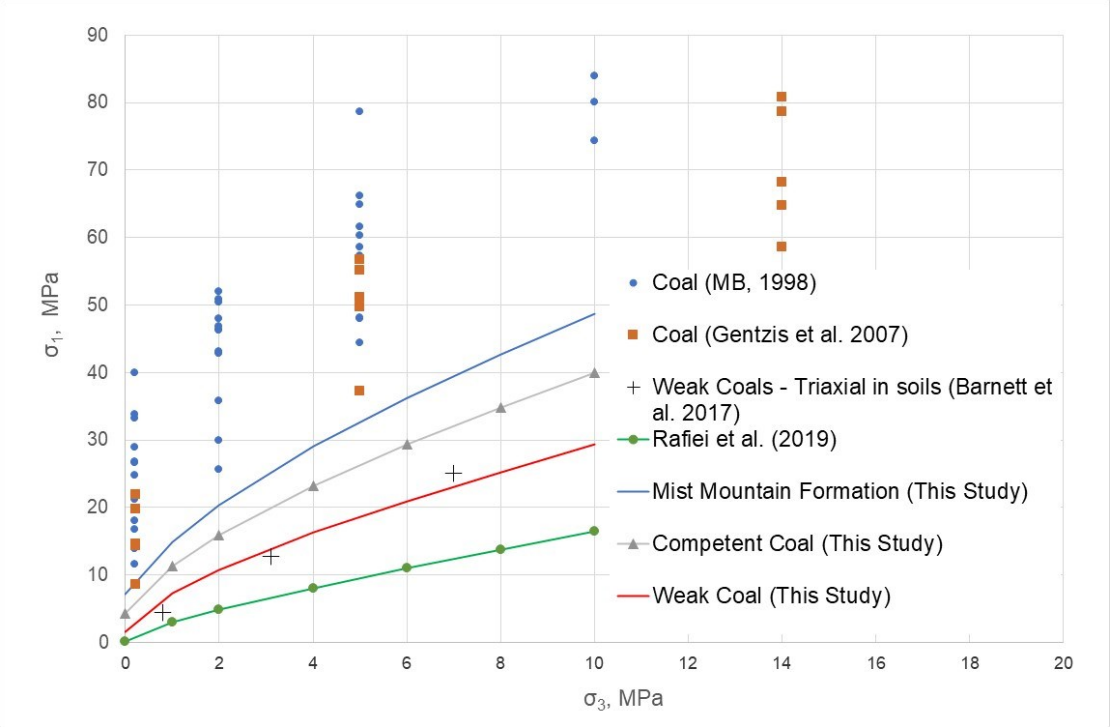

Figure 16: Hoek-Brown failure envelopes for the Interbedded sedimentary rock (Mist Mountain Formation), competent coal, weak coal for the base case study, and test results from others reported in literature

3.4 Evaluation of Rock Strength Variability – methods adopted

The deterministic strength envelope of the rock mass materials using the Hoek-Brown failure criterion is shown in Figure 16. To account for the probabilistic approach, it is necessary to consider the uncertainty of at least one parameter of the Hoek-Brown criterion and treat it as a random variable. The rock mass strength variability was determined using Monte Carlo simulations (Baecher and Cristian, 2003) involving 10 000 random values from defined distributions for the strength parameters considered random. To explore the variability of the rock mass strength in terms of the cohesion and friction components, we employed the criteria proposed by Rafiei et al. (2009). Estimates of the equivalent Mohr-Coulomb parameters were calculated from the Hoek-Brown envelopes using the relationships provided by Hoek et al. (2002) and Rafiei and Martin (2019)

hereafter referred to as HCC2002 and RM2019, respectively. Monte Carlo simulations are used to translate the variation of the Hoek-Brown strength parameters into the variation of equivalent cohesion and friction angle following univariate and bivariate distributions scenarios.

The bivariate distribution scenarios are idealized scenarios that help explore how the correlation of parameters impact the rock mass characterization for PSSA. The analyses are based on the coupling of data in the context of a bivariate distribution as presented by Phoon and Ching (2015). This distribution is defined as two pairs of data that are corelated (or dependent) using the Pearson correlation coefficient (δ_{12}), also referred to as the cross-correlation coefficient (Javankhoshdel and Bathurst 2016, Javankhoshdel et al. 2016). The random variables m_i and σ_{ci} were selected, and combinations of σ_{ci} with m_i were applied as inputs to the relationships provided by HCC2002 and RM2019. Lognormal distributions were assigned to these random variables based on Prakoso (2002), Zhang et al. (2018), and Rafiei et al. (2019). All the scenarios are conducted for a constant slope height (H) of 150 m, a slope angle (β) of 52 degrees, and the parameters indicated in Table 3.

3.4.1 RSV based on the equivalent Mohr-Coulomb parameters from univariate distributions

The first group of scenarios considered univariate distribution scenarios. Initially, the rock mass strength variability is generated from the distribution of the σ_{ci} ($COV_{\sigma ci}$ equal to 0.4) to estimate the mean and COV in major principal stress (σ_1) and the deviatoric stress ($\sigma_1 - \sigma_3$) space based on the Hoek-Brown failure criterion. The results are then evaluated based on the Mohr-Coulomb failure criterion in terms of COV_c and COV_φ for different

values of $COV_{\sigma ci}$. Trends are estimated by combining the result pairs (equivalent cohesion and friction angle) obtained from all four rock mass materials. Afterward, the variable m_i is then introduced independently, both as a univariate distribution and as a pair of univariate distributions (correlation coefficient equals zero) with σ_{ci}. Trends are only estimated for the interbedded sedimentary rock. Furthermore, when evaluating σ_{ci} and m_i together, COV_{mi} is fixed at 0.4 and then at 0.8, the latter being twice the $COV_{\sigma ci}$ of the material (consistent with literature observations discussed earlier). Four different scenarios (scenario number "N" 1, 2, 3, and 4) of univariate distributions are evaluated.

3.4.2 RSV based on the equivalent Mohr-Coulomb parameters from bivariate distributions

The second group of scenarios considered bivariate distribution scenarios (correlation coefficient not equal to zero) which is a more realistic scenario for studying the rock mass strength variability in terms of COV_c and COV_φ. The correlation coefficient between σ_{ci} and m_i was set at - 0.9 based on the results from Zhang et al. (2018). Similar to the previous case, trends are only estimated for the interbedded sedimentary rock with COV_{mi} fixed at 0.4 and 0.8. Two scenarios (N=5 and 6) of bivariate distributions are evaluated.

3.5 Results and discussion

3.5.1 Results of RSV from σ_{ci} as a univariate distribution – all rock mass materials

The variability of the Hoek-Brown failure envelope considering a $COV_{\sigma ci}$ at 0.4 for the interbedded sedimentary rock and the weak coal is shown in Figure 17. The variation in COV in σ_1 and 'σ_1-σ_3' space for these and the other materials are shown in Figure 18. As expected, the COV estimated in σ_1 and 'σ_1 - σ_3'space is initially equal to that considered for σ_{ci} when σ_3 equals zero. As σ_3 increases, the COV rapidly decreases, and this

reduction is more significant for the weak coal compared to the interbedded sedimentary rock. For instance, when σ_3 equals 1 MPa the interbedded sedimentary rock has a COV in σ_1 of 0.23, while the weak coal has a COV in σ_1 of 0.18, and Unit 1 has a COV in σ_1 of 0.13. The reduction of COV in σ_1 space continues as σ_3 increases and becomes nearly constant once σ_3 is above 12 MPa. A similar trend is evident on the σ_1 - σ_3 case. Unit 1 exhibits the lowest value of COV in σ_1-σ_3, being the weakest material among the data. However, in this plot, the four rock mass materials converge to a COV in σ_1-σ_3 of approximately 0.2. These results are in agreement with those reported by Prakoso (2002).

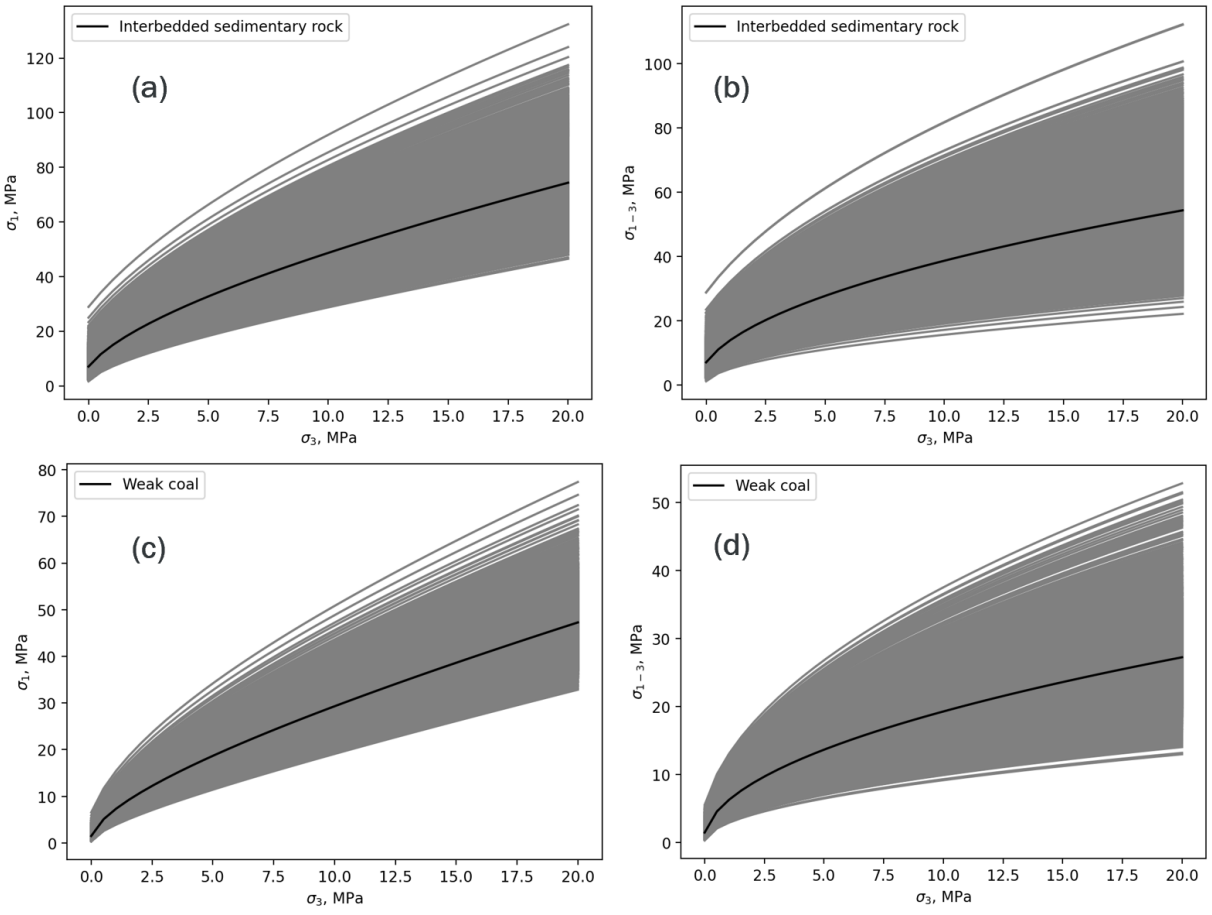

Figure 17: Variability of the Hoek-Brown envelope for a $COV_{\sigma ci}$ equal to 0.4 in the Interbedded sedimentary rock (a) in σ_1 and (b) in σ_1-σ_3, and in the weak coal (c) in σ_1 and (d) in σ_1-σ_3

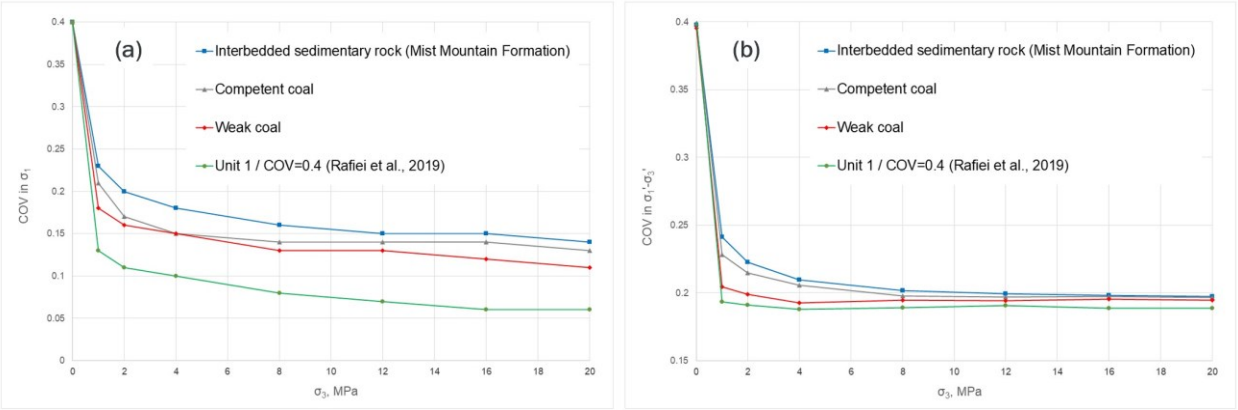

Figure 18: Variability of COV for different values of σ_3 in (a) σ_1 and (b) σ_1- σ_3

The relationship between the COV of the equivalent Mohr-Coulomb parameters and the $COV_{\sigma ci}$ for the interbedded sedimentary rock and the weak coal is shown in Figure 19. As an example, the interbedded sedimentary rock unit, for a $COV_{\sigma ci}$ at 0.4, the COV_c and COV_φ are 0.24 and 0.06, respectively, using HCC2002; and 0.36 and 0.03, respectively, using RM2019.

The COV of the equivalent Mohr-Coulomb parameters increases by increasing $COV_{\sigma ci}$, as was also shown by Rafiei et al. (2019). However, this increase is greater in cohesion using RM2019 and greater in friction angle using HCC2002. Moreover, as the rock becomes more competent, the ratio of COV_c / $COV_{\sigma ci}$ increases while COV_φ / $COV_{\sigma ci}$ decreases. The ratio of COV of the Mohr-Coulomb parameters to $COV_{\sigma ci}$, plotted to the mean values of cohesion and friction angle for the materials evaluated is shown in Figure 20. In this plot the trend is clear, showing larger increases in COV_c using the RM2019 than with HC2002. It is observed that the minimum ratio COV_c / $COV_{\sigma ci}$, and the maximum ratio COV_φ / $COV_{\sigma ci}$, correspond to the weakest rock material presented by Rafiei et al. (2019).

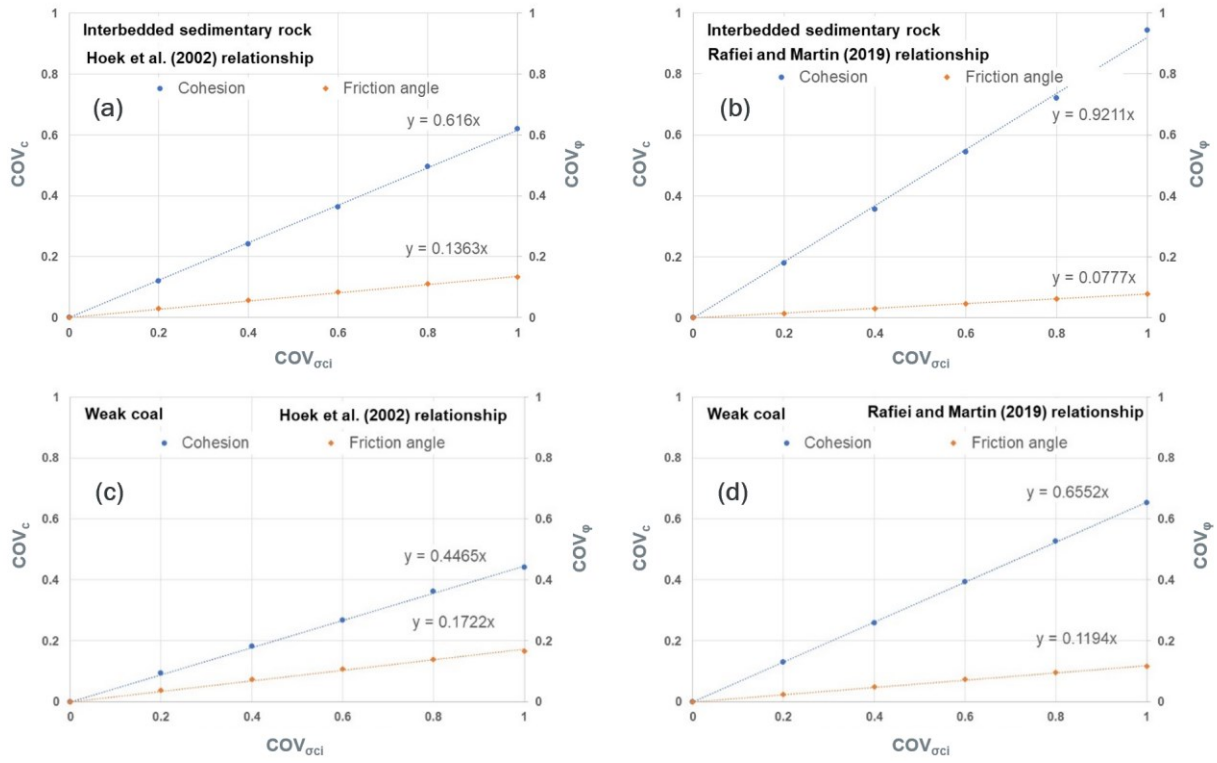

Figure 19: Scenario N=1: Relationship between the COV of the equivalent Mohr-Coulomb parameters and $COV_{\sigma ci}$ in the Interbedded sedimentary rock (a) with HCC2002 (b) with RM2019, and in the weak coal (c) with HCC2002 (d) with RM2019

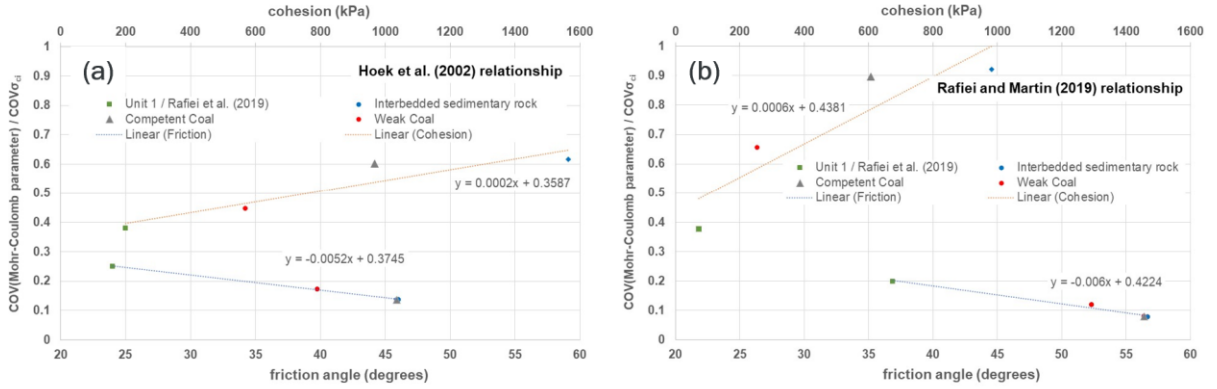

Figure 20: Relationship between the ratio of COV(Mohr-Coulomb parameter)/ $COV_{\sigma ci}$ with the mean value of equivalent cohesion and equivalent friction angle (a) with HCC2002 (b) with RM2019

3.5.2 Results of RSV from σ_{ci} and m_i as univariate distributions – interbedded sedimentary rock

The variation of COV in cohesion and friction when only m_i is taken as the random variable is shown in Figure 21. Compared to Figure 19 and Figure 20, which only consider σ_{ci} as the random variable, the case of m_i as a random variable generates less variability in cohesion but high variability in friction angle. It is also observed that HCC2022 leads to higher COV in friction than cohesion, while RM2019 shows the opposite. Nonetheless, it is worth noting that we can generate significant variability in the friction angle by considering m_i as a random variable.

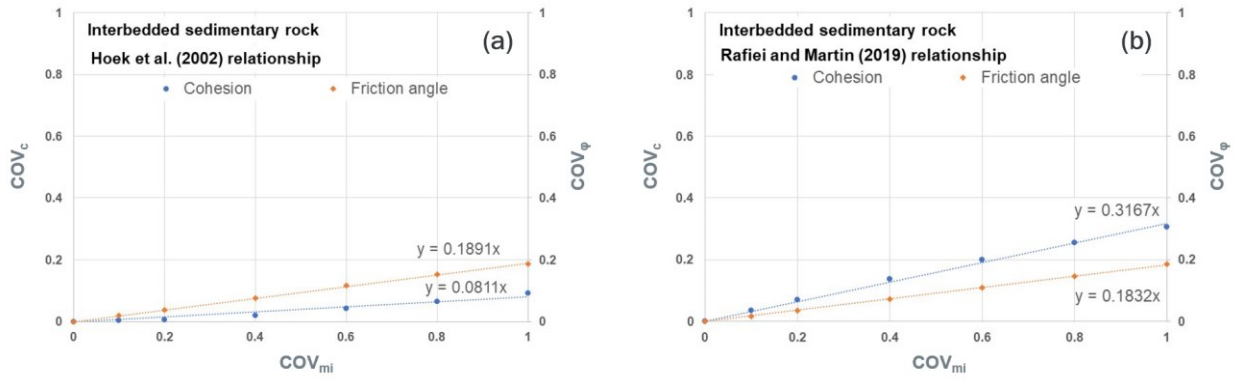

Figure 21: Scenario N=2: Relationship between the COV of the equivalent Mohr-Coulomb parameters and COV_{mi} in the Interbedded sedimentary rock (a) with HCC2002 (b) with RM2019

The change in COV_c and COV_φ when the $COV_{\sigma ci}$ increases, and when COV_{mi} is set at 0.4 and 0.8 is shown in Figure 22 and Figure 23, respectively. Compared to the scenario N=1, considering COV_{mi} equal to 0.4 only slightly affects COV_c but increases the COV_φ. Increasing COV_{mi} to 0.8 results in a greater increase in both COV_c and COV_φ.

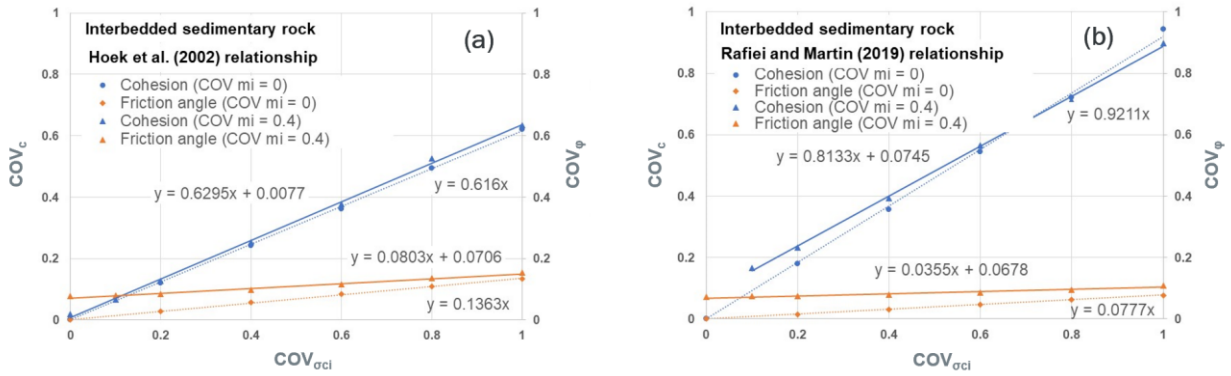

Figure 22: Scenario N=3: Relationship between the COV of the equivalent Mohr-Coulomb parameters and $COV_{\sigma ci}$ combined with a COV_{mi} at 0.4 in the Interbedded sedimentary rock (a) with HCC2002 (b) with RM2019 - no correlation coefficient

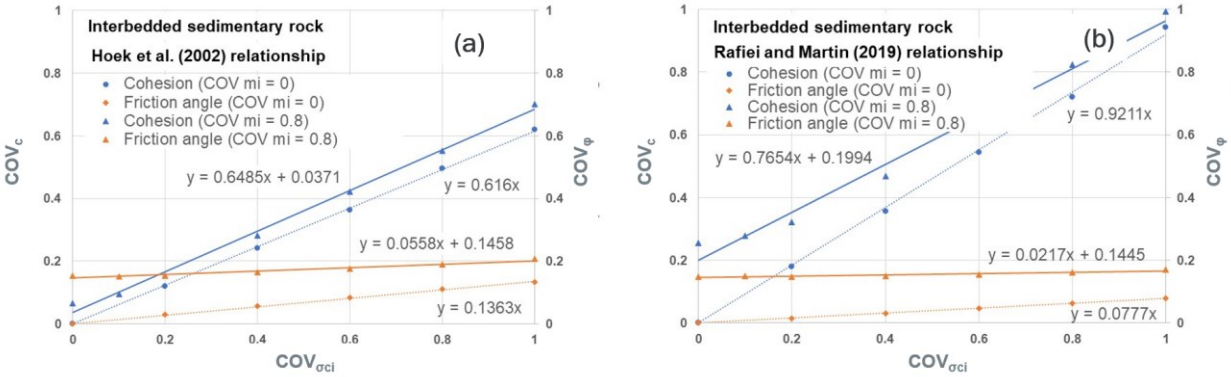

Figure 23: Scenario N=4: Relationship between the COV of the equivalent Mohr-Coulomb parameters and $COV_{\sigma ci}$ combined with a COV_{mi} at 0.8 in the Interbedded sedimentary rock (a) with HCC2002 (b) with RM2019 - no correlation coefficient

The same trends are observed for both HCC2002 and RM2019, further supporting the observation that m_i has a significant impact on the variability of the equivalent friction angle. In our case study, with $COV_{\sigma ci}$ set at 0.4, we expect COV_{mi} to be approximately 0.8 (based on previous findings from Zhang et al., 2018). In this case, COV_c and COV_φ are 0.28 and 0.16 using HCC2002, respectively, and 0.47 and 0.15 using RM2019. Compared to the results in scenario N=1, when σ_{ci} is the only random variable, COV_c shows an increment between 10% and 20%, meaning an increase in their variability.

However, it is COV_φ that shows an increment about three to five times (depending on the relationship used), suggesting that more variability will be added in the rock mass strength as a frictional component when m_i is added as another univariate distribution.

3.5.3 Results of RSV from bivariate distribution (σ_{ci} and m_i) – interbedded sedimentary rock

The change in COV_c and COV_φ when the $COV_{\sigma ci}$ increases, and when the COV_{mi} is set at 0.4 and 0.8 is shown respectively in Figure 24 and Figure 25 considering a correlation coefficient between σ_{ci} and m_i (referred to as $\delta_{\sigma m}$) of -0.9. Compared to the case when σ_{ci} is the only random variable, we observe significant changes in COV_c and COV_φ when COV_{mi} is 0.4 and even more so for 0.8. Regardless of the condition, and compared to the case where $\delta_{\sigma m}$ is 0 (Figure 22 and Figure 23), COV_c increases, while COV_φ decreases when $COV_{\sigma ci}$ is greater than COV_{mi}. The same trends are observed for both HCC2002 and RM2019, but with varying magnitudes of the COV. Assuming that the more representative condition for our case study has a $COV_{\sigma ci}$ of 0.4, a COV_{mi} of 0.8, and a $\delta_{\sigma m}$ of -0.9; means that COV_c and COV_φ are 0.39 and 0.11 using HCC2002, and 0.66 and 0.13 using RM2019. These values are higher for COV_c but lower for COV_φ when compared to the case where $\delta_{\sigma m}$ is 0. Nevertheless, compared to the scenario results when σ_{ci} is the only random variable, COV_c in this scenario shows an increment between 60% and 85% and COV_φ shows an increment of two to four times.

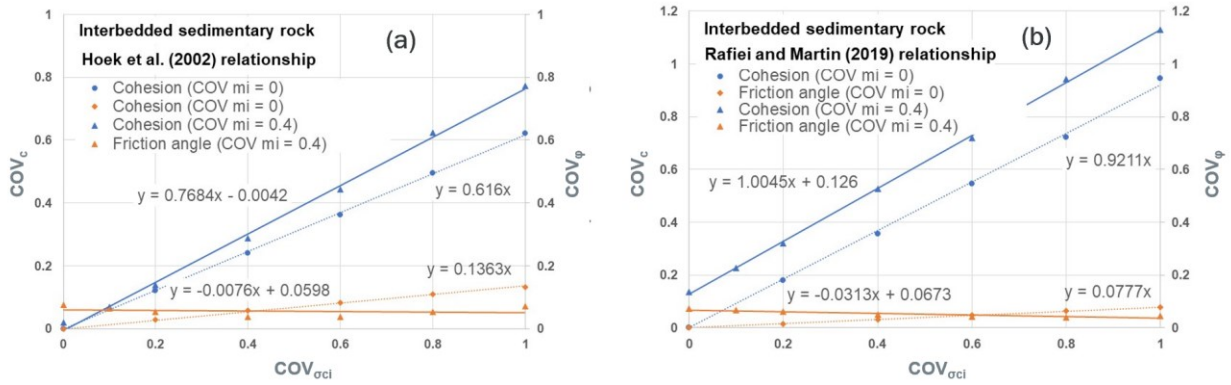

Figure 24: Scenario N=5: Relationship between the COV of the equivalent Mohr-Coulomb parameters and $COV_{\sigma ci}$ combined with a COV_{mi} at 0.4 in the Interbedded sedimentary rock (a) with HCC2002 (b) with RM2019 - $\delta_{\sigma m}$=-0.9

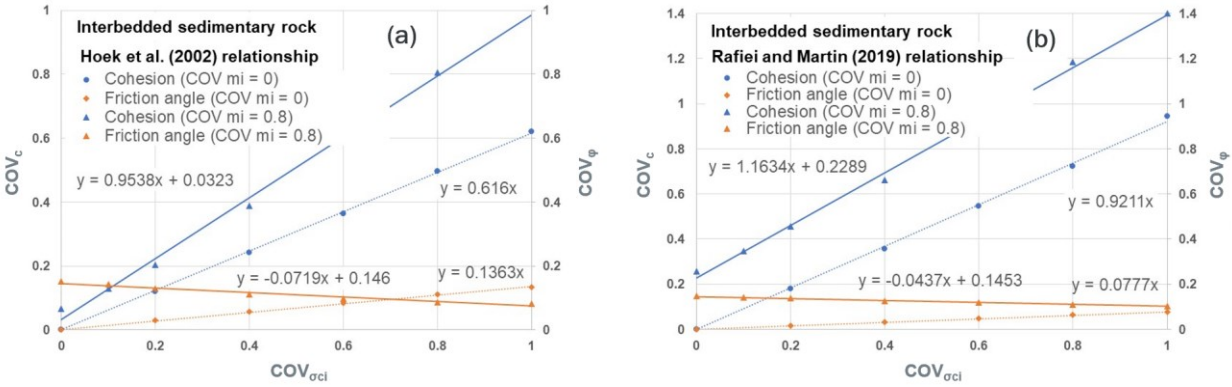

Figure 25: Scenario N=6: Relationship between the COV of the equivalent Mohr-Coulomb parameters and $COV_{\sigma ci}$ combined with a COV_{mi} at 0.8 in the Interbedded sedimentary rock (a) with HCC2002 (b) with RM2019 - $\delta_{\sigma m}$=-0.9

3.5.4 Inherent correlation in equivalent cohesion and friction angle

Up until this point, the analyses have treated cohesion and friction angle as independent variables. However, it is important to recognize that each cohesion and friction angle obtained corresponds to one pair of the many Monte Carlo realizations on the Hoek-Brown failure criterion, as they are being estimated using either HCC2002 or RM2019. Therefore, these parameters form an output of bivariate distributions defined by the conversion equations whether we are working with an input of univariate distributions or a bivariate distribution. This means there is an inherent correlation between equivalent

cohesion and friction angle. The values of this inherent correlation coefficient between the cohesion and friction angle (referred to as $\delta_{c\phi}$) obtained from the univariate distribution analyses are provided in Table 4.

Table 4: Inherent correlation coefficient ($\delta_{c\phi}$) from the univariate distribution analyses. COV is varied for σ_{ci} or m_i (left column) depending on the analysis settings (scenario N = 1, 2, 3, and 4). Interbedded sedimentary rock

COV (σ_{ci} or m_i)	varying $COV_{\sigma ci}$ (N=1)		varying COV_{mi} (N=2)		varying $COV_{\sigma ci}$ and COV_{mi} at 0.4 (N=3)		varying $COV_{\sigma ci}$ and COV_{mi} at 0.8 (N=4)	
	HCC2002	RM2019	HCC2002	RM2019	HCC2002	RM2019	HCC2002	RM2019
0.1	1.00	1.00	0.88	-1.00	0.21	-0.77	-0.22	-0.90
0.2	1.00	1.00	0.63	-1.00	0.36	-0.42	0.00	-0.73
0.4	0.99	0.98	0.10	-1.00	0.61	0.04	0.26	-0.40
0.6	0.98	0.97	-0.20	-0.99	0.73	0.29	0.44	-0.15
0.8	0.97	0.94	-0.43	-0.98	0.81	0.46	0.55	0.01
1.0	0.96	0.93	-0.53	-0.97	0.85	0.57	0.63	0.16

Scenario N=1 shows $\delta_{c\phi}$ ranges from 1.00 to 0.96 using HCC2002 and from 1.00 to 0.93 using RM2019. For example, Figure 26a illustrates the relationship between friction and cohesion when using HCC2002 for $COV_{\sigma ci}$ at 0.4 (N = 1). The value of 0.99 indicates a strong positive linear correlation between cohesion and friction, meaning that at a given value of σ_3, an increase in σ_{ci} results in an increase in both cohesion and friction angle. However, it should be noted that the plot in Figure 26a follows a clear non-linear trend, whereas the correlation coefficient from Pearson is indicative of the linearity of the correlation between parameters. Another correlation is the Spearman rank correlation ($\rho_{c\phi}$) (Phoon and Ching, 2015), which “quantifies how well the relationship between the

two variables can be described as a monotonic function". Figure 26b shows the Spearman ranks, with our data showing $\rho_{c\phi}$ is 1, indicating a perfect positive monotonic relationship between cohesion and friction angle at a given confinement stress, using σ_{ci} as a random variable in the HCC2002 relationship. As $COV_{\sigma ci}$ increases, the non-linearity of the trend increases, which is the reason for the slight decrease in $\delta_{c\phi}$. Similar findings are observed for N=1 using RM2019, where the equation is different but the variation in σ_{ci} is maintained.

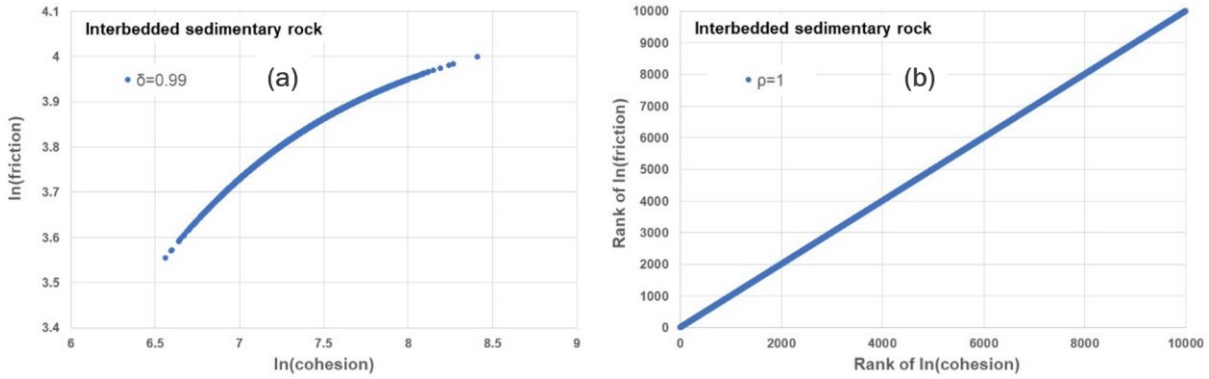

Figure 26: Inherent cross-correlation in Mohr-Coulomb parameters for N=1 for $COV_{\sigma ci}$ at 0.4 evaluated through (a) Pearson correlation ($\delta_{c\phi}$ = 0.99) and (b) Spearman rank correlation ($\rho_{c\phi}$= 1). Equivalent friction and cohesion following HCC2002 for the Interbedded sedimentary rock

The results of $\delta_{c\phi}$ for scenario N=2 (only m_i as a random variable) are shown in Figure 27. The trend observed is different from that presented in N=1. In the case of HCC2002, $\delta_{c\phi}$ changes from a positive to a negative correlation. This is because, for a small COV, most of the data tend to a positive linear correlation with only a small portion of the data showing a negative linear correlation. However, as COV_{mi} increases the data with negative linear correlation increases. For example, Figure 27 shows that there is a fairly equal amount of data in the negative and positive trend in the case of a COV_{mi} equal to 0.4, being the reason why $\delta_{c\phi}$ is close to 0. However, when COV_{mi} is higher than 0.4

the data in the negative trend increases leading to a negative value of $\delta_{c\phi}$. In the case of RM2019, the data show a strong negative linear correlation, as opposed to N=1.

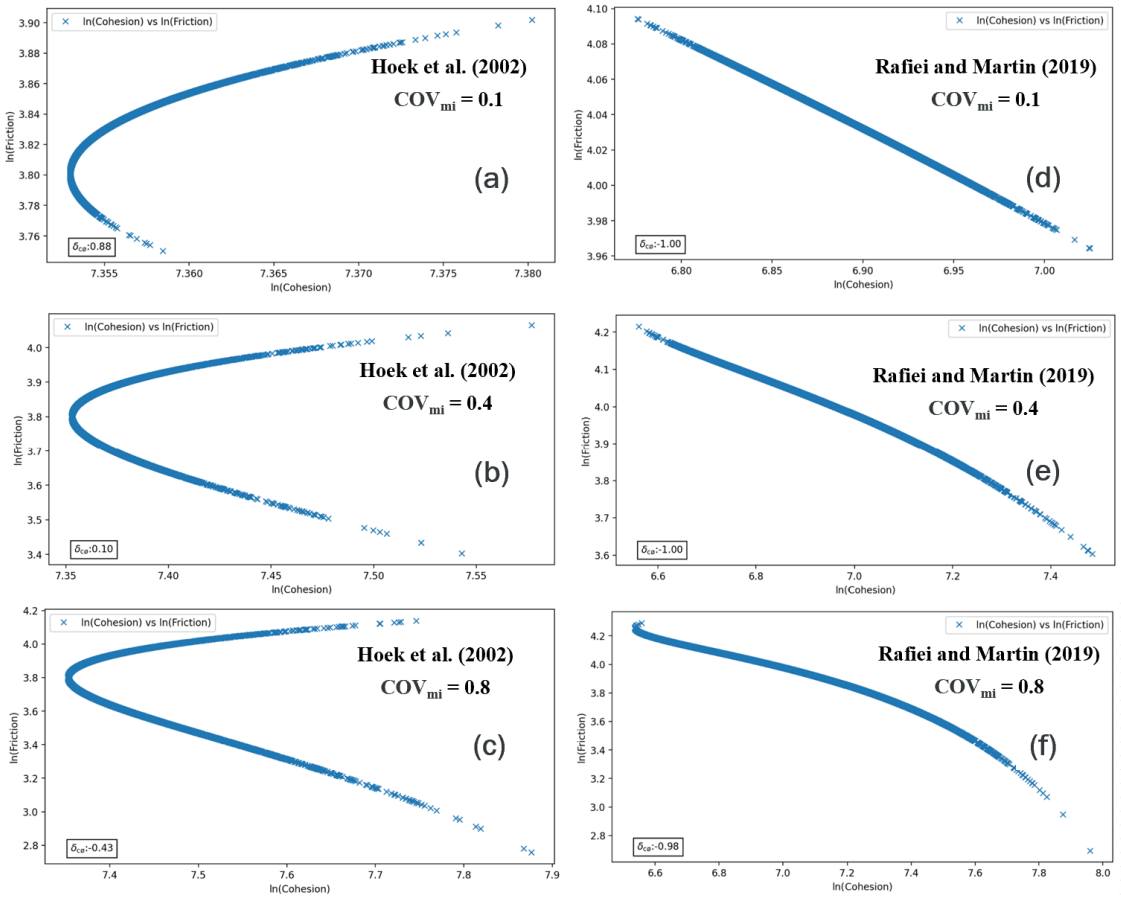

Figure 27: Inherent correlation coefficient in Mohr-Coulomb parameters for N=2 using HCC2002 for (a) COV_{mi} at 0.1, (b) COV_{mi} at 0.4, (c) COV_{mi} at 0.8, and using RM2019 for (d) COV_{mi} at 0.1, (e) COV_{mi} at 0.4, (f) COV_{mi} at 0.8

Figure 27 also illustrates the effect of random realizations of Hoek-Brown strength envelopes. For realizations that render relatively stronger material and using HCC2002, the non-linearity of the Hoek-Brown strength criterion allows for high values of cohesive intersect and steep equivalent Mohr-Coulomb linear criterion (high friction angle). Some realizations of weaker material can have a reduction in the equivalent friction angle (reduction in the steepness of the failure envelope) as the cohesive intersect is reduced.

Other realizations can show relatively high cohesive intersects and reduced steepness in the failure envelope. This then generates the possibility of two equivalent cohesion values for a given equivalent friction angle, depending on the selected confining stress for the conversion.

The results for scenarios N=3 (when the COV_{mi} is 0.4) and N=4 (when the COV_{mi} is 0.8) are also reported in Table 4. The results obtained for $COV_{\sigma ci}$ equal 0.4 and 0.8 and when COV_{mi} is 0.8 are shown in Figure 28. When the COV_{mi} is 0.4, most of the results show positive values of $\delta_{c\phi}$, except for some cases using RM2019, where negative $\delta_{c\phi}$ is obtained when $COV_{\sigma ci}$ is less than COV_{mi}. A similar trend is also presented in RM2019 when COV_{mi} is 0.8. For the case of using HCC2002, the only negative $\delta_{c\phi}$ is obtained when $COV_{\sigma ci}$ is 0.1. These results indicate that σ_{ci} has a strong influence on the HCC2002 relationship, leading to positive $\delta_{c\phi}$ in general. In the case of RM2019, the final value in $\delta_{c\phi}$ will depend on which of the two parameters have more variability, σ_{ci} or m_i, as both parameters appear to have equal influence on $\delta_{c\phi}$.

The values of $\delta_{c\phi}$ from the bivariate distribution analyses using HCC2002 and RM2019 are shown in Table 5. Compared to the previous results, $\delta_{c\phi}$ is now negative in all the scenarios using RM2019, and in most of the scenarios using HCC2002. For the latter, there is only positive $\delta_{c\phi}$ when $COV_{\sigma ci}$ is higher than COV_{mi}, and only when COV_{mi} is 0.4. These results suggest that the strong negative correlation between σ_{ci} and m_i leads to negative $\delta_{c\phi}$. The results for $COV_{\sigma ci}$ equal 0.4 and 0.8 and when COV_{mi} is 0.8 are shown in Figure 29.

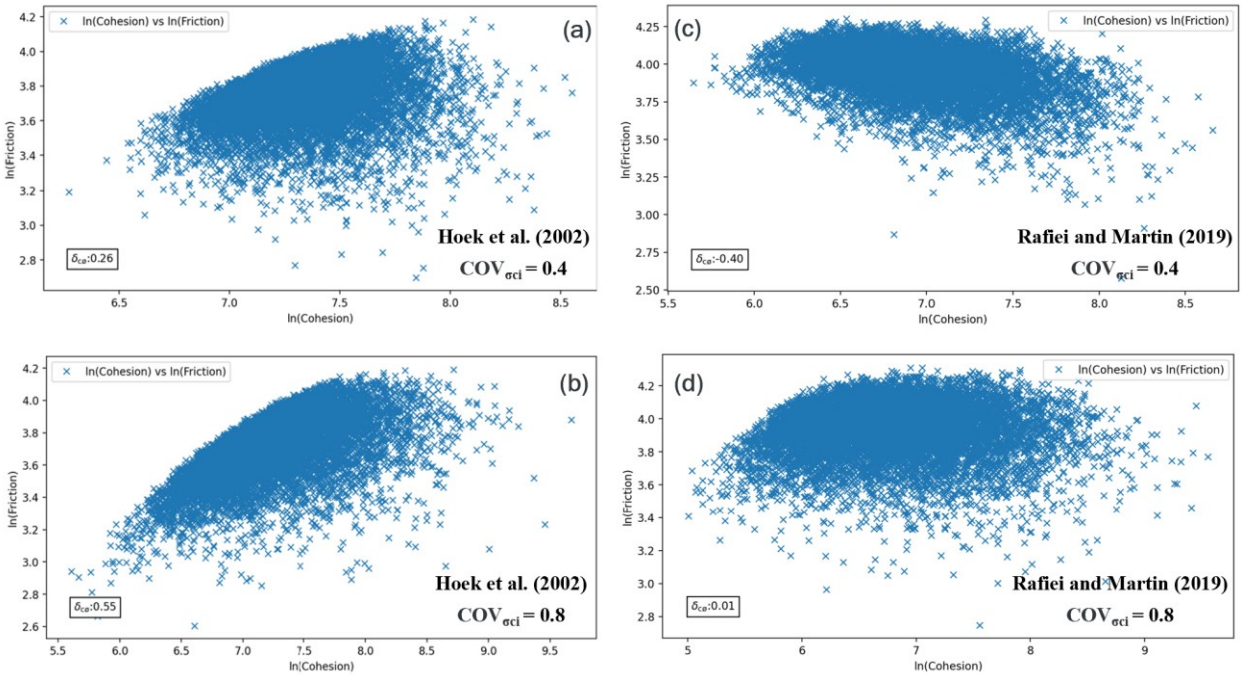

Figure 28: Inherent correlation coefficient in Mohr-Coulomb parameters for N=4 using HCC2002 for (a) $COV_{\sigma ci}$ equal to 0.4, (b) $COV_{\sigma ci}$ equal to 0.8 and RM2019 for (c) $COV_{\sigma ci}$ equal to 0.4, (d) $COV_{\sigma ci}$ equal to 0.8. All conditions with COV_{mi} at 0.8

Table 5: Inherent correlation coefficient ($\delta_{c\phi}$) from the bivariate distribution analyses. For different analysis settings (N 5 and 6) for COV values of σ_{ci} and m_i

$COV_{\sigma ci}$	Varying $COV_{\sigma ci}$ and COV_{mi} at 0.4 ($\delta_{\sigma m}$ =-0.9) - (N=5)		Varying $COV_{\sigma ci}$ and COV_{mi} at 0.8 ($\delta_{\sigma m}$ =-0.9) - (N=6)	
	HCC2002	RM2019	HCC2002	RM2019
0.1	-0.79	-0.97	-0.81	-0.97
0.2	-0.75	-0.92	-0.84	-0.95
0.4	-0.38	-0.82	-0.79	-0.91
0.6	0.21	-0.61	-0.71	-0.87
0.8	0.59	-0.33	-0.55	-0.81
1.0	0.74	0	-0.34	-0.75

Table 5 shows that for a condition where $COV_{\sigma ci}$ is 0.4 and COV_{mi} is twice $COV_{\sigma ci}$, $\delta_{c\phi}$ is between -0.79 and -0.91. These results suggest that the correlation coefficient in rocks will likely be negative, similar to what is usually estimated in soils (Hata et al. 2012 and Yucemen et al. 1973).

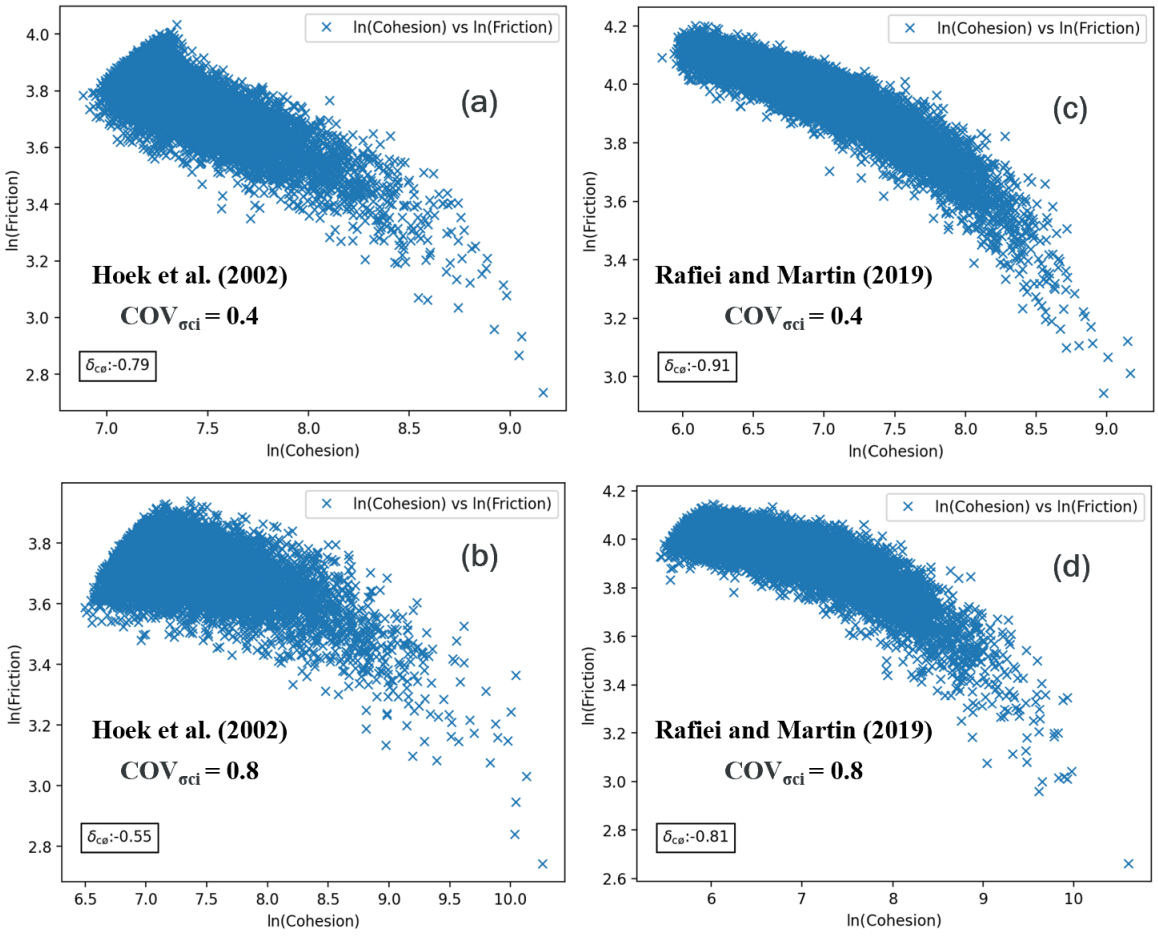

Figure 29: Inherent correlation coefficient in Mohr-Coulomb parameters for N=6 using HCC2002 for (a) $COV_{\sigma ci}$ equal to 0.4, (b) $COV_{\sigma ci}$ equal to 0.8 and RM2019 for (c) $COV_{\sigma ci}$ equal to 0.4, (d) $COV_{\sigma ci}$ equal to 0.8. All conditions with COV_{mi} at 0.8 and $\delta\sigma_m$=-0.9

The influence of GSI is illustrated in Figure 30. This Figure shows that when GSI is equal to 100, $\delta_{c\phi}$ is -1, indicating a strong negative correlation between cohesion and friction angle for intact rock. However, as GSI decreases, $\delta_{c\phi}$ increases, and can change from a negative to a positive correlation. In our case study, with a GSI equal to 59, the results indicate a negative $\delta_{c\phi}$ value whether we use HCC2002 or RM2019.

For the scenario when $COV_{\sigma ci}$ is 0.4 and COV_{mi} is 0.8, $\delta_{c\phi}$ will be positive when GSI is less than 37 and 15 using HCC2002 and RM2019, respectively. The RM2019 relationship shows more negative $\delta_{c\phi}$ results compared to HCC2002, which may be attributed to the different upper limit of the confining stress (σ_{3max}) estimated by each method. In our case study, the height of the slope (H) considered is 150 m, resulting in a σ_{3max} equal to 3.15 MPa using HCC2002 but 0.53 MPa using RM2019. To obtain a σ_{3max}=3.15MPa using RM2019, H would need to be 890 m. The results and comparisons between the two relationships assuming RM2019 for an H of 890 m are shown in Figure 31. As can be seen, the results are very close, confirming that difference is related to the assumptions considered for estimating σ_{3max}. As a result, $\delta_{c\phi}$ tends to increase (move towards a positive sign) as the confining stress increases. An internal verification demonstrated that the reason for the presence of solely negative $\delta_{c\phi}$ in Figure 27 using RM2019 is due to the difference in σ_{3max}. What is also observed is that the results of positive $\delta_{c\phi}$ in Figure 31 follow the same path presented in Figure 27, meaning that there are more data with a positive trend than in the negative.

As the confining stress increases, COV_c decreases. A decrease in COV was also presented in Figure 28 in terms of σ_1 and 'σ_1 - σ_3'. For the case of the friction angle, Table 7 shows that when $\delta_{\sigma m}$=0, the COV_ϕ increases as confining stress increases, but

when $\delta_{\sigma m}$=-0.9, the COV_{φ} decreases as confining stress increases. The results presented in Figure 31 are in good agreement with the results presented by Zhang et al. (2018).

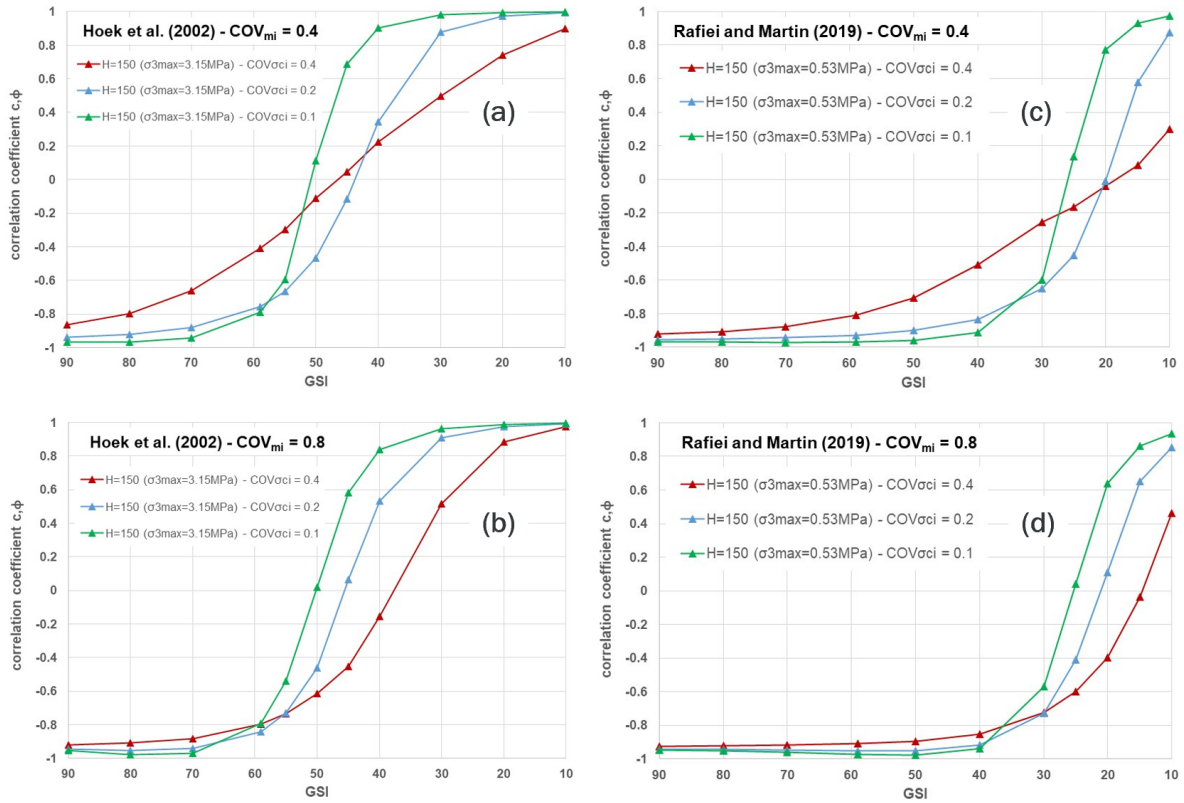

Figure 30: Influence of the GSI in $\delta_{c\phi}$ for bivariate distributions ($\delta_{\sigma m}$=-0.9) using HCC2002 for (a) COV_{mi} at 0.4, (b) COV_{mi} at 0.8 and RM2019 for (c) COV_{mi} at 0.4, (d) COV_{mi} at 0.8

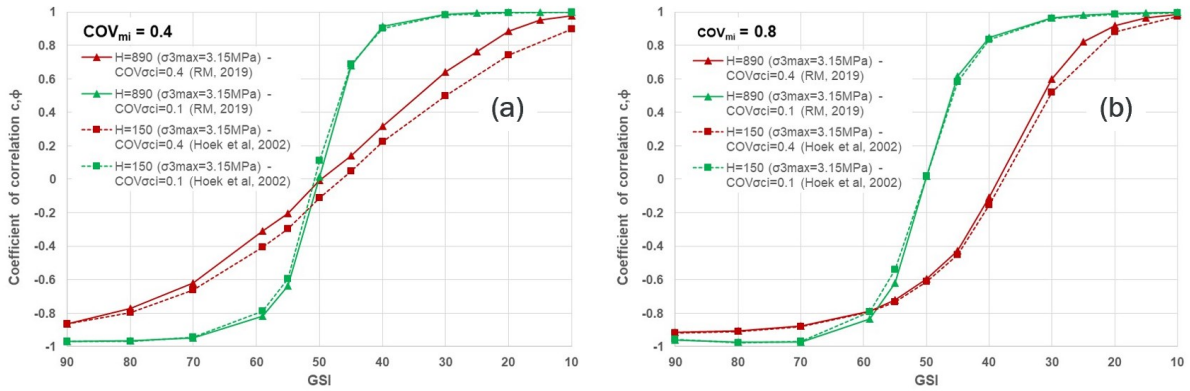

Figure 31: Comparison between HCC2002 and RM2019 in bivariate distributions considering σ_{3max} equal to 3.15 MPa for (a) COV_{mi} at 0.4 and (b) COV_{mi} at 0.8

3.6 Influence of the inherent correlation coefficient in equivalent Mohr-Coulomb parameters in PSSA

Two different groups of PSSA were carried out to estimate the influence of the inherent correlation coefficient in equivalent Mohr-Coulomb parameters combined with the COV values estimated from cohesion and friction angle. Five analyses were performed on each group, these are related to the different scenarios of COV values and correlation coefficients that were estimated previously (N=1, 3, 4, 5, and 6). Scenario N=2 is not considered as it was introduced to explore the variability solely of m_i. Group 1 used equivalent parameters estimated with HCC2002, while Group 2 used the parameters estimated with RM2019. Table 6 summarizes the Hoek-Brown and Mohr-Coulomb strength parameters, while Table 7 summarizes the variability in terms of COV and $\delta_{c\phi}$.

Table 6: Rock mass properties for the Hoek-Brown and equivalent Mohr-Coulomb failure criteria (using HCC2002 for Group 1 and RM2019 for Group 2)

Rock mass	γ (kN/m³)	σ_{ci} (MPa)	GSI	m_i	m_b	s	a	Parameters Group	Cohesion (kPa)	Friction (degrees)
Interbedded sedimentary rock	26	70	59	9	2.08	1.05E-2	0.50	1	1560	46
								2	982	56.7
Weak coal	17	-	-	-	-	-	-	-	50 COV: 0.26	23 COV: 0.05

γ: unit weight
σ_{ci}: Unconfined Compressive Strength
GSI: Geological Strength Index
m_i: Constant parameter for intact rock
m_b, s, and a: Constant parameters for the rock mass

Table 7: Summary of COV and $\delta_{c\phi}$ considered for the scenarios being evaluated

Case N	Variability	Group 1 – Hoek et al. (2002)			Group 2 – Rafiei and Martin (2019)		
		COV_c	COV_ϕ	$\delta_{c\phi}$	COV_c	COV_ϕ	$\delta_{c\phi}$
1	ln σ_{ci} (COV=0.4)	0.24	0.06	1	0.36	0.03	0.98
3	ln σ_{ci} (COV=0.4) and m_i (COV=0.4) ($\delta_{\sigma m}$=0)	0.25	0.10	0.61	0.39	0.08	0.04
4	ln σ_{ci} (COV=0.4) and m_i (COV=0.8) ($\delta_{\sigma m}$=0)	0.28	0.16	0.26	0.47	0.15	-0.40
5	ln σ_{ci} (COV=0.4) and m_i (COV=0.4) ($\delta_{\sigma m}$=-0.9)	0.29	0.04	-0.38	0.53	0.05	-0.82
6	ln σ_{ci} (COV=0.4) and m_i (COV=0.8) ($\delta_{\sigma m}$=-0.9)	0.39	0.11	-0.79	0.66	0.13	-0.91

The profile used for the LEA in Slide2 (Rocscience Inc 2023) is shown in Figure 32. The profile was derived from the section created by Clayton et al. (2020). Also, the phreatic surface considered in the analysis corresponds to the interpretation by Clayton et al. (2020). For the purposes of this study, some geological structures were not included in order to focus solely on the effects of the variations in the interbedded sedimentary rock. Specifically, only the weak coal in the profile was taken into account, with the parameters indicated in Table 6. This implies the exercise does not intend to model the case study described in Clayton et al. (2020) but use a realistic model for the purpose of the sensitivities in this paper. The analyses were performed using the Morgenstern-Price method (Morgenstern and Price 1965) and assuming a non-circular failure surface.

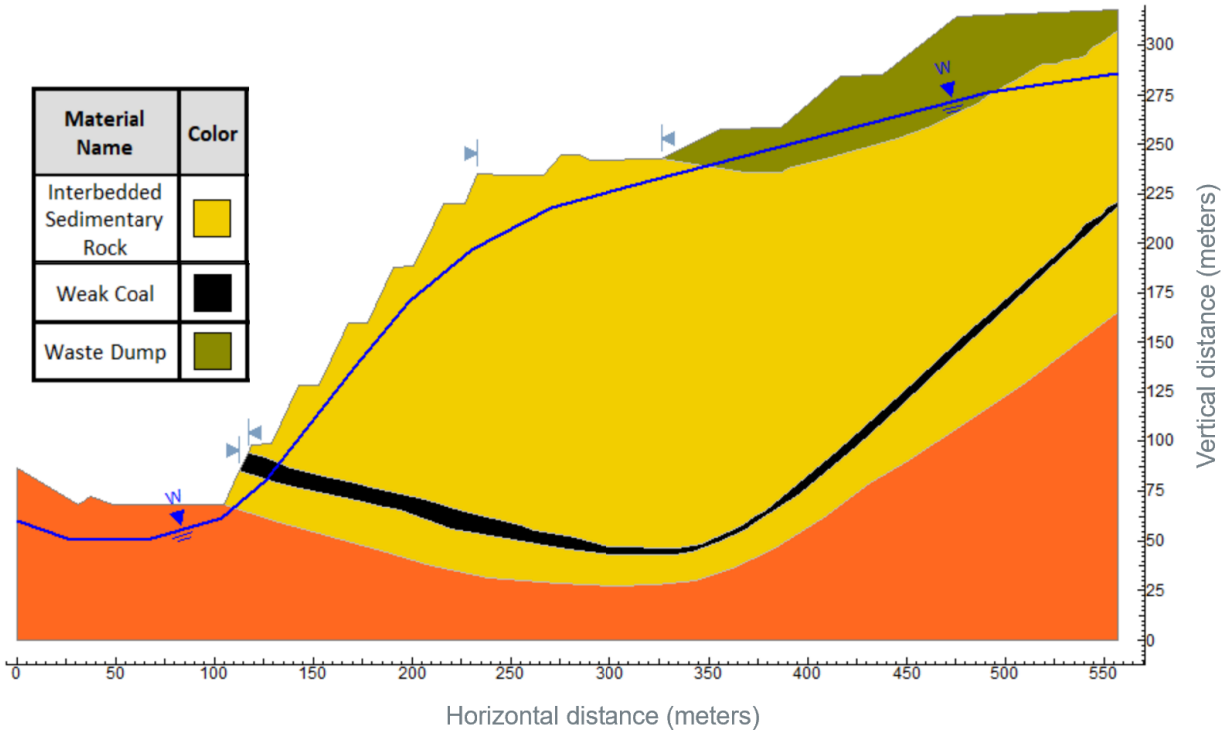

Figure 32: Geotechnical profile of the section in evaluation generated in Slide2 (H=150 m)

The outcomes of the PSSA are summarized in Table 8. The resulting mean FoS, PoF, and COV_{FoS} using the Hoek-Brown criterion are also shown. It can be observed that in the cases of univariate distribution (N=1, 3, and 4) the results obtained using the Hoek-Brown parameters are closer to those using the equivalent cohesion and friction angle from the RM2019 relationship (group 2). In contrast, using the equivalent Mohr-Coulomb strength parameters derived from the HCC2002 relationship leads to higher values of FoS and lower values of COV_{FoS}. This suggests that the parameters and variability estimated from the RM2019 relationship are more appropriate for representing the Hoek-Brown failure envelope.

Table 8: Summary of results of FoS, PoF, and COV_{FoS} from Groups 1 and 2

Case N	Variability	Hoek Brown FoS deterministic = 1.71	Group 1 FoS deterministic = 2.00			Group 2 FoS deterministic = 1.69		
		Failure criterion	FoS	PoF	COV_{FoS}	FoS	PoF	COV_{FoS}
1	ln σ_{ci} (COV=0.4)	Hoek-Brown	FoS=1.63, PoF=0.0, COV_{FoS}=0.06					
		Mohr-Coulomb	1.88	0.0	0.05	1.61	0.0	0.06
3	ln σ_{ci} (COV=0.4) and m_i (COV=0.4) ($\delta_{\sigma m}$=0)	Hoek-Brown	FoS=1.65, PoF=0.0, COV_{FoS}=0.08					
		Mohr-Coulomb	1.89	0.0	0.07	1.64	0.0	0.08
4	ln σ_{ci} (COV=0.4) and m_i (COV=0.8) ($\delta_{\sigma m}$=0)	Hoek-Brown	FoS=1.68, PoF=0.0, COV_{FoS}=0.10					
		Mohr-Coulomb	1.94	0.0	0.12	1.68	0.0	0.11
5	ln σ_{ci} (COV=0.4) and m_i (COV=0.4) ($\delta_{\sigma m}$=-0.9)	Hoek-Brown	No estimated					
		Mohr-Coulomb	1.92	0.0	0.04	1.61	0.0	0.06
6	ln σ_{ci} (COV=0.4) and m_i (COV=0.8) ($\delta_{\sigma m}$=-0.9)	Hoek-Brown	No estimated					
		Mohr-Coulomb	1.95	0.0	0.05	1.63	0.0	0.04

Figure 33 illustrates the critical slip surface for N=4 from Groups 1 and 2, depicted in red and green, respectively, along with that estimated using the Hoek-Brown failure envelope shown in blue. As reported by Rafiei and Martin (2019), using the HCC2002 relationship leads to a larger surface area than that expected from the original Hoek-Brown failure criterion.

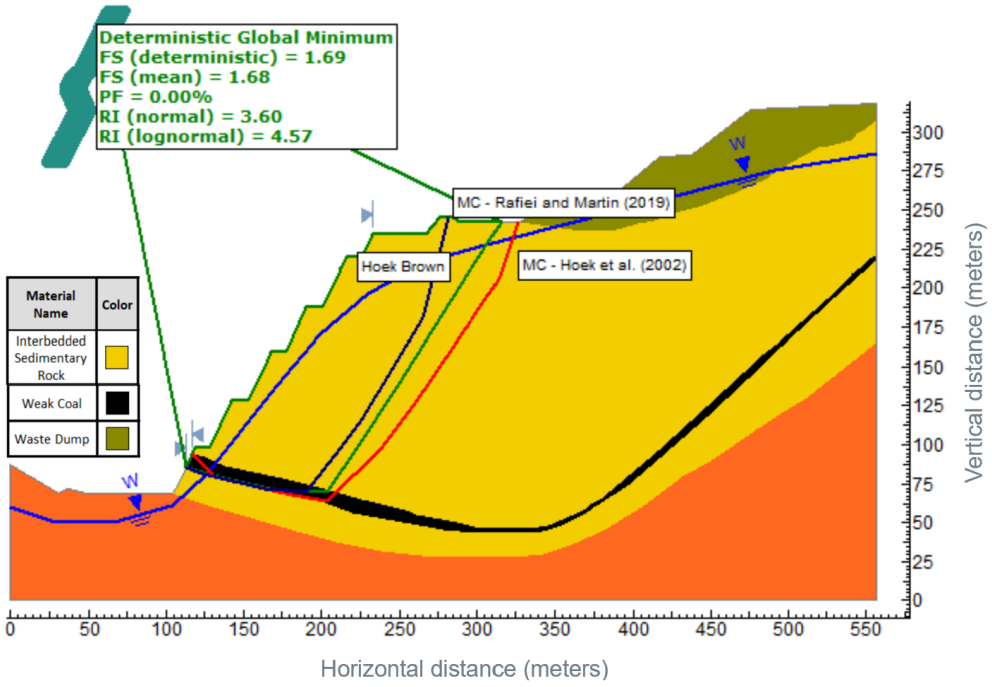

Figure 33: Mean FoS estimated in Slide N=4 comparison of critical slip surface with parameters from Groups 1 (red) and 2 (green) and original parameters from Hoek-Brown (blue)

For the bivariate distribution cases (N=5 and 6), it is important to note that none of these analyses can be carried out in Slide2 (version 9.027) using the Hoek-Brown failure criterion, since this version does not support the consideration of correlation coefficient between the Hoek-Brown parameters. However, our analysis using the RM2019 relationship has demonstrated that results can be obtained that closely approximate those obtained using the original Hoek-Brown parameters, with their associated variability and dependency, as shown in analyses N=1, 3, and 4. In our most realistic scenario of the case study (N=6), compared to analysis N=1, we observe an increase in FoS and a reduction in COV_{FoS}.

The influence on PoF was not determined for the work presented in Table 8 as it was 0, meaning that most of the results of FoS were above 1. Therefore, a third group of analyses was performed where a reduction in the strength parameters of the interbedded

sedimentary rock is considered. The reduction was made to study results close to the limit equilibrium and increase the critical slip surface's PoF for the five previous scenarios. For this third group, cohesion is 570 kPa and friction is 31 degrees, considered to be the residual strength of the sedimentary rock based on work at the University of British Columbia and the University of Alberta. It was assumed that the variability and correlation are those estimated previously for Group 2 (Table 7).

The results using parameters from this new Group 3 are shown in Table 9. From the univariate distribution analyses, it is observed that although the mean FoS has not changed, PoF and COV_{FoS} are increasing as more variability is considered in m_i. However, from the bivariate distribution analyses, it is observed that FoS is reduced, PoF increased, and COV_{FoS} is reduced as more variability is considered in m_i.

The result obtained in Slide2 for N=6 and parameters from Group 3 is shown in Figure 34. It is interesting to note that PoF increases from 19.59% in N=1 to more than 30% for analysis N=6, being the latter close to the real case scenario. In RBD criteria, like those presented by Macciotta et al. (2020), a PoF of 30% might represent the limit PoF for a structure of very low consequence but very high design reliability. It is also observed that COV_{FoS} decreases for the scenarios with correlation coefficient in the Hoek-Brown strength parameters. Therefore, considerations of the adequacy of selecting the equivalent Mohr-Coulomb parameter and the correlation between cohesion and friction could easily influence the acceptability of a design.

It is important to mention that LEA approaches would not capture the complexities of progressive failure in rock and coalescence of discontinuities to develop a kinematically

admissible failure mode; however this exercise illustrates the influence of uncertainty in the commonly adopted LEA for the design of open pit slopes.

Table 9: Summary of results of FoS, PoF, and COV_{FoS} (Group 3)

Case N	Variability	Failure criterion	Group 3 FoS det = 1.08		
			FoS	PoF	COV_{FoS}
1	ln σ_{ci} (COV=0.4)	Mohr-Coulomb	1.05	19.6%	0.06
3	ln σ_{ci} (COV=0.4) and m_i (COV=0.4) ($\delta_{\sigma m}$=0)	Mohr-Coulomb	1.05	22.1%	0.06
4	ln σ_{ci} (COV=0.4) and m_i (COV=0.8) ($\delta_{\sigma m}$=0)	Mohr-Coulomb	1.05	25.8%	0.07
5	ln σ_{ci} (COV=0.4) and m_i (COV=0.4) ($\delta_{\sigma m}$=-0.9)	Mohr-Coulomb	1.03	28.7%	0.06
6	ln σ_{ci} (COV=0.4) and m_i (COV=0.8) ($\delta_{\sigma m}$=-0.9)	Mohr-Coulomb	1.02	33.0%	0.06

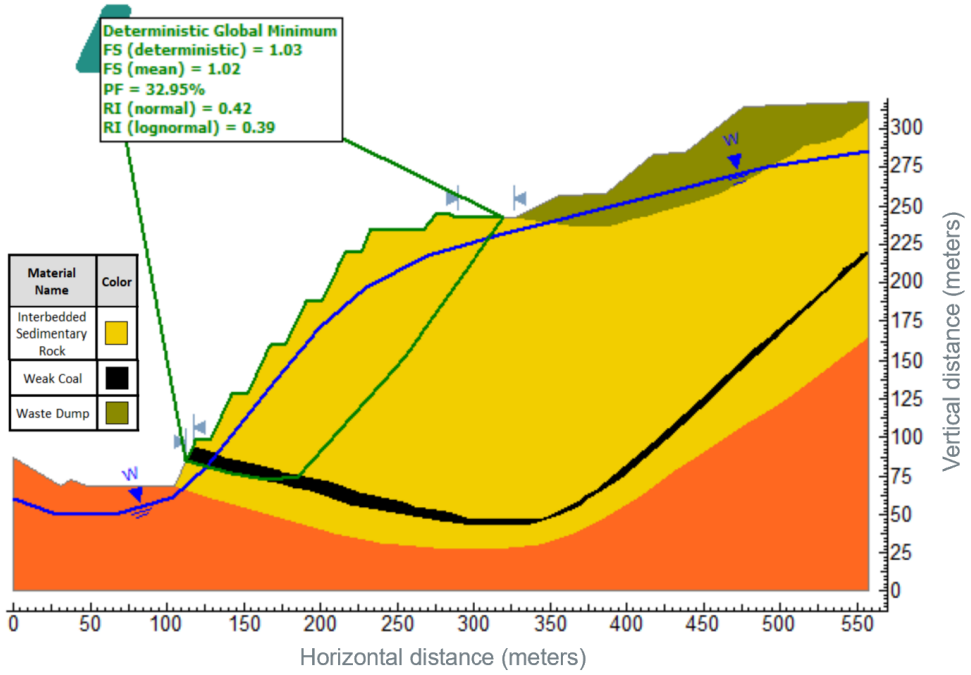

Figure 34: Mean FoS estimated in Slide N=6 with parameters from Group 3

3.7 Conclusion

This paper examines the variability of rock mass strength as modelled by the Hoek-Brown failure criterion and equivalent Mohr-Coulomb strength parameters based on the relationships provided by Hoek et al. (2002) and Rafiei and Martin (2019). The work is completed for a sedimentary rock at an open pit in Western Canada. Variability was initially associated with the Unconfined Compressive Strength, σ_{ci}. Subsequently, the variability was based on the equivalent Mohr-Coulomb parameters following the criteria presented by Rafiei et al. (2019) by using any of the two relationships indicated previously, and through Monte Carlo simulations. Univariate and bivariate distribution analyses were performed, considering σ_{ci} and m_i as random variables.

The results show that different trends in the variability of the equivalent cohesion and friction angle are associated with variability in σ_{ci} and m_i and the dependency between these parameters. Additionally, the study shows that the equivalent cohesion and friction angle form an output of bivariate distributions having an inherent correlation coefficient derived from the equation adopted to estimate the equivalent parameters. Also, it was observed that as the GSI decreases or the confining stress increases, the inherent correlation coefficient increases from negative values to positive values.

PSSA on a pit slope based on a real case study shows that equivalent parameters from Rafiei and Martin (2019) provide similar results compared to a PSSA using the original Hoek-Brown failure criterion. Also, it was observed that the inherent correlation coefficient has a significant effect on the calculated FoS, PoF, and COV_{FoS}. Results considering strength parameters close to limit equilibrium showed that the PoF increased when the

variability of the rock mass adopts bivariate distributions and the associated dependency of these parameters.

The differences found in FoS, PoF, and COV_{FoS} indicate that assumptions on correlation coefficient in strength parameters and the approaches to estimate the equivalent cohesion and friction can alter results in stability calculations that can make the difference between acceptable and unacceptable designs when adopting RBDAC. Our results are consistent with Rafiei and Martin (2019) relationships for equivalent Mohr-Coulomb parameters providing adequate results when compared to analyses that adopt the Hoek-Brown strength envelope. Nevertheless, more model uncertainty is added when using equivalent Mohr-Coulomb parameters for stability calculations derived from an original Hoek-Brown criterion. This would remain true whether Hoek et al. (2002) or Rafiei and Martin (2019) relationship are being used. Moving forward, it is recommended to model the variability in rock mass strength using the Hoek-Brown failure criterion, which will require software that supports the consideration of cross-correlation between the Hoek-Brown strength parameters.

It is important to mention that LEA approaches would not capture the complexities of progressive failure in rock and coalescence of discontinuities to develop a kinematically admissible failure mode; however, this exercise illustrates the influence of uncertainty, and how uncertainty is included in the analysis, in the commonly adopted LEA for the design of open pit slopes. In this regard, the practitioner needs to consider the plausible failure modes, the limits of LEA and the treatment of uncertainty when interpreting the results of a stability analysis in the commonly adopted LEA for open pit slopes.

4. Testing the Application of Reliability-Based Design Acceptance Criteria for Open Pit Slopes

This chapter was submitted for publication under the title *Testing the Application of Reliability-Based Design Acceptance Criteria for Open Pit Slopes* in the Geotechnical and Geological Engineering Journal on October 5th, 2023.

4.1 Introduction

Design Acceptance Criteria (DAC) have been proposed for open pit slopes to assess the adequacy of designs for both deterministic and probabilistic slope stability analysis (DSSA and PSSA, respectively). Some DACs focus solely on Factor of Safety (FoS) and Probability of Failure (PoF), as presented by Priest and Brown (1983), Swan and Sepulveda (2000), and Wesseloo and Read (2009) in the Guidelines for Open Pit Slope Design. Some consider the risk of the structure through the potential consequence of failure, including Adams (2015), Wesseloo and Read (2009), Gaida et al. (2021). A RBDAC approach presented by Macciotta et al. (2020), evaluates design reliability with simplified guidance on engineering effort in the design and data availability, and links the FoS and PoF targets by analyzing the resulting Coefficient of Variation (COV) of the FoS from PSSA (COV_{FoS}). The method was inspired by the work of Meyerhof (1970), Lambe (1985), and Silva et al. (2008), linking design reliability, FoS, and PoF for civil and mining earth structures.

This paper aims to evaluate the application of the RBDAC proposed by Macciotta et al. (2020). The study is conducted on an idealized configuration of an open pit based on an implemented pit slope previously reported by Valdivia and Macciotta (in press). The

RBDAC proposed by Macciotta et al. (2020) allows direct and simple comparisons of FoS and/or PoF results. However, the parametric study in this paper dives into the details of evaluating parameter and epistemic uncertainty as part of stress testing the proposed RBDAC matrix. Three different levels of design reliability (low, moderate, and high) are evaluated to explore different areas of the RBDAC matrix. These different reliability levels are created by utilizing diverse scenarios that account for the expected level of uncertainty in each design reliability level. These scenarios are inspired by the geotechnical, geological, and hydrological characteristics of the implemented pit slope.

4.1.1 DAC in terms of design reliability for open pit slopes

Macciotta et al. (2020) have proposed a RBDAC for operating open pit slopes, which builds upon the previous DAC proposed by Wesseloo and Read (2009) in the Guidelines for Open Pit Slope Design. The proposed RBDAC matrix is shown in Figure 35 and illustrates the relationship between FoS and PoF for different categories of the economic consequence of failure and design reliability. Target FoS and PoF vary depending on the level of design reliability and failure consequence. A higher reliability level corresponds to a reduction in the minimum required FoS, accompanied by an increase in the maximum allowable PoF. This adjustment reflects the understanding that as design reliability increases, there is a decrease in epistemic uncertainty (Macciotta et al. 2020). The matrix defines the pairs of FoS and PoF through mathematical correlations for values of COV_{FoS} adopting lognormal and normal distributions (in parenthesis).

The ranges of PoF in the matrix span from less than 5% to 30%, which is consistent with the annual PoF reported for open pits by Steffen et al. (2006). These ranges are in alignment with previous findings reported by Meyerhof (1970) and Lambe (1985).

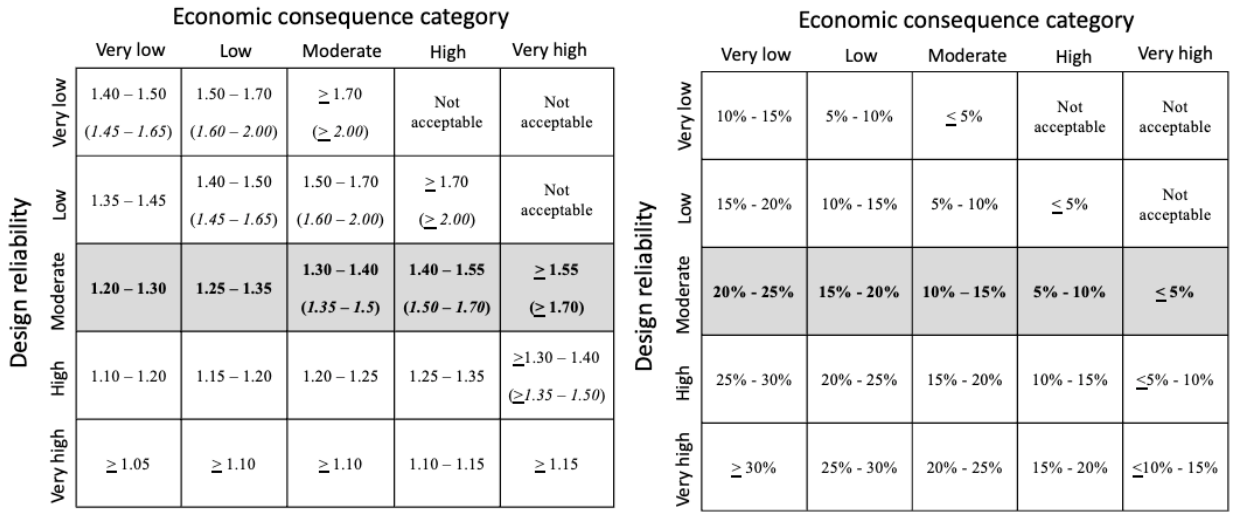

Design reliability \ Economic consequence category	Very low	Low	Moderate	High	Very high
Very low	1.40 – 1.50 (*1.45 – 1.65*)	1.50 – 1.70 (*1.60 – 2.00*)	≥ 1.70 (≥ *2.00*)	Not acceptable	Not acceptable
Low	1.35 – 1.45	1.40 – 1.50 (*1.45 – 1.65*)	1.50 – 1.70 (*1.60 – 2.00*)	≥ 1.70 (≥ *2.00*)	Not acceptable
Moderate	**1.20 – 1.30**	**1.25 – 1.35**	**1.30 – 1.40 (*1.35 – 1.5*)**	**1.40 – 1.55 (*1.50 – 1.70*)**	**≥ 1.55 (≥ 1.70)**
High	1.10 – 1.20	1.15 – 1.20	1.20 – 1.25	1.25 – 1.35	≥1.30 – 1.40 (≥*1.35 – 1.50*)
Very high	≥ 1.05	≥ 1.10	≥ 1.10	1.10 – 1.15	≥ 1.15

Design reliability \ Economic consequence category	Very low	Low	Moderate	High	Very high
Very low	10% - 15%	5% - 10%	≤ 5%	Not acceptable	Not acceptable
Low	15% - 20%	10% - 15%	5% - 10%	≤ 5%	Not acceptable
Moderate	**20% - 25%**	**15% - 20%**	**10% – 15%**	**5% - 10%**	**≤ 5%**
High	25% - 30%	20% - 25%	15% - 20%	10% - 15%	≤5% - 10%
Very high	≥ 30%	25% - 30%	20% - 25%	15% - 20%	≤10% - 15%

Figure 35: Proposed design acceptance criteria for open pits slopes (Macciotta et al., 2020, with permission)

4.1.2 Rock Strength Variability (RSV)

RSV can be described by two key aspects: parameter variability and parameter correlation. Parameter variability refers to the range of variation exhibited by any (strength) parameter associated with the rock mass. In the context of rock slopes and open pits, these parameters typically correspond to the failure criteria of Hoek-Brown or the equivalent Mohr-Coulomb (Hoek et al. 2002). Each parameter of these failure criteria can be represented as a univariate distribution (random variable), meaning it is described by a specific probability distribution. However, relying solely on univariate distributions may overlook the interdependencies that exist between parameters. To account for these dependencies, bivariate or multivariate distributions are necessary. These statistical analyses require parameter correlation to capture the relationship between random variables. Valdivia and Macciotta (in press) summarized some works related to PSSA in open pit and rock slopes highlighting that variability expressed through the Hoek-Brown failure criterion can also be translated into the equivalent Mohr-Coulomb failure criterion following previous works by Rafiei and Martin (2019) and Rafiei et al. (2019). However, it

is important to consider an inherent correlation coefficient between equivalent cohesion and friction angle that stems from the expressions used to calculate equivalent Mohr-Coulomb parameters from Hoek-Brown parameters. In PSSA, considering this inherent correlation becomes important to ensure the consistency of PSSA results between the Hoek-Brown and equivalent Mohr-Coulomb approaches.

The considerations mentioned earlier regarding strength parameter variability and the correlation between parameters can be used to develop models of rock units with homogeneous strength parameters, which vary for each simulation in a PSSA. However, the strength parameters of the rock mass exhibit variability throughout the rock slope space. The spatial variability of strength can be modelled through random field generation techniques. A parameter called the spatial correlation length (θ) is used to determine how similar the strength parameters are between samples in different locations. When the distance between two different locations is below θ, it means that the strength parameter values are close to each other. The closer they are, the stronger the relationship between them.

Previous works on spatial variability have been reported in soil slopes by Griffiths and Fenton (2004), Griffiths et al. (2009), Javankhoshdel et al. (2016), and Javankhoshdel et al. (2023), among others. However, there are relatively few publications specifically focusing on rock slopes and open pits, such as the works reported by Rafiei et al. (2019), and Duran (2019), which indicate that PoF experiences a drastic decrease, from approximately 20% to less than 1%, when spatial variability is considered in PSSA for rock slopes. This observation is consistent with previous findings reported in soil slopes, particularly when the ratio between the spatial correlation length (θ) and the height of the

slope (H) is below one order of magnitude. This finding has particular relevance for open pit designs that involve excavations greater than 150 m. Additionally, although the available information is limited, Prakoso (2002) has reported that the spatial correlation length of strength parameters in rocks may vary between 0.5 m and 1.5 m. The results presented by Rafiei et al. (2019), and Duran (2019) have drawn attention not only to the reduced PoF when spatial correlation is considered, but also to its influence on COV_{FoS} as well as the position of the results within the DAC proposed by Macciotta et al. (2020).

4.2 Open pit slope case study

The open pit slope considered in this study is a modified slope based on a case study previously described by Valdivia and Macciotta (in press) and reported in the works of Barnett et al. (2017) and Clayton et al. (2020). The case study focuses on an open pit located in southeastern British Columbia, Canada, specifically in the Elk Valley Coalfield. The geological characteristics of the research site involve the presence of two formations: the Mist Mountain Formation and the Moose Mountain Formation. These formations are part of the Kootenay Group, which is a geological period spanning from the Lower Jurassic to the Lower Cretaceous (Grieve and Price, 1987).

A cross-section of the referenced case study under operating conditions is shown in Figure 36. The modified open pit slope being studied is shown in Figure 37. The base cross-section used in this study adopts certain characteristics of the case study that include the lithologic units, coal seams, main geometry of the pit wall, and a steeply dipping fault, as reported by Clayton et al. (2020). However, one geological structure, specifically the reverse fault, was excluded from the original profile to focus on failure modes that involve structural control and rock mass strength rather than structural control

exclusively. In terms of parameter variability, the strength parameters of certain geological materials are treated as random variables, including the Mist Mountain Formation (also defined as the Interbedded Sedimentary Rock), the west fault, and the competent and weak coal. On the other hand, the strength parameters of the waste Dump and the Moose Mountain Sandstone are considered constant variables since they do not impact the determination of the critical slip surface with the minimum FoS, as per a preliminary analysis performed on the modified open pit slope.

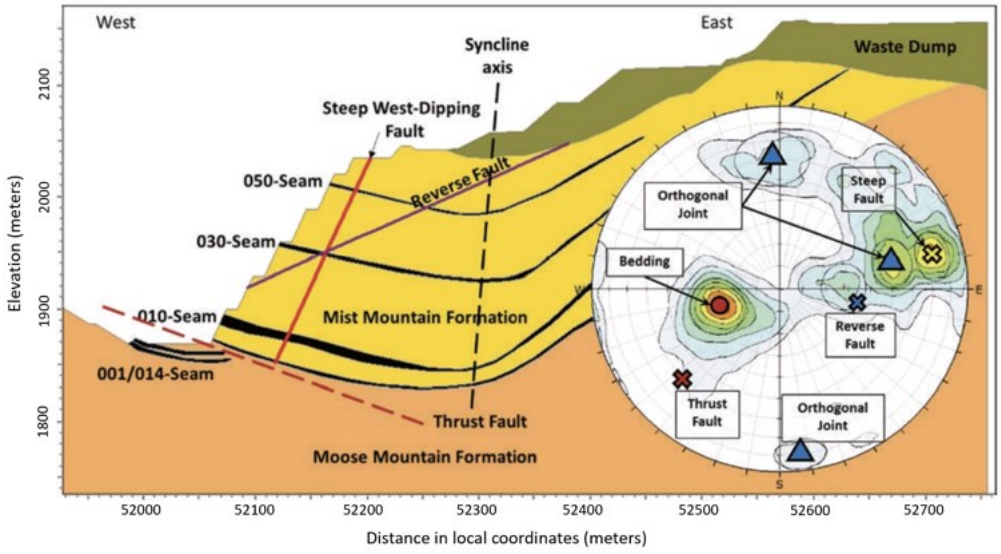

Figure 36: Cross section of the case study (Clayton et al. 2020, with permission)

The piezometric elevation depicted in the profile represents a constant and plausible level for operating conditions based on the case study. Additionally, there is a slight increase in the Mohr-Coulomb strength parameters of the competent coal, weak coal, and the west fault compared to the values reported by Clayton et al. (2020). This increment in the strength parameters is intended to establish a stable slope under operating conditions, without altering the original geometry of the open pit slope. Given this slope corresponds to the final configuration (final pushback), the study considers that the economic

consequence of inter-ramp or overall failure would be moderate or less and the design could be more aggressive.

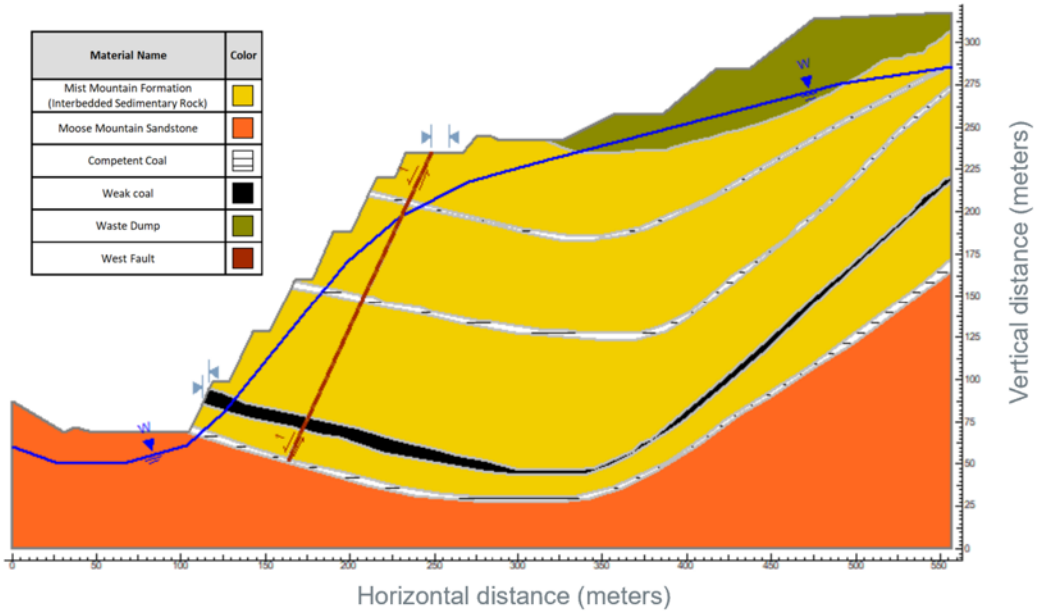

Figure 37: Cross section of modified open pit slope

A summary of the strength parameters and their corresponding COV is presented in Table 10. It should be noted that this information pertains to parameters with high reliability based on expected COV values from the authors' experience. The strength parameters for the Interbedded Sedimentary Rock are expressed in terms of equivalent Mohr-Coulomb parameters and were previously reported by Valdivia and Macciotta (in press). Table 10 also summarizes COV values for the equivalent cohesion and friction angle (referred to as COV_c and COV_φ) as well as the correlation coefficient between them ($\delta_{c\varphi}$). These COV values are estimated using Monte Carlo simulations based on the relationship proposed by Rafiei and Martin (2019), which allows for the estimation of variability in Mohr-Coulomb strength parameters from Hoek-Brown strength parameters. Definition of the Hoek-Brown strength parameters and COV values were presented in

Valdivia and Macciotta (in press). COV for the Unconfined Compressive Strength (σ_{ci}) is set at 0.4 (referred to as $COV_{\sigma ci}$), COV of the parameter m_i (referred to as COV_{mi}) is 0.8 considered as twice $COV_{\sigma ci}$ following the results presented by Zhang et al. (2018). Furthermore, there is a strong negative correlation coefficient ($\delta_{\sigma m}$) of -0.9 between these two parameters (Refer to Valdivia and Macciotta, in press). The height (H) and the slope angle (β) used in the relationship proposed by Rafiei and Martin (2019) are 150 m and 52 degrees, respectively. The random variables are assigned lognormal distributions according to Prakoso (2002), Zhang et al. (2018), and Rafiei et al. (2019). For the West Fault, COV for the Mohr-Coulomb strength parameters is defined solely based on literature. It should be noted that lognormal distributions are also employed for the Mohr-Coulomb strength parameters of all materials considered as random variables in the analysis.

Table 10: Summary of strength parameters based on Mohr-Coulomb failure criteria - high reliability in parameters

Material	γ (kN/m^3)	Cohesion (kPa)	COV_c	Friction (degrees)	COV_φ	$\delta_{c\varphi}$
Interbedded sedimentary rock	26	982	0.66	57	0.13	-0.91
Competent coal	17	50	0.66	30	0.12	-0.90
Weak coal	17	50	0.48	24.5	0.10	-0.85
West Fault	-	30	0.35	20	0.25	-0.50

γ: unit weight
note 1: COV estimated with $COV_{\sigma ci}$ at 0.4, COV_{mi} at 0.8, and $\delta_{\sigma m}$: -0.90 in all materials.
note 2: All the other parameters not indicated can be found in Valdivia and Macciotta (in press).

4.3 Methodology for evaluating the open pit slope in the RBDAC

A parametric study is conducted to evaluate the slope configuration and test the applicability of the RBDAC matrix proposed by Macciotta et al. (2020) for different design reliability levels. The workflow is presented in Figure 38.

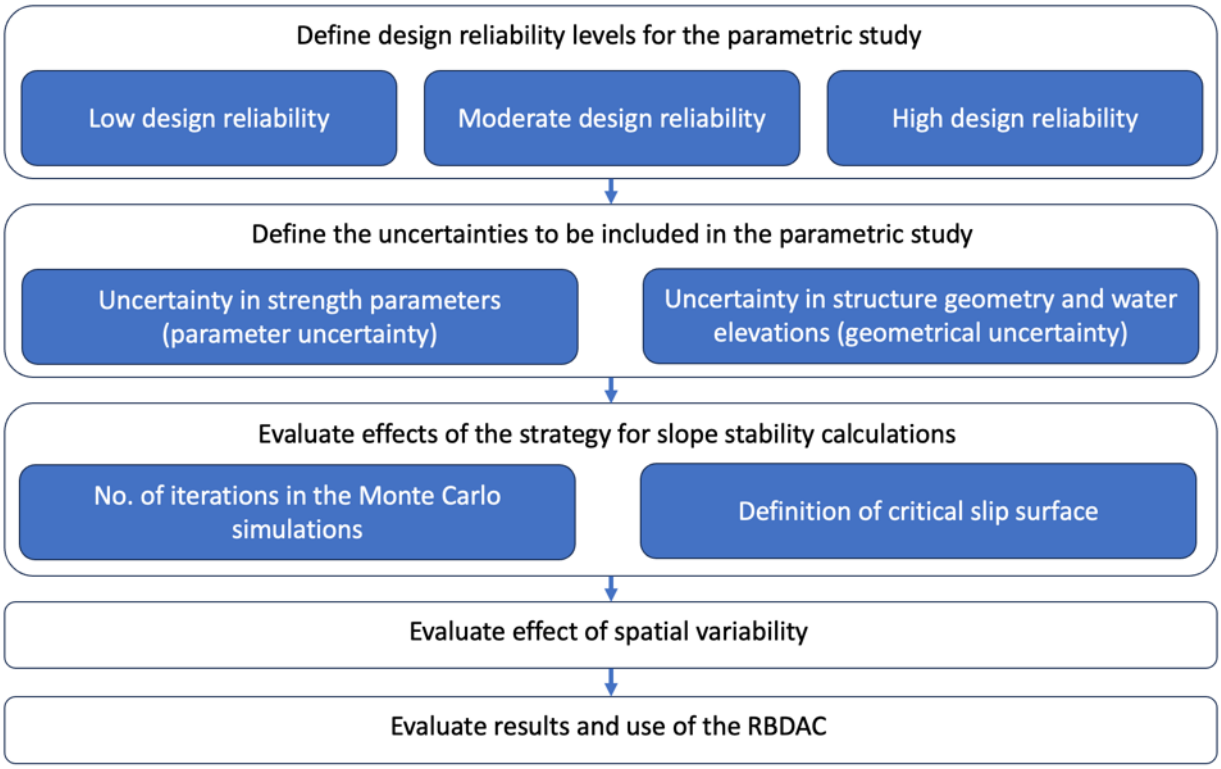

Figure 38: Workflow chart for the case study

We first establish the different levels of design reliability (low, moderate, and high) for the modified open pit case study. Both parameter and geometrical uncertainty are considered, the first through strength inputs as probability density functions and the second as models where structural geometry (dip of major structures) is varied to simulate uncertainty in structural models. The latter also considered the position of the piezometric level in the models, in an explicit manner. Therefore, the differentiation between each reliability level is based on the magnitude of uncertainty in the parameter inputs and

variability of the structural and piezometric characteristics. Combining the results from models with different structure geometry and piezometric levels generated an aggregated result set referred to as the global result. This approach weighted the different structure geometries equally, with a similar approach followed by the variation in piezometric elevation for the models.

The results obtained from the global scenario were contrasted with those obtained from the mean scenario (geometry of discontinuities and piezometric elevation corresponding to the original case, assumed here to correspond to the highest model reliability). The mean scenario would also represent the common approach to PSSA in open pit design. The mean scenario considered a dip of 14 degrees for the coal seam, a dip of 65 degrees for the fault, and the piezometric elevation at operating conditions (as shown in Figure 37). A summary of the test models is presented in Table 11. We reiterate this is not required for the application of the RBDAC matrix, and we adopt it to stress test the matrix under a variety of uncertainty scenarios.

Prior to the parametric study, it was necessary to assess the influence of the number of realizations in the probabilistic analysis using Monte Carlo simulations. This was done by running models through 1000 and 10 000 iterations and comparing the resulting distribution of FoS. Similar results would suggest that representative FoS distributions for the model would have been reached by 1000 iterations. Furthermore, the PSSA calculation allowed to iterate for the critical slip surface for each iteration, or to define a critical slip surface for the mean parameters and fix the slip surface for all other iterations (significantly reducing the computational effort). Models were run for the fixed critical slip surface and for the iteration-specific slip surface search to evaluate the need for the

computation effort associated with generating iteration-specific critical slip surfaces. These tests were only conducted in the mean scenario, without variation in the geometry, and for each design reliability level. We also investigate the effect of modelling spatial variability in the high design reliability, mean scenario.

Results of each scenario are presented as histograms to illustrate the distribution of FoS and fitted to common probability density functions (PDF) (e.g. normal and log-normal distributions). The Kolmogorov-Smirnov test (KS test) and q-q plots were used to evaluate the goodness-of-fit of the PDF to the results. Finally, the results were plotted in the RBDAC matrix.

Table 11: Summary of test models

Design Reliability	**Mean Scenario**	**Global scenario**		
		Variable coal dip	**Variable coal and fault dip**	**Variable coal dip, fault dip and piezometric elevation**
Low	1 scenario	3 scenarios (Coal dip 8, 14, and 20 degrees)	15 scenarios (Fault dip 55, 60, 65, 70, and 75 degrees)	45 scenarios (Lower, average, and upper piezometric elevation)
Moderate	1 scenario	3 scenarios (Coal dip 8, 14, and 20 degrees)	9 scenarios (Fault dip 60, 65, and 70 degrees)	Not applicable
High	1 scenario	Not applicable	Not applicable	Not applicable

4.3.1 Design reliability scenarios

The profile of the high design reliability level is presented in Figure 37. Only one scenario is evaluated due to the expected reduced epistemic uncertainty. Parameter uncertainty is mainly attributed to the natural variability of the parameters indicated in Table 10. In terms of geometrical uncertainty, the piezometric elevation is assumed as known with high reliability (seasonal fluctuations are out of the scope of this work). The dip of the coal and fault at 14 and 65 degrees, respectively, are assumed well-established at this level of design reliability. The fault was modeled as fully persistent.

For the moderate design reliability level, a total of 9 scenarios are evaluated. Parameter uncertainty includes both natural variability and epistemic uncertainty. Consequently, COV values reported in Table 10 were increased with some modifications to the strength parameters (Table 12) based on the authors' experience and reported COV values in literature (Valdivia and Macciotta, in press). In terms of geometrical uncertainty, the piezometric elevation is assumed as known with high reliability. The coal dip varies across the scenarios, with angles of 8, 14, and 20 degrees. The fault dip is also varied with angles of 60, 65, and 70 degrees. This assumes that epistemic uncertainty in structural geometry at the moderate design reliability level could be approximated as +/- 6 degrees for the coal dip and +/- 5 degrees for the fault. It is acknowledged this is an oversimplification of epistemic uncertainty in practice, however, attempts to evaluate the order of magnitude of the impact of the structure geometry in PSSA and the use of an RBDAC.

For the low design reliability level, a total of 45 scenarios are evaluated. Similar to the moderate design reliability, there is a variation in parameters and an increase in their COV (Table 13). This reliability level assumes there is no distinction between competent coal

and the weaker coal, and only the parameters for the competent coal are considered. Two additional geometries for the piezometric elevation are considered, representing plausible higher and lower piezometric elevation conditions. The range of coal dip angles remains the same as in the moderate reliability level. However, the fault dip angles are expanded to include 55, 60, 65, 70, and 75 degrees. Similar to the moderate level, all scenarios (piezometric elevations and structure geometries) share the same Probability of Occurrence (POO).

It is important to acknowledge that, in reality, it is not possible to estimate all sources of epistemic uncertainty for a design. The ones mentioned above are the most common and have a plausible range of variation for the considered levels of reliability. The aim is to investigate the influence of epistemic uncertainty, although in a simplified manner, in the COV_{FoS}.

A summary of the strength parameters, COV_c, COV_φ, and $\delta_{c\varphi}$ is presented in Table 12 and Table 13 for the moderate and low design reliability, respectively. These follow the same criteria described previously for the high reliability level. However, for the low design reliability, it is assumed that there is no correlation adopted between σ_{ci} and m_i for the interbedded sedimentary rock and competent coal, reflecting the lack of knowledge at those reliability levels. Nevertheless, although they follow a pair of univariate distributions in Hoek-Brown failure criteria, there will still be a correlation between the equivalent cohesion and friction angle given the expressions used to calculate their equivalency, as indicated by Valdivia and Macciotta (in press). This is included in Table 13. The moderate and low design reliability models consider the fault is not fully persistent, with 10 m trace lengths followed by 10 m of rock mass.

Table 12: Strength parameters – moderate design reliability

Material	γ (kN/m^3)	Cohesion (kPa)	COV_c	Friction (degrees)	COV_φ	$\delta_{c\varnothing}$
Interbedded sedimentary rock (note 1)	26	635	0.705	54	0.14	-0.91
Competent coal (note 2)	17	50	0.820	33	0.16	-0.90
Weak coal (note 2)	17	40	0.636	23	0.13	-0.85
West Fault	-	40	0.45	23	0.35	-0.50

γ: unit weight
note 1: COV estimated considering σ_{ci} equal to 42 MPa and $COV_{\sigma ci}$ equal to 0.45
note 2: COV estimated considering $COV_{\sigma ci}$ equal to 0.50
note 3: COV_{mi} is twice $COV_{\sigma ci}$ and $\delta_{\sigma m}$: -0.90 in all materials.

Table 13: Strength parameters – low design reliability

Material	γ (kN/m^3)	Cohesion (kPa)	COV_c	Friction (degrees)	COV_φ	$\delta_{c\varnothing}$
Interbedded sedimentary rock (note 1)	26	610	0.52	54	0.19	-0.25
Competent coal (note 2)	17	50	0.73	36	0.22	-0.45
West Fault	-	80	0.65	28	0.50	-0.50

γ: unit weight
note 1: COV estimated considering σ_{ci} equal to 40 MPa and $COV_{\sigma ci}$ equal to 0.50
note 2: COV estimated considering $COV_{\sigma ci}$ equal to 0.60
note 3: COV_{mi} is twice $COV_{\sigma ci}$ and $\delta_{\sigma m}$: 0 in all materials.

All 55 scenarios were analyzed in slide2 (Rocscience Inc 2013) which is a common tool for designing open pit slope design. The Morgenstern-Price method (Morgenstern and Price, 1965) with non-circular slip surfaces was adopted. Monte Carlo simulation is used for the sampling method in the PSSA.

Prior to the parametric study, and as previously mentioned, initial tests were run to evaluate the influence of the number of realizations in the results of the PSSA and the use of fixed critical slip surfaces versus iteration-specific critical slip surfaces.

4.3.2 Influence of spatial variability for the high design reliability level

This involved five separate analyses, each varying spatial correlation lengths (θ) between 1, 2.5, 5, 10, and 20 m. For simplicity, the sensitivity analysis assumes isotropic θ values that are equal for all materials specified in Table 10. The Mohr-Coulomb failure criterion is used for these analyses due to two reasons: firstly, the current software packages do not account for correlation $\delta_{\sigma m}$ in the Hoek-Brown failure criterion, and secondly, they do not incorporate spatial variability using Hoek-Brown failure criterion. Each scenario in the sensitivity analysis considers 10 000 realizations as well as the variation in the slip surface for each iteration. In addition, another comparison was performed considering 1000 realizations for these 5 analyses in order to evaluate if the use of spatial correlation has an effect on the required number of iterations in PSSA.

4.4 Results and discussion

The resulting distributions of FoS for the different design reliabilities and scenarios tend to a closer fit to a log-normal distribution rather than a normal distribution, for the case study analyzed. However, some FoS outliers were observed. Although these outliers do not critically affect the calculation of mean FoS and PoF, they can affect the visual selection of the optimal statistical distribution. Some outliers are characterized by FoS values near zero, which were tracked to unrealistic stress values along the slip surface. Despite their presence, the authors have chosen not to remove these outliers but to show the results in terms of histograms for the purpose of comparing the performance of other statistical distributions such as normal distributions.

4.4.1 Results of initial tests

4.4.1.1 Number of realizations

A comparison of results using iteration-specific critical slip surfaces for 1000 and 10 000 realizations of the mean scenarios and for each design reliability level is presented in Table 14. A summary of the differences in FoS (ΔFoS), PoF (ΔPoF), and COV_{FoS} (ΔCOV) is also presented in Table 14. Figure 39 shows a comparison of the resulting FoS histograms for the low design reliability. In terms of computational time, the mean scenario considering 1000 realizations with iteration-specific critical slip surfaces takes approximately one hour, while scenarios considering 10 000 realizations require approximately seven hours and a half. These computations were conducted on a computer equipped with an AMD Ryzen 9 5950X 16-Core Processor, and 66GB of RAM, ensuring adequate and sufficient computer resources.

Table 14: Comparison of results using different numbers of realizations in PSSA. 3 decimal places are shown to better show some of the differences

Design reliability	1000 realizations			10 000 realizations			Comparisons		
	FoS	PoF (%)	COV_{FoS}	FoS	PoF (%)	COV_{Fos}	ΔFos	ΔPoF (%)	ΔCOV_{FoS}
Low	1.457	4.00	0.209	1.464	3.75	0.215	0.007	0.25	0.006
Moderate	1.336	1.90	0.189	1.332	2.56	0.198	0.004	0.66	0.009
High	1.151	18.80	0.208	1.148	18.51	0.197	0.003	-0.29	0.011

The results in ΔFoS, ΔPoF, and ΔCOV are very small, indicating that the results are consistent, and the difference is not significant for PSSA. This suggests that the analysis with 1000 realizations exhibits minimal differences compared to the analysis with 10 000

realizations. Therefore, the results obtained using 1000 realizations still demonstrate consistency and can provide reliable insights, even though the analysis with 10 000 realizations offers a more robust statistical sample.

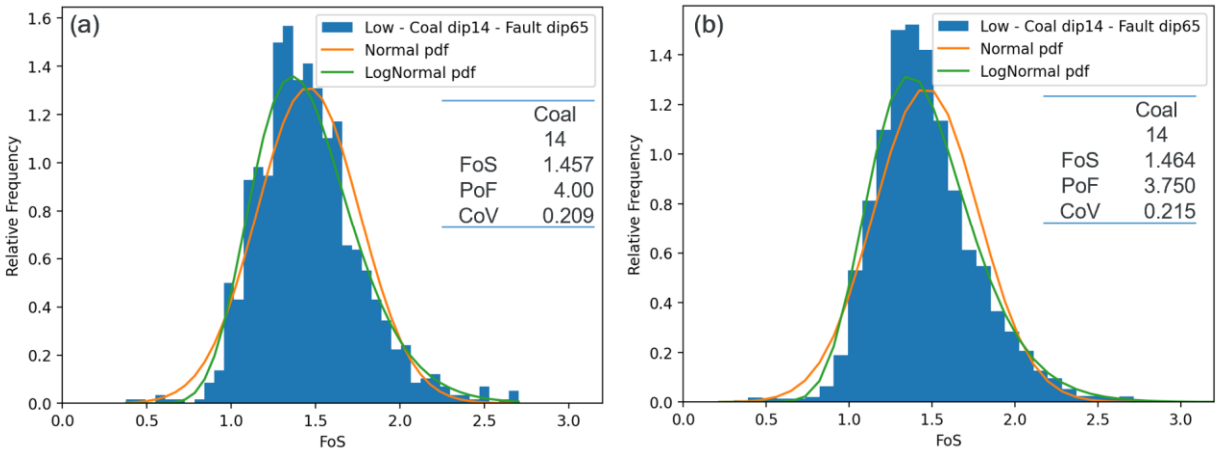

Figure 39: Comparison of histograms for the mean scenario, low design reliability level for (a) 1000 realizations and (b) 10 000 realizations

4.4.1.2 Fixed and iteration-specific critical slip surfaces

The PSSA results for the fixed and the iteration-specific critical slip surfaces are presented in Table 15. For the high design reliability level, a comparison of the resulting histograms is presented in Figure 40. In terms of computational time, each scenario considering 10 000 realizations with the fixed critical slip surface takes less than two minutes to complete. For the iteration-specific analysis, the time required is approximately seven and a half hours, a considerable increase in the computational requirements.

ΔPoF and ΔCOV are significant enough that evaluation of the stability of a slope in terms of FoS and/or PoF could deviate from one approach to the other. Results show lower PoF and COV_{FoS} for each reliability level in the case of the fixed critical slip surface. The difference is attributed to the wide range of slip surfaces between the weak coal and the

competent coal (at the toe of the slope) when iteration-specific critical slip surfaces are evaluated. This contributes to the higher COV_{FoS} compared to that obtained with a fixed critical slip surface.

Importantly, the effect of adopting a significantly less computationally expensive but simplified approach, in our example, leads to an overestimation of the design in terms of PoF and for the low design reliability also in terms of FoS.

Table 15: Comparison of results between adopting fixed and iteration-specific critical slip surfaces in PSSA. 3 decimal places are shown to better show some of the differences

Design reliability	Iteration-specific critical slip surface			Fixed critical slip surface			Comparison		
	FoS	PoF (%)	COV_{FoS}	FoS	PoF (%)	COV_{FoS}	ΔFos	ΔPoF (%)	ΔCOV_{FoS}
Low	1.464	3.750	0.215	1.693	0.098	0.196	0.229	3.652	0.019
Moderate	1.332	2.56	0.198	1.330	0.017	0.080	0.002	2.543	0.118
High	1.148	18.51	0.197	1.124	6.631	0.083	0.024	11.879	0.114

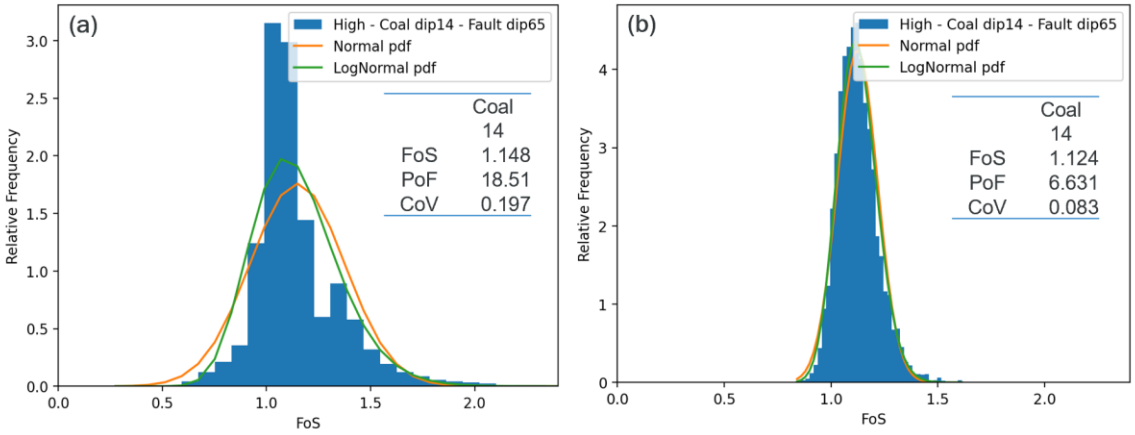

Figure 40: Histogram for the high reliability level (a) iteration-specific critical slip surfaces and (b) fixed critical slip surface

4.4.1.3 Spatial variability

A summary of the results of incorporating spatial variability for the high design reliability scenario is presented in Table 16. The infinite spatial correlation length shown in Table 16 corresponds to the state where spatial variability in strength parameters is not considered and are those results previously presented in Table 14. In terms of computational time, each scenario considering 1000 and 10 000 realizations with different iteration-specific critical slip surfaces and considering spatial variability takes approximately two hours and a half (1000 realizations) and thirteen hours (10 000 realizations) to complete, respectively. Histograms of the results for spatial correlation lengths (θ) of 2.5 m, 20 m, and infinite, and for both 1000 and 10 000 realizations are shown in Figure 41 and Figure 42, respectively.

Table 16: Summary of results considering spatial variability in strength parameters and for the high design reliability model. 3 decimal places are shown to better show some of the differences

Spatial correlation length, m (θ)	1000 realizations			10 000 realizations			Comparison		
	FoS	PoF (%)	COV_{FoS}	FoS	PoF (%)	COV_{Fos}	ΔFos	ΔPoF (%)	ΔCOV_{FoS}
1	1.186	1.6	0.147	1.189	1.7	0.146	0.003	0.1	0.001
2.5	1.203	3.3	0.154	1.207	3.5	0.155	0.004	0.2	0.001
5	1.211	5.8	0.164	1.215	6.0	0.165	0.004	0.2	0.001
10	1.221	9.1	0.178	1.218	9.6	0.179	0.003	0.5	0.001
20	1.209	14.8	0.193	1.214	13.4	0.192	0.005	1.4	0.001
∞	1.151	18.0	0.208	1.148	18.5	0.197	0.003	0.5	0.011

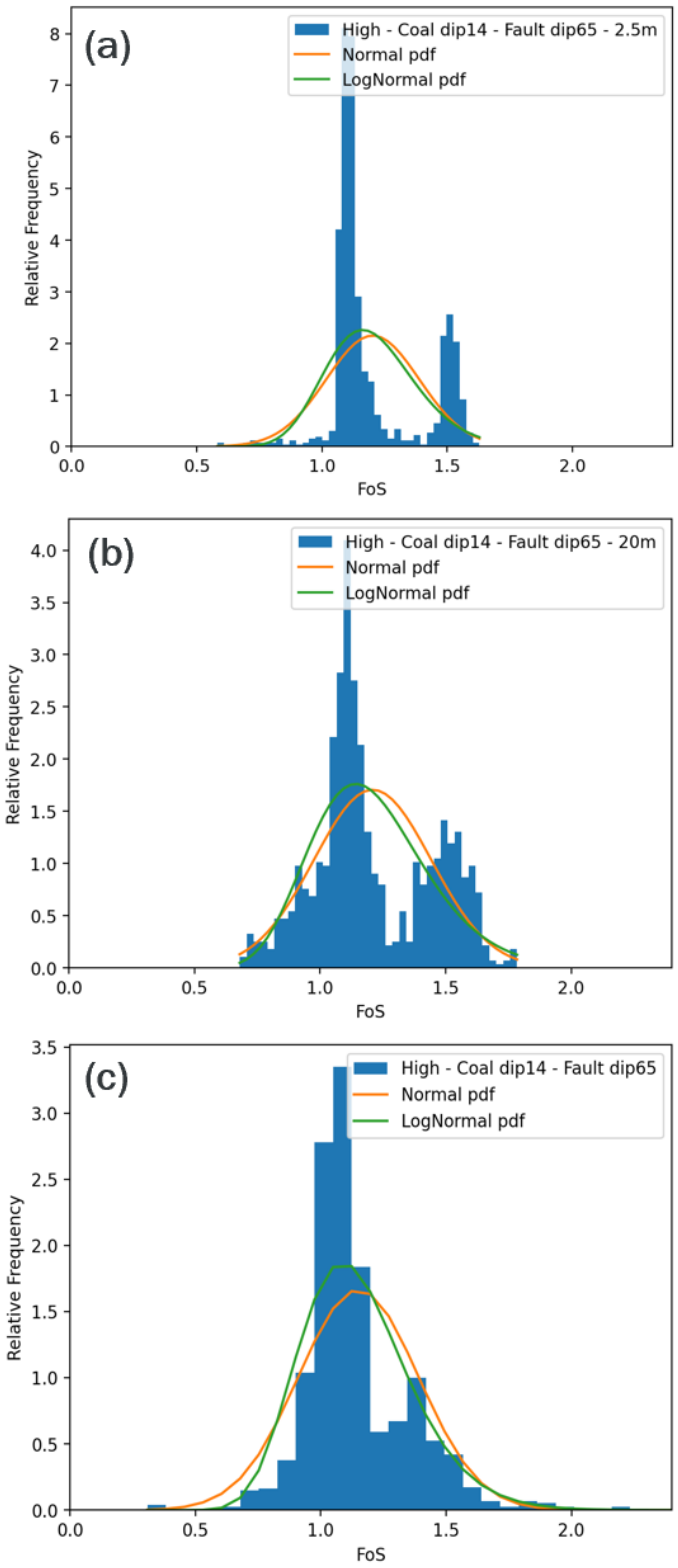

Figure 41: Histograms results for θ (a) 2.5 m, (b) 20 m, and (c) infinite - Analysis with 1000 realizations

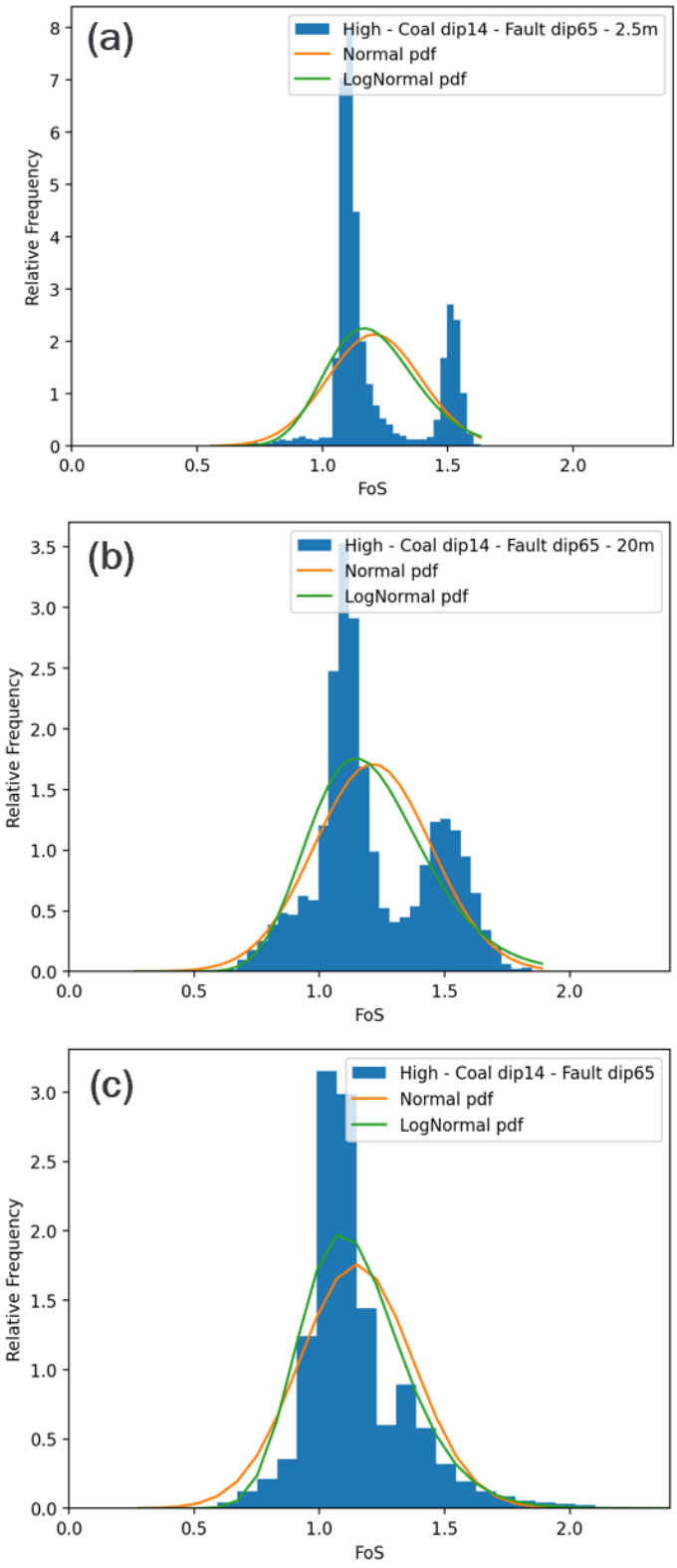

Figure 42: Histogram results for θ (a) 2.5 m, (b) 20 m, and (c) infinite - Analysis with 10 000 realizations

The results for both 1000 and 10 000 realizations exhibit similarities, like those previously observed, suggesting that adopting spatial variability for strength parameters did not influence the required number of realizations for our case study. It is observed that as θ decreases, both COV_{FoS} and PoF decrease. The decrease in PoF is considerable, and the difference between not considering spatial variability and a correlation length of 5m (as an example) could already differentiate between acceptable and unacceptable designs.

Results from the incorporation of spatial variability have a bimodal distribution of resulting FoS, which was not previously observed for the infinite θ case (Figure 41c and Figure 42c). This is attributed to the effect of spatial correlation in the development of the critical slope surfaces leading towards two failure modes (depending on the realization) for the case modelled in this study.

The results of the different slip surfaces and FoS values for spatial correlation lengths (θ) of 2.5 m, and infinite, and for 1000 realizations are shown in Figure 43. For the case of θ equal to infinite, two failure mode are observed. One is observed daylighting through the weak coal and the second one through the competent coal. It is also observed that these slip surfaces are somewhat evenly distributed within an area in the open pit slope section. For the case of θ equal to 2.5 m, these slip surfaces clearly show the two failure modes (clustering of FoS results between 1.0 and 1.1 - in yellow according to the legend - and FoS results between 1.4 and 1.5 - in purple). This is consistent with the observation of value of COV_{FoS} for the high design reliability level for iteration-specific critical slip surfaces compared to the fixed critical slip surface (Table 15). This result highlights the

importance of properly capturing spatial variability for the evaluation of potentially different failure volumes.

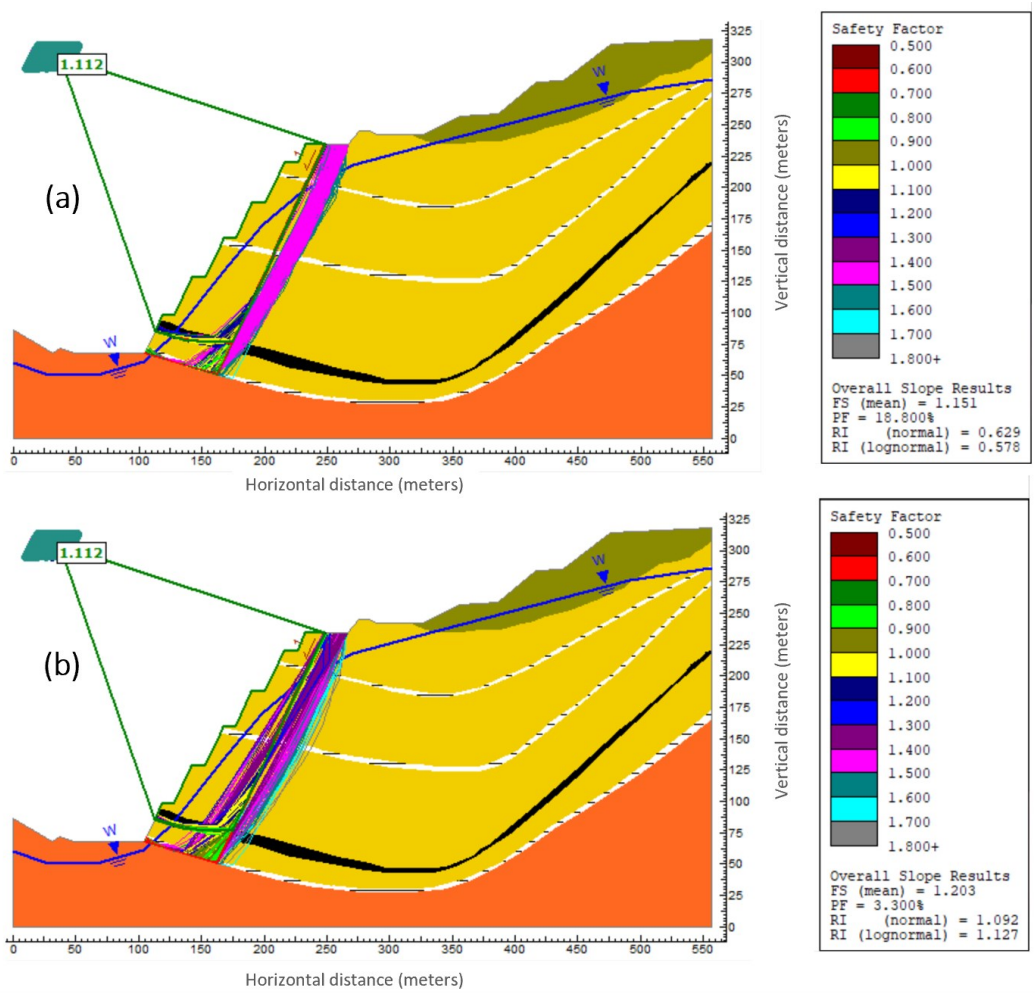

Figure 43: FoS results for θ (a) 2.5 m and (b) infinite - Analysis with 1000 realizations

The results for 10 000 realizations considering spatial variability are also shown in the RBDAC matrix in Figure 44. The arrow indicates the direction of the results as spatial correlation length increases. The data in terms of FoS increase from θ equal to 1 m to 10 m, then it slightly decreases for θ equal to 20 m to infinite (no spatial correlation). In terms of PoF, PoF increases as θ increases. Interestingly, considering the potential for a large multi-bench failure, these results would have not been acceptable if the economic

consequences had been considered higher and either the reliability in design would need to be increased through further engineering effort, or the slope configuration changed.

Finally, it is important to note that these analyses considering spatial variability are limited to the use of Mohr-Coulomb criterion due to the current software package limitations. These limitations introduce more model uncertainty as they do not consider parameter correlation (Valdivia and Macciotta, in press) and spatial variability in the Hoek-Brown failure criterion.

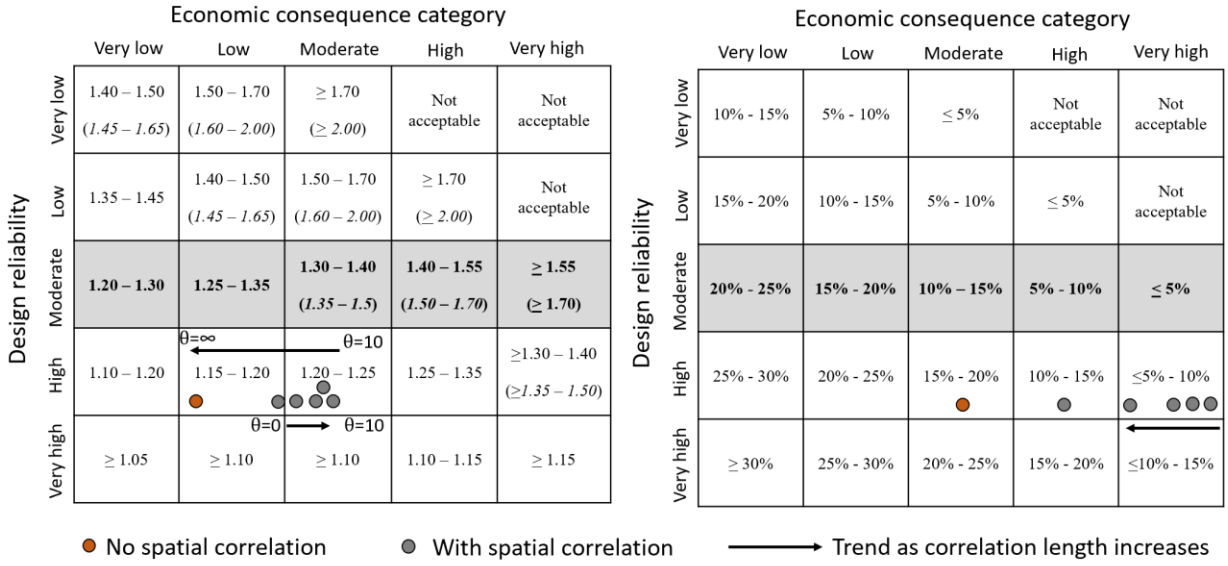

Figure 44: Interpretation of results for 1 000 realizations and iteration-specific critical slip surface when considering spatial variability in the high design reliability scenario. Results plotted on the RBDAC proposed by Macciotta et al. (2020)

4.4.2 Parametric results on different design reliabilities

Results of the parametric analysis for the low, moderate, and high design reliability levels are presented in Figure 45, Figure 46, and Figure 47, respectively. In each figure, the blue contours represent the mean scenario, characterized by a coal dip of 14 degrees, fault dip of 65 degrees, and piezometric elevation at operating conditions. The green bars

represent the global scenario, which combines results from models that vary piezometric elevation and dip of the structures (as applicable for the different design reliability levels). In the low reliability design, the global scenario in Figure 45a represents 3 combinations of coal dip (8, 14, and 20 degrees). The global scenario in Figure 45b represents 15 combinations of coal dip (8, 14, and 20 degrees) and fault dip (55, 60, 65, 70, and 75 degrees). The global scenario in Figure 45c represents 45 combinations, considering the variation of the piezometric elevation (high, average, and low levels) along with the previous 15 scenarios. For the moderate reliability design, the global scenario in Figure 46a represents 3 combinations of coal dip (8, 14, and 20 degrees). The global scenario in Figure 46b represents 9 combinations of coal dip (8, 14, and 20 degrees) and the fault dip (60, 65, and 70 degrees). The result presented for the high reliability level is that considering no spatial variability. Each figure illustrates the result in terms of FoS, PoF, and COV_{FoS}. A summary of these values is also presented in Table 17. It is evident from the global scenario results, in the low and moderate reliability level, that the introduction of additional uncertainties leads to an increase in the COV_{FoS}, as expected. For the low and moderate reliability, the increase in COV_{FoS} is 0.045 and 0.022, respectively, when comparing the mean scenario with the final global scenario.

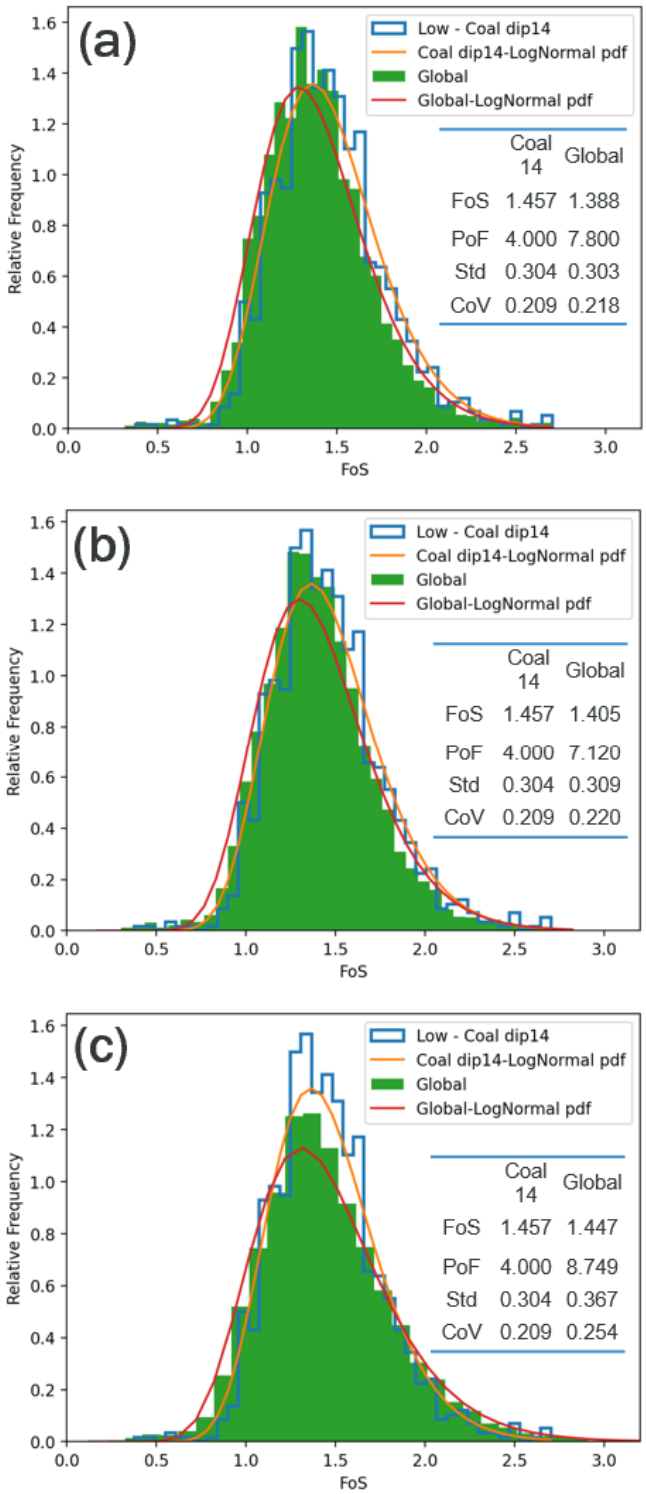

Figure 45: FoS results for the low reliability level: (a) Global results from 3 combinations of the coal dip, (b) Global results from 15 combinations of the coal and fault dip, (c) Global result from 45 combinations of the coal and fault dip and change in the piezometric elevation

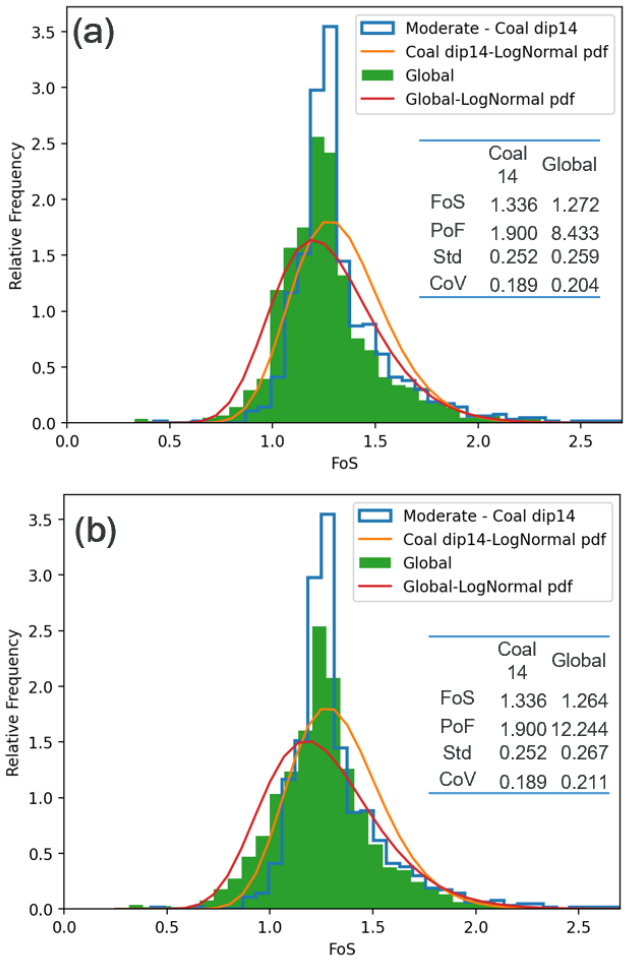

Figure 46: FoS results for the moderate reliability level: (a) Global results from 3 combinations of the coal dip, (6b) Global results from 9 combinations of the coal and fault dip

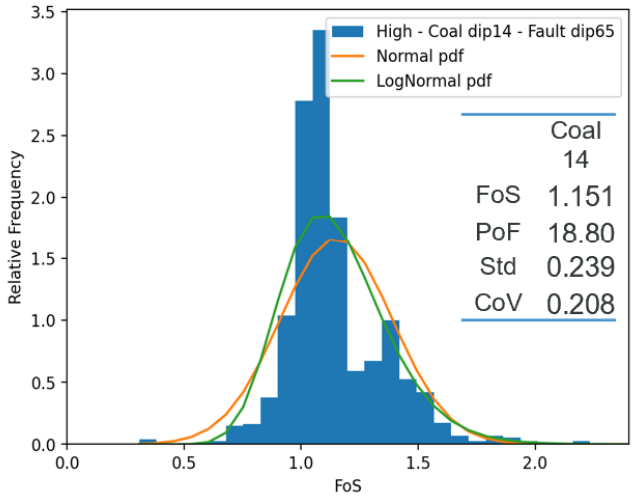

Figure 47: FoS results for the high reliability level

Table 17: Summary of results for the low, moderate, and high reliability for the parametric study. 3 decimal places are shown to better show some of the differences

Design Reliability	Mean Scenario			Global scenario								
				Variable coal dip			Variable coal and fault dip			Variable coal dip, fault dip and piezometric elevation		
	FoS	PoF (%)	COV_{FoS}	FoS	PoF (%)	COV_{FoS}	FoS	PoF (%)	COV_{FoS}	FoS	PoF (%)	COV_{FoS}
Low	1.457	4.00	0.209	1.388	7.800	0.218	1.405	7.120	0.220	1.447	8.749	0.254
Moderate	1.336	1.90	0.189	1.272	8.433	0.204	1.264	12.244	0.211	Not applicable		
High	1.151	18.80	0.208	Not applicable			Not applicable			Not applicable		

These results are plotted in the RBDAC matrix in terms of FoS and PoF as shown in Figure 48. Results have been plotted considering the design reliability as defined when creating the scenarios. Mean scenarios (no epistemic uncertainty modelled) are indicated by unfilled markers, while filled markers indicate results when some epistemic uncertainty is modelled (dip of discontinuities, location of piezometric level). In general, resulting FoS and PoF aligned with expected targets (shaded areas in the matrices). This is due to the design of the parametric study, targeting moderate economic consequences and the design reliabilities mentioned. Small deviations are observed (e.g. FoS for the low design reliability scenarios appears to be lower than recommended by the RBDAC, some PoF for the moderate and low design reliability scenarios appear to be higher than recommended). The arrows in the matrix show the trend of results (when observed) as models included epistemic uncertainty as the geometry of discontinuities and piezometric elevations. These trends were observed for the PoF results, as the FoS did not show variation. This is attributed to the approach to model epistemic uncertainty associated

with structure geometry and piezometric level, where deviations were modelled to both sides of expected (e.g. structure dip variations modelled as expected mean +/- a set value). Although this approach would have balanced FoS iterations, providing for a consistent mean value of FoS, the COV_{FoS} would increase, therefore increasing the resulting PoF.

The observed variation from the mean scenario to the global scenario underscores the importance of considering multiple sources of uncertainty in slope stability assessments. This requires consideration as the variation in results, particularly in terms of PoF, could make the difference between designs that are considered acceptable and those that are not.

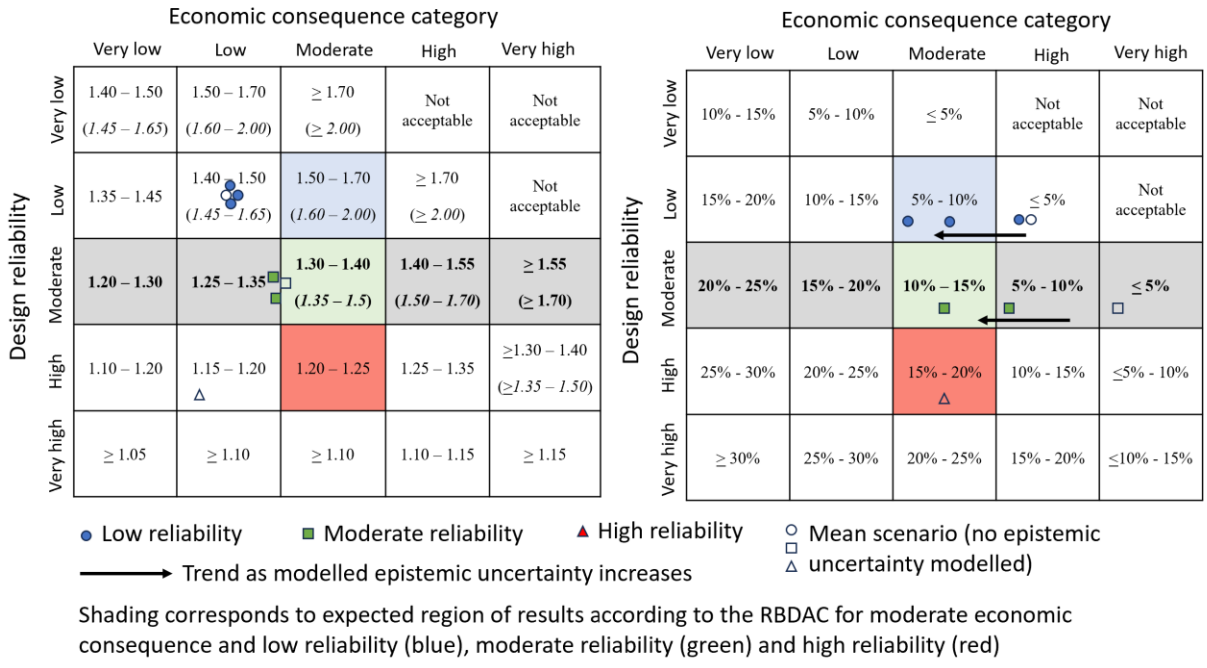

Figure 48: Interpretation of results in the RBDAC proposed by Macciotta et al. (2020) for low (blue), moderate (green) and high (orange) reliability – All scenarios

4.5 Conclusion

This paper presents a parametric study on Probabilistic Slope Stability Analyses (PSSA) in an open pit and its applicability in the RBDAC proposed by Macciotta et al. (2020). The study aims to assess the influence of different sources of uncertainty on PSSA and, consequently, on the proposed RBDAC matrix for different design reliability levels. The adoption of an RBDAC requires slope stability results and an assessment of the reliability of the models used in the analyses, however, this paper develops diverse scenarios of uncertainty to stress-test the applicability of the RBDAC approach. The results from this parametric study also provide insights into the essential considerations necessary to perform PSSA, and further illustrates how to interpret results plotted in the RBDAC matrix.

The design reliability levels considered in the study are low, moderate, and high, each associated with different magnitude of parameter uncertainty, related to the variability in the strength parameters, and geometrical uncertainty, related to the variability in the geometry and piezometric elevation. This variability is taken into account by creating multiple scenarios corresponding to each reliability level. The magnitude of uncertainty is linked with knowledge uncertainty, with higher variability in designs at lower reliability levels and reduced variability at higher reliability levels. The evaluation is conducted on a modified open pit slope based on a real case study. The authors acknowledge that the results presented correspond to one particular case study, and that not all sources of uncertainty can be explicitly modelled in slope stability calculations. However, the results provide some insights into the quantitative significance of increased uncertainty in the relevance of calculated FoS and PoF in slope design. The following observations can be drawn:

- The results of the case study support the adoption of lognormal distributions for the development of the RBDAC matrix.
- In terms of the number of realizations required in PSSA, the results indicate minimal differences between the outcomes obtained from 1000 and 10 000 realizations, suggesting that PSSA with 1000 realizations can still yield consistent results with minimal influences of statistical uncertainty. This finding implies that the computational time for PSSA can be reduced without compromising the reliability of the analysis required for evaluating COV_{FoS}, FoS and PoF required in the evaluation of the RBDAC. It is recommended this test be performed in at least one scenario during the design process to confirm the required number of iterations in PSSA.
- Significant differences are observed between PSSA with fixed and iteration-specific slip surface generation. Adopting a fix slip surface leads to significant over-estimation of the design stability, even if computational effort is significantly reduced.
- Spatial correlation becomes a critical aspect for high design reliabilities that have the required information to model spatial correlation and that aim at open pit design optimization. As spatial correlation length decreases, PoF decreases, consistent with existing findings in existing literature. Additionally, COV_{FoS} also decreased in our case in the range of 0.051 to 0.061 compared to the results obtained without spatial correlation. This range applies to the case study with bimodal histograms. Although the difference in COV_{FoS} is small, the reduction in PoF is significant.

- Resulting FoS from PSSA can result in bimodal distributions that correspond to different potential slope failure modes. It is recommended that this distribution be inspected by the designer and the possible failure modes driving each distribution understood in order to make informed decisions regarding design acceptability and required monitoring strategies. These observations can lead to enhancements in understanding of the design through numerical techniques for selected sectors of the pit.

Overall, the results presented in this work indicate the applicability of the proposed reliability-based design acceptance criteria (RBDAC) framework presented in Macciotta et al. (2020), and the practicability of the thresholds in their proposed RBDAC matrices. Practical adoption of the RBDAC matrix requires evaluating slope stability results against the thresholds in the matrix for an assessed consequence of failure and reliability of the stability models. It is highlighted that the categorization of a design in terms of potential economic consequence and, perhaps more importantly, categorization of the reliability of a design; requires proper assessment by qualified practitioners. Similarly, target values of FoS and PoF should be validated for each operation in light of the risk appetite of the operator, their knowledge of the pit slope deformation mechanisms, and the maturity of their Triger Action and Response Plans (TARPS), where the target values in the RBDAC matrix in Macciotta et al. (2020) represent good starting points, as a reflection of general industry practice.

5. Conclusion

Reliability-based design codes have been progressively adopted for the design of different geotechnical structures since the mid-1970s. In slope stability analysis and design, its adoption has helped geotechnical designers understand the importance that uncertainty plays for the structure's safety and design optimization. The application of this methodology requires understanding the potential consequence of inadequate design, and the different sources of uncertainty that could lead to inadequate design. Although uncertainty is quantified by probabilistic analysis, some types of uncertainty are not usually accounted for in the design. Therefore, different results can be obtained in a slope stability analysis for different types of uncertainty considered, which can lead to different decisions whether the design is acceptable or not. Nonetheless, it is common in practice to only consider parameter uncertainty as the only variability in the system.

This work is carried out to test the applicability of a reliability-based design acceptance criteria for open pit slopes, and the impact of different sources of uncertainties in the evaluation. The application was performed on a modified open pit slope, inspired by the geotechnical, geological, and hydrological characteristics of an implemented pit slope located in British Columbia, Canada.

In terms of parameter uncertainty, a review of different works presented in the last 13 years showed that different approaches were considered for estimating the variability of the rock mass strength in terms of the Hoek-Brown failure criterion as well as the equivalent Morh-Coulomb failure criterion. The former was usually used considering univariate distributions, therefore, ignoring any parameter correlation between the strength parameters. The latter was most frequently used due to users' familiarity with

cohesion and friction angle, nevertheless the parameter correlation considered was that usually estimated for soils. The analysis presented in this thesis demonstrated that consistency of results can be achieved by the consideration of an inherent parameter correlation in the equivalent Mohr-Coulomb parameters estimated through current conversion equations from Hoek-Brown failure to Mohr-Coulomb failure criterion. These conversion equations are also required for estimating variability of the equivalent cohesion and friction angle from the variability of the Hoek-Brown strength parameters. The conclusion of this work is that equivalent Mohr-Coulomb strength parameters will always follow a bivariate distribution whether univariate or bivariate distribution is considered in the Hoek-Brown strength parameters. The inherent correlation estimated tends to be negative, following the same criteria in soils, however, it changes to positive values as the GSI decreases or the confining stress increases. Finally, although univariate and bivariate distribution were studied in the Hoek-Brown failure criterion, considering bivariate distributions, which follow more real scenarios, tend to higher probability of failure compared to those observed using univariate distributions. Consequently, the attention given to the variability of the rock mass strength parameters can have a significant impact on the acceptability of the design.

Parameter uncertainty is also affected by epistemic uncertainty, which mathematically can increase the coefficient of variation of the rock mass strength parameters. More epistemic uncertainty reduces the level of reliability in the design, and this was evaluated in the reliability-based design acceptance criteria for different design reliability levels. Geometrical uncertainty, and computational uncertainty were also considered in this part of the work.

Computational uncertainty was evaluated in terms of the computational simplifications by reducing the number of realizations and whether to consider a fixed slip surface or an iteration-specific surface generation. The former showed that our case study can be optimized in time by reducing the number of realizations from 10 000 to 1000, showing slight differences attributed to statistical uncertainty. The latter showed that the design is overestimated if fixed slip surface is considered in the design by obtaining lower values of coefficient of variation and probability of failure, suggesting a better level of reliability in the design than those obtained with an iteration-specific surface generation. Therefore, although fixed slip surface is less computationally expensive, its simplified approach leads to high computational uncertainty by ignoring the uncertainty associated in the failure mechanisms.

Spatial variability was also investigated in the high reliability design. It was observed that as spatial correlation decreases, probability of failure decreases from 18% to 1.6%, as similar works in literature for soil slopes. Coefficient of variation was observed to decrease in this trend, nevertheless in our case study the reduction is very small compared to the reduction in the probability of failure.

Geometrical uncertainty was evaluated - in combination with parameter uncertainty - in terms of variability in the geometry and piezometric elevation. This was considered by creating multiple scenarios (considering they all share equal probability of occurrence) with different orientation of major structures and different positions of the piezometric level in the model. This was performed for different reliability levels, where variation increases as the reliability level reduces. This also means the addition of more scenarios as the design reliability decreases, which helps in creating a global scenario. This global

scenario is different from the usual mean scenario, which usually only accounts for parameter variability and corresponds to the highest model reliability. The criteria considered for obtaining the global scenario is a simplified criteria which aims to evaluate the impact of the variation of structures and piezometric elevation in probabilistic analysis.

Comparisons of the global scenario and the usual mean scenario for probabilistic analysis show that variation in the coefficient of variation increases as more epistemic uncertainty is considered in the design. This means an increase in the probability of failure while maintaining a consistent factor of safety. The evaluation of these results in the reliability-based design matrix highlighted the influence of multiple sources of uncertainties by making a difference between designs deemed acceptable or not, as per the matrix criteria. Importantly, the use of the matrix for the multiple scenarios considered was simple and intuitive, allowing direct interpretation of results.

The results in this thesis indicate that a RBDAC matrix allows evaluation of design slope stability considering the reliability of these designs in a practical and transparent manner.

5.1 Recommendation for Future Research

The recommendations for future research based on this study are the following:

- Once software packages allow for bivariate distribution with the Hoek-Brown failure criterion, it is recommended to complete similar studies using variability in the Hoek-Brown strength parameters and compare against the outcomes using Mohr-Coulomb strength parameters to understand the effect of adopting the simplified equivalent Mohr-Coulomb strength parameters in PSSA.

- Develop parallel studies as the one presented here considering other open pit cases, in different geological contexts, particularly for hard and soft rocks and different structural geometries.
- It is recommended that future similar works can test the applicability of the proposed reliability-based design matrix for a different economic consequence category than the one evaluated here (moderate economic consequence).
- Explore the range of variation in the probability of failure and coefficient of variation as more uncertainty is considered in the open pit design from the mean scenario to the global scenario and determine whether these additional uncertainties influence in the acceptability of the design in a similar magnitude presented in this work, through their comparison against the RBDAC matrix.
- Finally, although geometrical uncertainty was performed in the simplest way, the work demonstrated that this form of uncertainty can easily influence the acceptance of an open pit slope design, and this means that other types of uncertainties not considered can also influence in a similar way. The RBDAC approach is a systematic way to consider these other uncertainties in the evaluation of open pit slope designs. This requires future research to evaluate adequate methods and criteria to define design reliability based on all sources of uncertainty in pit slope design, such that the use of the RBDAC matrix is consistent across industry.

References

Adams, B. M. (2015, February 22-25). Slope stability acceptance criteria for opencast mine design. G. Ramsay (Ed.), Proceedings of the 12th Australia New Zealand Conference on geomechanics (pp. 8), Wellington, New Zealand.

Abdulai, Musah & Sharifzadeh, Mostafa. (2021). Probability Methods for Stability Design of Open Pit Rock Slopes: An Overview. Geosciences. 11. 319. 10.3390/geosciences11080319.

Alonso EE (1976). Risk analysis of slopes and its application to slopes in Canadian sensitive clays. Geotech 26:453-472.

Amoushahi, Sina & Grenon, Martin & Locat, Jacques & Turmel, Dominique. (2018). Deterministic and probabilistic stability analysis of a mining rock slope in the vicinity of a major public road – case study of the LAB Chrysotile mine in Canada. Canadian Geotechnical Journal. 55. 10.1139/cgj-2017-0298.

Baecher, Gregory and Christian, John. (2003). Reliability and Statistics in Geotechnical Engineering. John Wiley & Sons.

Barnett, R., Azizian, A., Clayton, C. and Slater, M. (2017). Geomechanical characterization of a sheared coal seam and implications for open pit slope design. Proceedings of the 51st US Rock Mechanics/Geomechanics Symposium, American Rock Mechanics Association, Alexandria.

Bieniawski, Z. T. (1968). The effect of specimen size on compressive strength of coal. International Journal of Rock Mechanics and Mining Sciences & Geomechanics Abstracts, 5(4), 325–335. doi:10.1016/0148-9062(68)90004-1.

British Columbia Ministry of Energy, Mines and Petroleum Resources (2018). The East Kootenay Coalfields. British Columbia Geological Survey Information Circular 2018-6.

Chiwaye HT, Stacey TR (2010) A comparison of limit equilibrium and numerical modelling approaches to risk analysis for open pit mining. J South Afr Inst Min Metal 110:571–580.

Clayton, C., Barnett, R. and Slater, M. (2020), Case study: back-analysis of a historical open pit highwall failure at a coal mine in Canada, in PM Dight (ed.), Slope Stability 2020: Proceedings of the 2020 International Symposium on Slope Stability in Open Pit Mining and Civil Engineering, Australian Centre for Geomechanics, Perth, pp.873-888, https://doi.org/10.36487/ACG_repo/2025_57

Christian, J. T., Ladd, C. C., and Baecher, G. B. (1994). Reliability applied to slope stability analysis. J. Geotech. Engr., 20, Dec., 2180– 2207.

Doruk, P. (1991) Analysis of the Laboratory Strength Data Using the Original and Modified Hoek-Brown Criteria. MS Thesis. Toronto, University of Toronto. 124 pp.

Eberhardt, E. (2012). The Hoek–Brown Failure Criterion. Rock Mech Rock Eng 45, 981–988. https://doi.org/10.1007/s00603-012-0276-4.

Evans, I., and Pomeroy, C.D. (1966) The Strength, Fracture and Workability of Coal. Pergamon Press, London.

Gaida, M, Cambio, D, Robotham, ME & Pere, V (2021). Development and application of a reliability-based approach to slope design acceptance criteria at Bingham Canyon Mine, in PM Dight (ed.), SSIM 2021: Second International Slope Stability in Mining, Australian Centre for Geomechanics, Perth, pp. 83-94, https://doi.org/10.36487/ACG_repo/2135_02.

Gentzis, T., Deisman, N., & Chalaturnyk, R. J. (2007). Geomechanical properties and permeability of coals from the Foothills and Mountain regions of western Canada. International Journal of Coal Geology, 69(3), 153–164. doi:10.1016/j.coal.2006.02.007.

Grieve, Da. and Price, RA. (1987). Geological Setting of the South Half of the Elk Valley Coalfield Southeastern British Columbia. Preliminary Map 63. Ministry of Energy, Mines and Petroleum Resources, Geological Survey Branch.

Griffith, A. A. (1924). Theory of rupture. In C. B. Biezeno and J. M. Burgers, editors, Proc. First International Congress on Applied Mechanics, Delft, pages 55–63.

Guo, Jia & Du, Xiaoping. (2007). Sensitivity Analysis with Mixture of Epistemic and Aleatory Uncertainties. AIAA Journal - AIAA J. 45. 2337-2349. 10.2514/1.28707.

Harr ME (1977). Mechanics of particulate media – a probabilistic approach. McGraw-Hill, New York.

Hata Y., Ichii K., and Tokida K. (2012). A probabilistic evaluation of the size of earthquake induced slope failure for an embankment. Georisk 6:73–88.

Hoek E., Brown ET. (2018). The Hoek–Brown failure criterion and GSI-2018 edition. J Rock Mech Geotech Eng. https ://doi.org/10.1016/j.jrmge .2018.08.001.

Hoek E., Carranza-Torres C., Corkum B. (2002). Hoek-Brown criterion - 2002 edition. In: Hammah R, Bawden W., Curran J., Telesnicki M., editors. Mining and tunnelling innovation and opportunity, proceedings of the 5th North American rock mechanics symposium and 17th tunnelling association of Canada conference. Toronto, Canada. Toronto: University of Toronto; 2002. p. 267-273.

Huan, Z., Zhenghong, G., Fang, X. et al. Review of Robust Aerodynamic Design Optimization for Air Vehicles. Arch Computat Methods Eng 26, 685–732 (2019). https://doi.org/10.1007/s11831-018-9259-2.

Huan, Zhao & Zhenghong, Gao & Xu, Fang & Zhang, Yidian. (2018). Review of Robust Aerodynamic Design Optimization for Air Vehicles. Archives of Computational Methods in Engineering. 26. 10.1007/s11831-018-9259-2.

Javankhoshdel S. and Bathurst RJ. (2016) Influence of cross correlation between soil parameters on Probability of Failure of simple cohesive and c–ϕ slopes. Can Geotech J 53:839–853.

Javankhoshdel, S., Luo, N., and Bathurst, R. (2016). Probabilistic analysis of simple slopes with cohesive soil strength using RLEM and RFEM. Georisk: Assessment

and Management of Risk for Engineered Systems and Geohazards. 11. 1-16. 10.1080/17499518.2016.1235712.

Lambe, T. W. (1985). Amuay landslides. 11th International Conference on soil mechanics and foundation engineering (pp. 137–158), San Francisco, CA: A.A. Balkema.

Langford, J.C., Diederichs, M.S. (2015). Quantifying uncertainty in Hoek-Brown intact strength envelopes. Int. J. Rock Mech. Min. Sci. 74, 91–102.

Macciotta R., Creighton A., and Martin C. D. (2020). Design acceptance criteria for operating open-pit slopes: An update, CIM Journal, 11:4, 248-265, DOI: 10.1080/19236026.2020.1826830.

Medhurst TP., Brown ET. (1998). A study of the mechanical behaviour of coal for pillar design. Int J Rock Mech Min Sci 35:1087–1105.

Meyerhof, G. G. (1970). Safety factors in soil mechanics. Canadian Geotechnical Journal, 7(4), 349–355. https://doi.org/10.1139/t70-047.

Morgenstern NR, Price VE (1965). The analysis of the stability of general slip surfaces. Geotech 15:79–93.

Peck, R. B. (1969). Advantages and limitations of the observational method in applied soil mechanics. Geotechnique. 19(2), 171-187. https://doi.org/10.1680/geot.1969.19.2.171.

Phoon, K.-K., and Ching, J. (Eds.). (2015). Risk and Reliability in Geotechnical Engineering (1st ed.). CRC Press. https://doi.org/10.1201/b17970.

Phoon, K.K. and Kulhawy, F.H. (1999a). Evaluation of geotechnical property variability, Canadian Geotechnical Journal, 36 (4), 625–6639.

Phoon, K.K. and Kulhawy, F.H. (1999b). Characterization of geotechnical variability. Canadian Geotechnical Journal, 36 (4), 612–624.

Phoon, K.K. Prakoso, Widjojo, Wang, Yu and Ching, Jianye. (2016). Chapter 3 Uncertainty representation of geotechnical design parameters. In the book: Reliability of Geotechnical Structures in ISO2394.

Pozo, Raul. (2022). Comparative analysis of different calculation methods of the geological strength index (GSI) based on qualitative and quantitative approaches. Rudarsko-geološko-naftni zbornik. 38. 121-138. 10.17794/rgn.2022.3.10.

Prakoso, W.A. (2002) Reliability-Based Design of Foundations on Rock for Transmission Line & Similar Structure. PhD Thesis. New York, Cornell University.

Priest, S. D., & Brown, E. T. (1983). Probabilistic stability analysis of variable rock slopes. Transactions of the Institution of Mining and Metallurgy, 92, A1–A12.

Rafiei Renani, H., Martin, C. D., Varona, P., and Lorig, L. (2019). Stability analysis of slopes with spatially variable strength properties. Rock Mechanics and Rock Engineering, 52(10), 3791-3808.

Rafiei Renani, H., and Martin, C. D. (2019). Slope Stability Analysis using Equivalent Mohr–Coulomb and Hoek–Brown criteria. Rock Mechanics and Rock Engineering. doi:10.1007/s00603-019-01889-3.

Rocscience Inc (2023). Slide2 Modeler – 2D limit Equilibrium Analysis for Slopes, version 9.027, Toronto, Canada.

Silva, F., Lambe, T. W., & Marr, W. A. (2008). Probability and risk of slope failure. Journal of Geotechnical and Geoenvironmental Engineering, 134(12), 1691–1699. https://doi.org/10.1061/(ASCE) 1090-0241(2008)134:12(1691).

Steffen OKH, Terbrugge PJ, Wesseloo J & Venter J (2006). A risk consequence approach to open pit slope design. In Proceedings of International Symposium on Stability of Rock Slopes in Open Pit Mining and Civil Engineering, Cape Town, pp. 81–96. South African Institute of Mining and Metallurgy, Johannesburg.

Swan, G., and Sepulveda, R. (2000). Slope stability at Collahuasi. In: W. A. Hustrulid, K. M.McCarter, & D. J. A.Van Zyl (Eds.), Slope stability in surface mining (pp. 163–170). SME.

Tang WH, Yucemen MS, And AHS (1976). Probability based short-term design of slopes. Can Geotech J 13:201-215.

The Mining Association of Canada (2023). The Canadian Mining Story: Economic Impacts and Drivers for the Global Energy Transition 2023.

Valdivia M. and Macciotta R. (in press). Rock mass strength variability for probabilistic open-pit slope stability analyses. Submitted to the Geotechnical and Geological Engineering Journal in October 2023.

Vanmarcke, E. H. (1977). Reliability for earth slopes. J. Geotech. Engrg. Div., ASCE, 103(11), 1227-1246.

Wesseloo, J., and Read, J. (2009). Acceptance criteria. In: J. Read & P. Stacey (Eds.), Guidelines for open pit slope design (pp. 221–236). CRC Press/ Balkema.

Yucemen MS., Tang WH., and Ang AHS. (1973). A probabilistic study of safety and design of earth slopes. Civil Engineering Studies, Structural Research Series 402, University of Illinois.

Zhang, F.P., Li, D.Q., Cao, Z.J., Xiao, T., Zhao, J. (2018). Revisiting statistical correlation between Mohr–Coulomb shear strength parameters of Hoek–Brown rock masses. Tunn. Undergr. Space Technol. 77, 36–44.